ANALYSIS OF THE ALTITUDE TRACKING PERFORMANCE OF AIRCRAFT-AUTOPILOT SYSTEMS IN THE PRESENCE OF ATMOSPHERIC DISTURBANCES

by

JAMES LUCKETT STURDY

S.B., Massachusetts Institute of Technology
(1986)

SUBMITTED IN PARTIAL FULFILLMENT
OF THE REQUIREMENTS FOR THE
DEGREE OF

MASTER OF SCIENCE IN
AERONAUTICS AND ASTRONAUTICS

at the

MASSACHUSETTS INSTITUTE OF TECHNOLOGY

February 1988

Signature of Author _____
Department of Aeronautics and Astronautics
January 15, 1988

Certified by _____
Associate Professor R. John Hansman
Thesis Supervisor, Department of
Aeronautics and Astronautics

Accepted by _____
Professor Harold Y. Wachman
Chairman, Department Graduate Committee

ANALYSIS OF THE ALTITUDE TRACKING PERFORMANCE OF AIRCRAFT-AUTOPILOT SYSTEMS IN THE PRESENCE OF ATMOSPHERIC DISTURBANCES

by

JAMES LUCKETT STURDY

Submitted to the Department of Aeronautics and Astronautics on January 15, 1988 in partial fulfillment of the requirements for the degree of Master of Science in Aeronautics and Astronautics

ABSTRACT

The dynamic response of aircraft-autopilot systems to atmospheric disturbances was investigated by analyzing linearized models of aircraft dynamics and altitude hold autopilots. Four jet aircraft (Boeing 737-100, McDonald Douglas DC9-30, Lockheed L-1011, and Cessna Citation III) were studied at three flight levels (FL290, FL330, and FL370).

The models were analyzed to determine the extent to which pressure surface fluctuations, vertical gusts, and horizontal gusts cause assigned altitude deviations by coupling with the aircraft-autopilot dynamics.

The results of this analysis were examined in light of meteorological data on disturbance magnitudes and wavelengths collected from observations of mountain wave activity. This examination revealed that atmospheric conditions do exist which can cause aircraft to exhibit assigned altitude deviations in excess of 1,000 ft. Pressure surface fluctuations were observed to be the dominant source of altitude errors in flights through extreme mountain wave activity. Based on the linear analysis the maximum tolerable pressure surface fluctuation amplitude was determined as a function of wavelength for an allowable altitude error margin of 300 ft. The results of this analysis provide guidance for the determination of vertical separation standards in the presence of atmospheric disturbances.

Thesis Supervisor: Dr. R. John Hansman Jr.
Associate Professor of
Aeronautical Engineering

ACKNOWLEDGEMENTS

This work would not have been possible without the efforts of Richard Hueschen of the NASA Langley Research Center, Bill Carter of Honeywell, and Randy Nelson of Cessna who provided aircraft and autopilot data as well as technical support. Professor R. John Hansman, my advisor, provided valuable advice and criticism. I would like to thank my wife, who served as an editor and a link to the world of the sane, and the other inmates of 37-450 -- may their efforts soar long and far.

TABLE OF CONTENTS

LIST OF FIGURES

Chapter 1

Chapter 2

Chapter 3

Chapter 4

LIST OF TABLES

Chapter 3

NOMENCLATURE

$\underline{A}$	state space state coefficient matrix
$\underline{B}$	state space input coefficient matrix
f	disturbance encounter frequency
g_x	amplitude of horizontal gust
g_z	amplitude of vertical gust
h	perturbed aircraft height
$\dot{h}$	aircraft vertical velocity
$\ddot{h}$	aircraft vertical acceleration
h_e	aircraft altitude error
h_p	perturbed height of assigned pressure surface
q	aircraft pitch rate
S	Laplace transform variable
$\underline{u}$	state space vector of inputs
u_b	perturbed aircraft forward velocity in body axes
u_g	X_b component of change in relative wind due to gusts
U_b	aircraft forward velocity in body axes
U_{b_o}	equilibrium forward velocity in body axes
w_b	perturbed aircraft vertical velocity in body axes
w_g	Z_b component of change in relative wind due to gusts
W_b	aircraft vertical velocity in body axes
W_{b_o}	equilibrium vertical velocity in body axes
v	perturbed aircraft velocity
v_g	relative wind velocity change due to horizontal gust
V	aircraft velocity
V_o	equilibrium aircraft velocity
$\underline{x}$	vector of state variables

α perturbed aircraft angle of attack

$\dot{\alpha}$ rate of change of angle of attack

α_g angle of attack change due to vertical gust

A aircraft angle of attack

γ perturbed aircraft flight path angle

$\dot{\gamma}$ rate of change of flight path angle

Γ aircraft flight path angle

Γ_o equilibrium flight path angle

δ_e elevator deflection

δ_{e_c} commanded elevator deflection

θ perturbed aircraft pitch angle

θ_c perturbed commanded aircraft pitch angle

Θ aircraft pitch angle

Θ_o equilibrium pitch angle

λ wavelength of disturbance measured along flight path

λ_w wavelength of mountain lee wave

Chapter 1

INTRODUCTION

1.1 Overview

This work seeks to determine the altitude tracking performance of aircraft-autopilot systems in the presence of atmospheric disturbances. The accuracy with which aircraft are able to track a specified barometric pressure altitude is an important consideration in determining the minimum regulated vertical separation that should be retained between aircraft whose paths may cross. The process of tracking altitude properly can be broken down into two stages. First, the altimetry system onboard the aircraft must measure altitude fairly accurately. Second, the pilot or autopilot must respond appropriately to any altitude deviations indicated by the altimeter.

Altitude tracking performance can deteriorate when errors occur in either the measurement or control of the aircraft's altitude. If the altimetry system does not measure the aircraft's altitude well, the pilot or autopilot will try to make the aircraft fly at the wrong altitude. If the pilot or autopilot doesn't respond so as to instantaneously eliminate altitude deviations, the aircraft will again deviate from its assigned altitude. The sources of measurment errors in the altimetry system are well documented.[1,2,3,4,5,6] This work concentrates on errors in

the control of the aircraft's altitude, especially those that result when atmospheric disturbances act on aircraft which are controlled by an altitude hold autopilot.

The effect of three types of atmospheric disturbances on the tracking performance of aircraft-autopilot systems was studied by analyzing linear models of the aircraft and autopilot dynamics. The three disturbances considered were fluctuations in the desired pressure surface, vertical gusts, and horizontal gusts. Four aircraft and their associated autopilots were studied: a Boeing 737-100, a McDonald Douglas DC9-30, a Lockheed L-1011, and a Cessna Citation III. The results of this analysis were then viewed in the context of available meteorological data to assess the magnitude of potential tracking errors.

Section 1.2 discusses the motivation for this work. Section 1.3 gives a more detailed description of the various sources of altitude error. Chapter 2 presents the derivation of the various linear aircraft and autopilot dynamic models and descriptions of the techniques used to analyze the models. In Chapter 3 the results of the analysis are presented. Chapter 4 examines the results in the context of atmospheric phenomena, specifically mountain waves. A summary of the conclusions is presented in Chapter 5.

1.2 Motivation

In recent years changes to the international vertical separation standards for aircraft have been proposed which would reduce the minimum altitude separation for aircraft in level flight above 29,000 feet (Flight Level, FL, 290). Vertical separation between aircraft is established by the air traffic control system which assigns aircraft to specific altitudes that correspond to fixed values of atmospheric pressure rather than to a height above ground or sea level. This pressure-referenced system is used because aircraft measure their altitude using barometric altimeters which measure the ambient pressure.

Current Federal Aviation Regulations (FAR) require aircraft flying different courses at and above FL290 to be separated vertically by a minimum of 2,000 feet and those flying below FL290 to be separated vertically by at least 1,000 feet as a means of providing a margin of safety against collisions. This standard was established in the late 1950's. The higher margins above FL290 reflect the degradation in altitude measurement accuracy at higher altitudes due to the decrease in the rate of change of pressure with changes in altitude. The significant improvements in altimetry system accuracy and autopilot performance that have occurred over the last thirty years as well as the potential benefits of increasing the number of usable flight levels have led to the introduction of a proposal for reducing the vertical separation standard for

flights at and above FL290 from 2,000 to 1,000 feet. The potential benefits of reducing the separation standard include: increased flexibility in ATC traffic routing, increased system capacity at high altitudes, and fuel conservation by allowing aircraft to fly closer to their most efficient altitude.

In order to ensure that reductions in the vertical separation standard will not seriously affect flight safety, the magnitude of the various components of altitude error need to be examined. These various components are enumerated in the next section.

1.3 Altitude Error Components

An aircraft's total vertical error, which is the difference between the aircraft's height and the height of the constant pressure surface to which it has been assigned, has two components which are illustrated in Figure 1-1. The first component, which is alternately referred to as Assigned Altitude Deviation (AAD) or tracking error, is a result of the pilot or autopilot allowing the aircraft's indicated altitude to deviate from the assigned altitude. These tracking errors typically occur when the height of the assigned pressure surface is fluctuating so that the aircraft has to 'chase' it or when gusts cause the aircraft to depart from equilibrium flight. An example of an assigned altitude deviation is presented in Figure 1-2. This Figure shows data that has been obtained by monitoring the Mode C altitude reporting transponder of a twin-engine Sabreliner jet

aircraft flying at FL370 with its altitude hold autopilot engaged during a period of reported mountain wave activity in the Denver, Colorado area. The data shows that the aircraft's altimeter detected a 700 foot assigned altitude deviation during a period of unsteady flight.

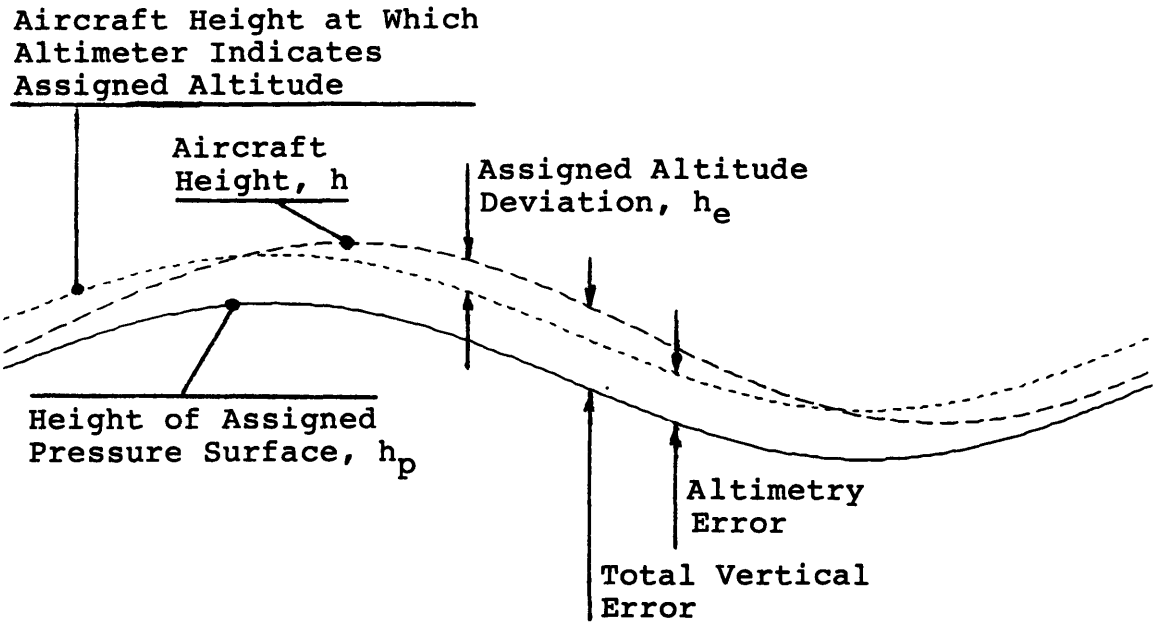

Figure 1-1 Altitude error components.

The second component, which is also illustrated in Figure 1-1, is due to measurement errors in the altimetry system. These error sources, which include such factors as calibration error, hysteresis in the pressure transducer, pressure leaks, measurement lags, and position error, cause the aircraft's indicated altitude to be different the aircraft's true barometric altitude. (Position error is a result of the aircraft's motion affecting the local pressure

at the measurement point). These error sources have been investigated in previous studies.[1,2,3,4,5,6]

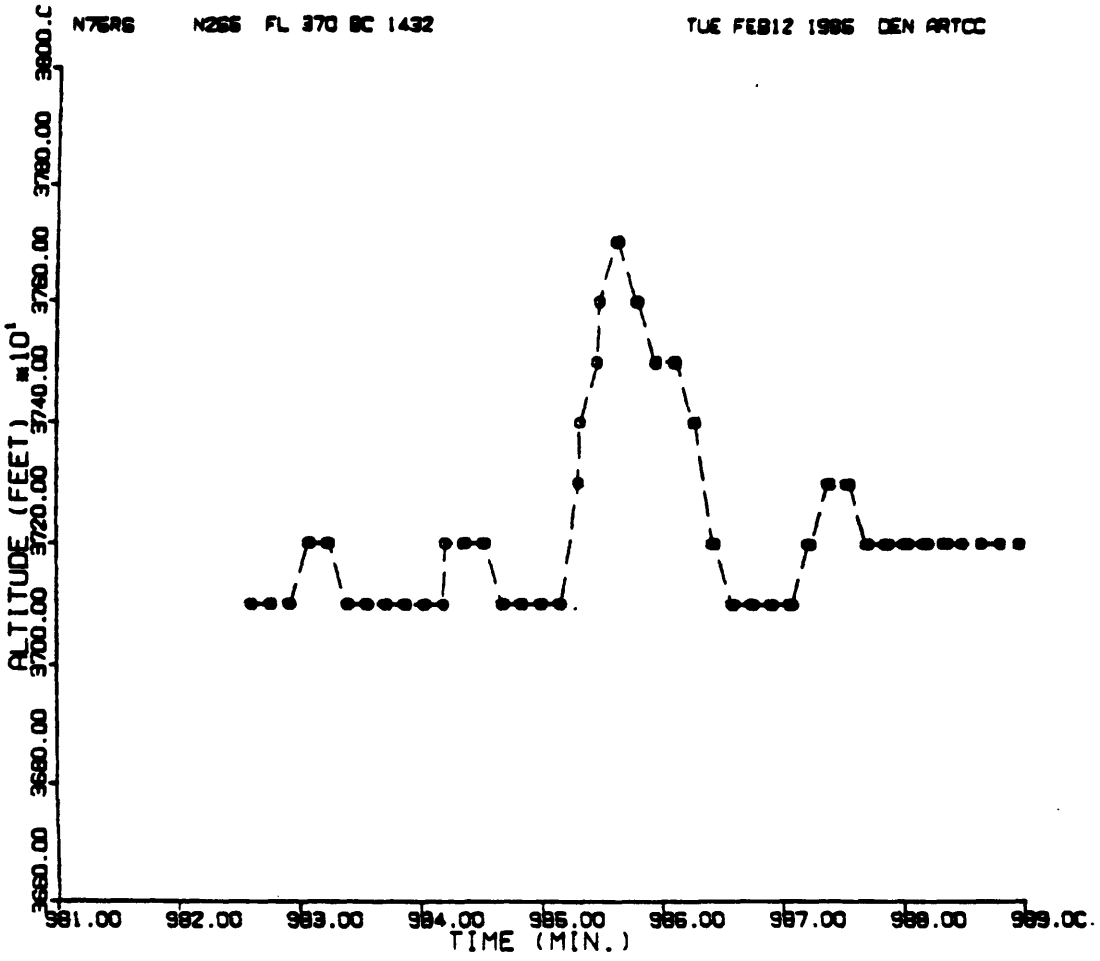

Figure 1-2 Mode C data showing an assigned altitude deviation of 700 feet.

This work concentrates on the tracking errors that can result when an aircraft is flown on autopilot in the presence of three types of disturbances which have been observed in the atmosphere: pressure surface fluctuations, vertical gusts, and horizontal gusts. The surface of constant pressure which aircraft try to follow is not always at a

uniform height. Fluctuations in the height of the pressure surface can be approximated by a series of sinusoidal fluctuations of varying amplitudes and wavelengths, where the amplitude measures the peak deviation from the mean height and the wavelength is the distance between successive peaks or troughs along an aircraft's flight path. Vertical gusts, which represent variations in the atmosphere's vertical motion along the flight path, and horizontal gusts, which represent variations along the flight path of the atmosphere's motion parallel to the direction of flight, can also be approximated in this manner.

Chapter 2

METHODOLOGY

2.1 Overview

Linearized mathematical models of the dynamics of several aircraft and autopilots were developed. These models were then analyzed to determine the altitude tracking performance of the various aircraft-autopilot systems in the presence of atmospheric disturbances. Details of the model derivation and their interpretation are given in Section 2.2. The techniques used in analyzing the models are covered in Section 2.3.

2.2 Model Derivation

In order to investigate the ability of aircraft to track their assigned altitude in the presence of atmospheric disturbances, a representation of specific aircraft and autopilot dynamics was needed. This representation, which is herein referred to as a model, consists of a set of differential equations which approximates the behavior of the aircraft. For this investigation, the typically nonlinear equations of motion were linearized about a nominal condition which represents steady level flight at a specified altitude. In these linearized models, each variable, such as velocity or pitch angle, is expressed as a perturbation from its steady state value. One advantage of a linear model is that

output or response amplitudes scale directly with input or disturbance amplitudes, such that doubling the input amplitude will double the output amplitude and superposition can be used to combine the effects of multiple disturbances.

Models were generated for the longitudinal dynamics of the various aircraft at several altitudes at and above FL290 and for the dynamics of an altitude hold autopilot commonly used on each aircraft. These components are shown in Figure 2-1. The aircraft and autopilot models were then combined to form a model of the aircraft-autopilot system's dynamics. The four aircraft studied, which are depicted in Figure 2-2, were: a Boeing 737-100, a McDonald Douglas DC9-30, a Lockheed L-1011, and a Cessna Citation III. The first three are commercial aircraft certified under FAR Part 25 and were chosen because they represent a range of transport category aircraft for which stability and autopilot data were available. The Cessna Citation III is representative of general aviation business jets. Each aircraft has been analyzed at three altitudes (FL290, FL330, and FL370), and Mach numbers of 0.8 for the transport aircraft and 0.7 for the Citation III. The DC9-30 had insufficient thrust to reach FL370 at the weight for which its linear models were generated and was therefore evaluated at FL357 instead.

The analysis was limited to flight with an altitude hold autopilot engaged because this is the normal procedure in high altitude cruise flight and because an autopilot's response can be modeled more accurately than a pilot's

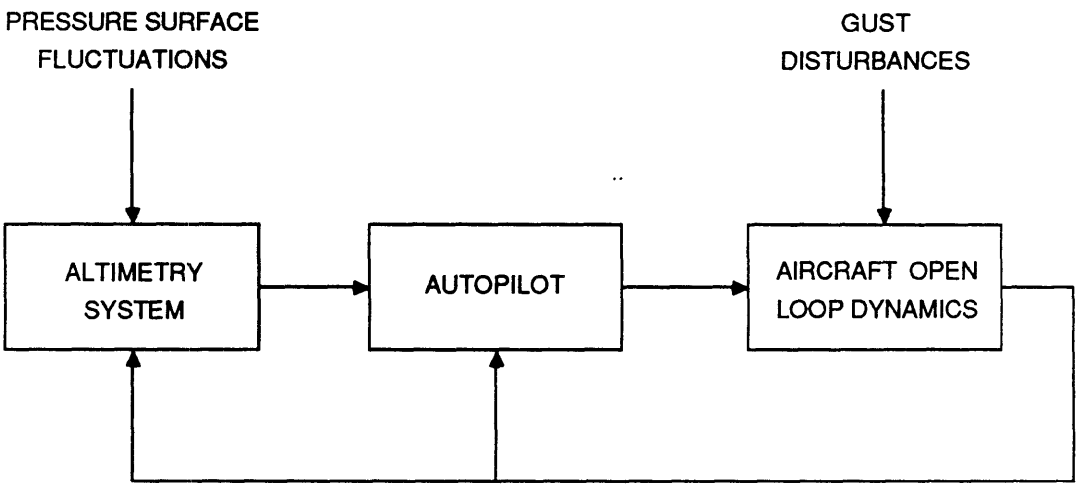

Figure 2-1 Linearized model components.

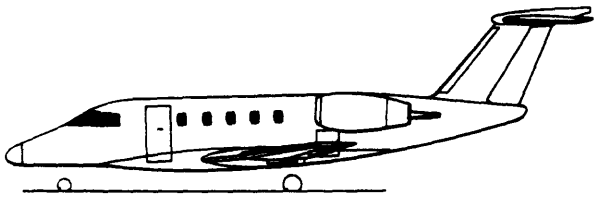

Cessna Citation III

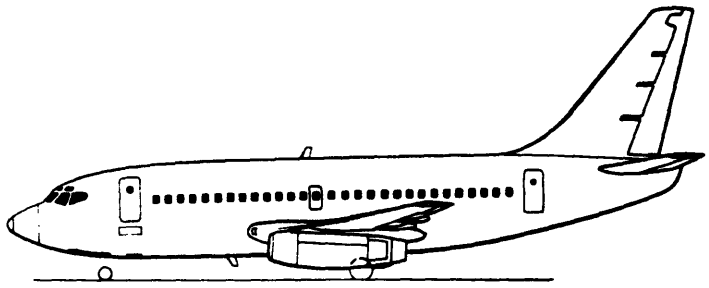

Boeing 737-100

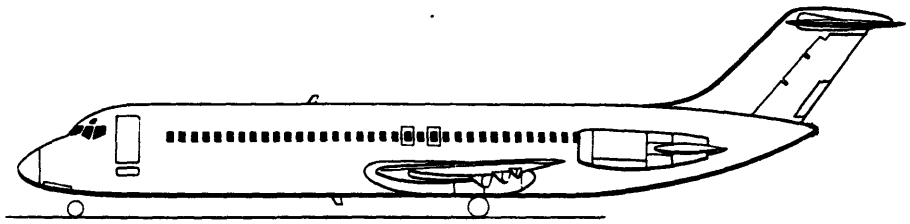

McDonald Douglas DC9-30

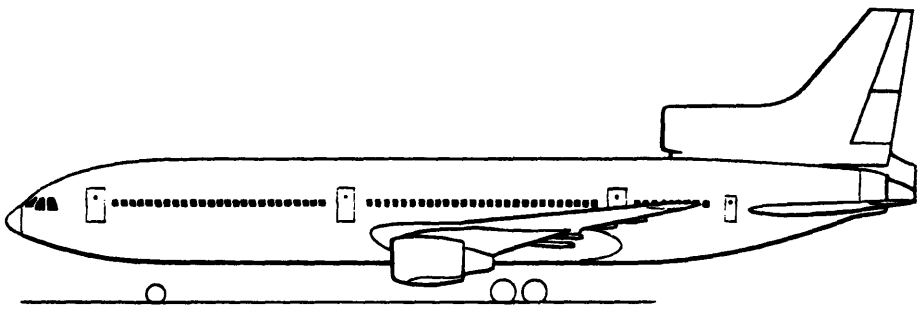

Lockheed L-1011

Figure 2-2 Aircraft studied.

response. Turbulent autopilot modes were not investigated because they typically involve continuous pilot input.

The atmospheric disturbances that were used as inputs to the model are pressure surface fluctuations, vertical gusts, and horizontal gusts. Pressure surface fluctuations are the variations in the height of the surface of constant pressure which the aircraft is assigned to fly along. Vertical gusts are the variations in the vertical component of atmospheric motion encountered along the aircraft's flight path. Horizontal gusts are the variations in the longitudinal component of atmospheric motion encountered along the aircraft's flight path.

Altitude error, h_e, was used as the output of the model in the analysis. The altitude error is defined as:

$$h_e = h_p - h \qquad (2\text{-}1)$$

where h_p is the height of the assigned pressure surface and h is the aircraft's height.

The following sections cover the derivation of the models for each aircraft and autopilot in more detail.

2.2.1 Frames of Reference and Sign Conventions

The three sets of axes used in this study, body axes, stability axes, and flight axes, are shown in Figure 2-3 for an aircraft in unyawed flight. The body axes, denoted by the subscript 'b', have their origin at the center of gravity of the aircraft and the X and Z axes in the aircraft's plane of symmetry and oriented so that all of the aircraft's cross products of inertia are zero. The stability axes, denoted by

the subscript 's', are similar to the body axes except that the X axis is aligned with the wind vector (when the aircraft is not yawed). The flight axes, denoted by the subscript 'f', have the Z axis directed towards the center of the earth and the X axis directed along the aircraft's flight path.

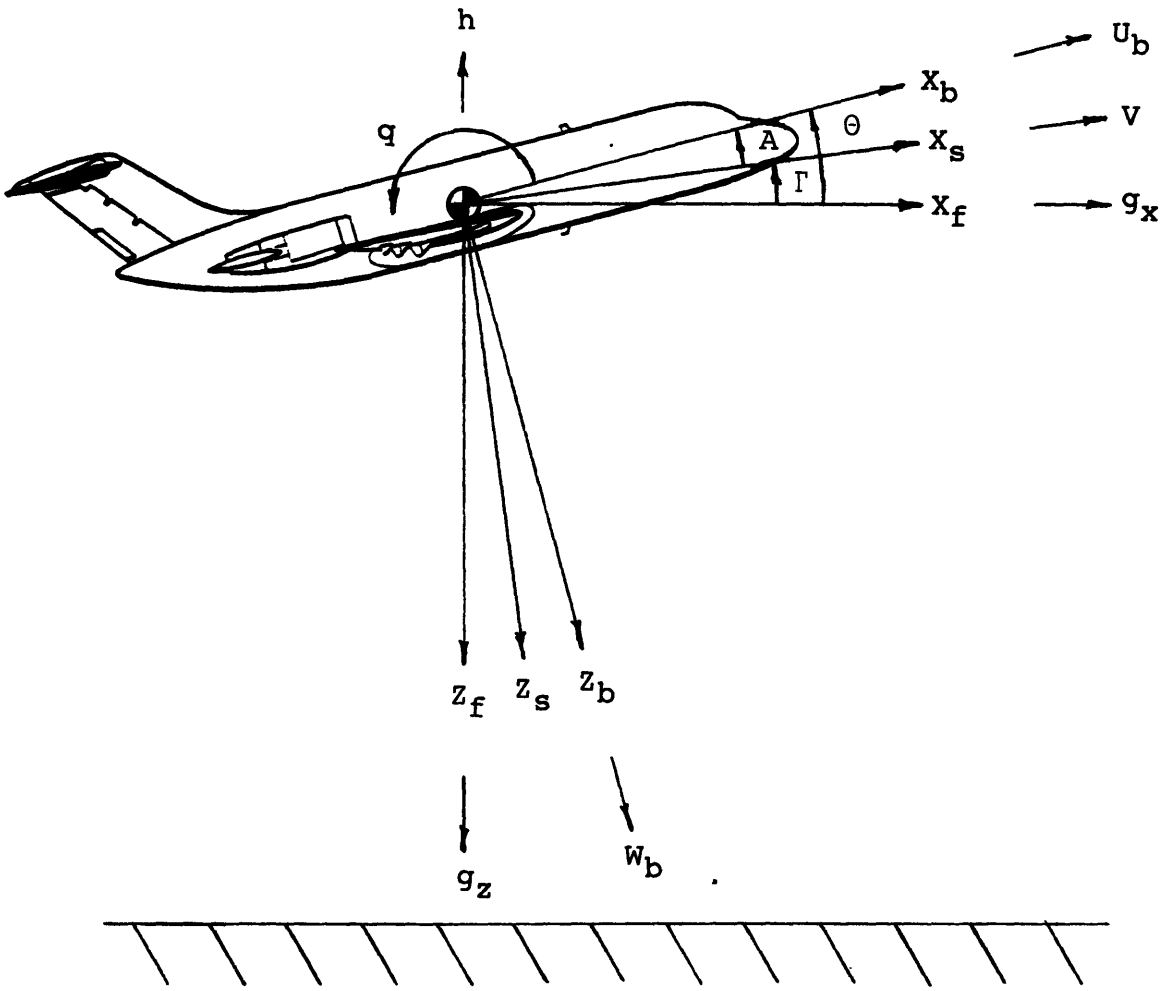

Figure 2-3 Frames of reference.

As can be seen in the figure, the flight axes can be transformed into body axes through a rotation by the aircraft's pitch angle, Θ. The stability axes can be transformed into body axes through a similar rotation by the aircraft's angle of attack, A. Note that when the pitch angle equals the angle of attack the aircraft is in level flight and the stability axes line up with the flight axes.

Figure 2-3 also shows the sign conventions used for the various flight parameters and gust inputs. The aircraft velocity components in body axes, U_b and W_b, are positive forward and down respectively. The aircraft's velocity V, which is in the direction of X_s, is positive for forward flight. The components of the wind fluctuation in the flight axes, g_x and g_z, are positive for tailwinds and downdrafts respectively. The positive direction for measuring the aircraft's height is up. The elevator deflection, δ_e, and the commanded elevator deflection, δ_{e_c}, use the sign convention that a positive deflection results in a negative pitch rate, -q.

2.2.2 Aircraft Models

When the dynamics of an aircraft are linearized, the longitudinal dynamics, which include translations and rotations in the aircraft's plane of symmetry, decouple from the lateral dynamics. Because the parameters of interest in this work (altitude, velocity, pitch angle, etc.) are all in the plane of symmetry, only the longitudinal dynamics need to be modeled.

Linearized models, which are derived using perturbation theory, are given in state space form.[7] The state is a vector, $\underline{x}$, composed of the important dynamic parameters in the equations of motion. For an aircraft, these parameters typically include such quantities as velocities, orientations, and rotation rates. The rate of change of the state vector, $\dot{\underline{x}}$, is then written in the form

$$\dot{\underline{x}} = \underline{A}\underline{x} + \underline{B}\underline{u} \qquad (2\text{-}2)$$

where $\underline{A}$ is a matrix made up of the coefficients found from performing a first order Taylor series expansion of the aircraft's equations of motion, $\underline{u}$ is a vector of control inputs, and $\underline{B}$ is a matrix of coefficients which also come from the Taylor series expansion. It is important to note that all of the variables used in the state space description are perturbed quantities which reflect changes from equilibrium.

In formulating the models of the aircraft dynamics, the following assumptions were made:

1. The mass of the aircraft is constant.

2. The airframe is a rigid body.

3. The earth is fixed in inertial space.

4. Longitudinal motion can be decoupled from lateral motion.

5. The linearized equations of motion are an accurate

approximation of the true aircraft behavior.

6. The spatial scale of all disturbances is sufficiently large that the disturbance acts uniformly over the entire aircraft.

7. The aircraft's pressure altitude is measured at the center of gravity of the aircraft.

8. The altimetry system measures the aircraft's pressure altitude perfectly.

Assumptions 2, 4, 5, and 6 are valid only for small perturbations from equilibrium flight and for input frequencies well below the unmodeled resonances of the airframe.

The state space models for the three transport aircraft were derived from the best available data[8] and are included in Appendix A along with the corresponding trim condition data. The state space models for the Citation III were derived from stability derivative data obtained from Cessna[9,10]. Trim condition data for the Citation III may be found in Appendix B.

2.2.2.1 737 and DC9 Models

The models for the 737 and the DC9 were derived in body axes and use the body axes components of velocity, u_b and w_b, pitch angle, θ, and pitch rate, q, as state variables. The DC9 model also has a state variable corresponding to the aircraft's height, h, and a state variable for the deflection

of the elevator, δ_e, which is required for simulating the lag in the elevator servo (the elevator servo lag is neglected in the 737 model). A variable for the aircraft's height, h, was added to the state space model of the 737 by linearizing the equation for altitude rate:

$$\dot{h} = U_b \text{Sin}(\Theta) - W_b \text{Cos}(\Theta) \qquad (2\text{-}3)$$

where U_b, W_b, and Θ represent total values (as opposed to perturbed quantities, which are indicated by lower case letters). Linearizing this equation using a first order Taylor series expansion, the expression becomes:

$$\dot{h} = \text{Sin}(\Theta_o)u_b - \text{Cos}(\Theta_o)w_b + (U_{b_o}\text{Cos}(\Theta_o)+W_{b_o}\text{Sin}(\Theta_o))\theta \qquad (2\text{-}4)$$

where U_{b_o}, W_{b_o}, and Θ_o are the steady state values of the variables. Since changes in altitude have only minor effects on the rate of change of the remaining state variables, no attempt was made to approximate these effects.

2.2.2.2 L-1011 and Citation III Models

The models for the L-1011 and the Citation III were derived in stability axes and use the aircraft's velocity, v, pitch angle, θ, pitch rate, q, angle of attack, α, aircraft height, h, and elevator position, δ_e, as state variables. Because the autopilots for each of these aircraft use measurements of vertical acceleration, $\ddot{h}$, an expression for it needed to be derived. By taking the derivative of the equation for vertical velocity:

$$\dot{h} = V\text{Sin}(\Gamma) \qquad (2\text{-}5)$$

where V is the aircraft's velocity and Γ is the aircraft's flight path angle in radians ($\Gamma=\Theta-A$), one obtains:

$$\ddot{h} = V\dot{\gamma}\,Cos(\Gamma) + \dot{V}Sin(\Gamma) \qquad (2\text{-}6)$$

which upon linearizing about the level flight equilibrium condition $\Gamma_o=0$ and making the substitution $\dot{\gamma}=q-\dot{\alpha}$ becomes:

$$\ddot{h} = V_o(q-\dot{\alpha}) \qquad (2\text{-}7)$$

where expressions for q and $\dot{\alpha}$ can be obtained from the state space model.

2.2.3 Autopilot Models

In the absence of any control input, most aircraft tend to exhibit a very lightly damped vertical oscillation, commonly called the phugoid mode, during which the aircraft slowly rises and sinks, exchanging kinetic and potential energy. They also have a second mode, the short period, which is much faster than the phugoid and is fairly well damped. This mode typically involves changes in pitch angle and angle of attack with minimal change in speed or altitude.

The primary role of an altitude hold autopilot is to add damping to the phugoid mode and shorten its period so that the aircraft will track its assigned altitude better. The autopilot is normally designed to control the aircraft's height by using the elevator to adjust the aircraft's pitch angle. Typically, the autopilot will also be designed to shorten the period and increase the damping of the short period mode so that the aircraft will follow the autopilot's pitch commands more accurately.

The control laws of the autopilots for each aircraft[8,11], which are depicted in block-diagram form in Figures 2-4 - 2-7 for each aircraft, are relatively similar to each other in form. Each has an inner feedback loop which uses measurements of pitch angle, θ, and pitch rate, q, to control the aircraft's pitch angle. (The Citation III autopilot uses a high pass filtering of the pitch angle instead of a measured pitch rate). An altitude tracking outer feedback loop uses measurements of the aircraft's altitude error, h_e, which is determined by an (ideal) altimetry system that in essence compares the aircraft's height to the height of the assigned pressure surface, and vertical velocity, $\dot{h}$, to generate a pitch angle command for the inner loop. The outer loops in the L-1011 and Citation III autopilots also use vertical acceleration information. Values for the gains and time constants indicated in the block diagrams of the three transport aircraft's autopilots are included in Appendix C. The block diagrams can be transformed directly into state space descriptions[7].

The model of the closed-loop aircraft-autopilot system is formed by combining the aircraft and autopilot models. The state variables of the aircraft model provide the input data for the autopilot (θ, q, h, $\dot{h}$, $\ddot{h}$). The output of the autopilot is a commanded elevator deflection which serves as the input to the aircraft model.

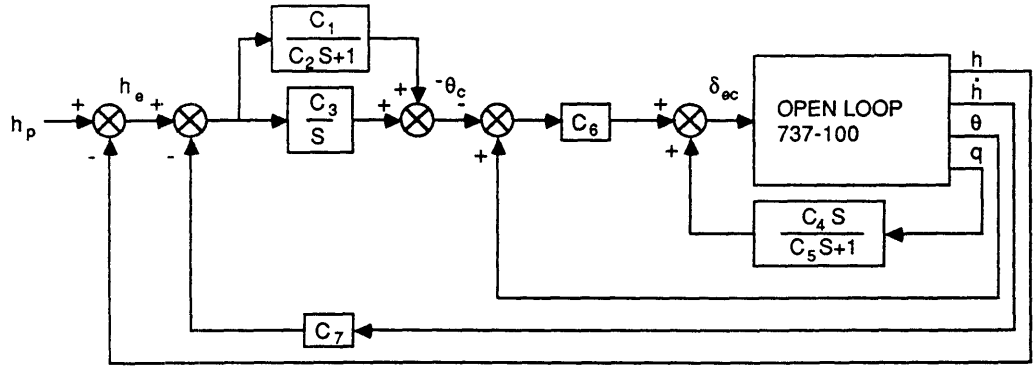

Figure 2-4 Block diagram of autopilot for Boeing 737-100.

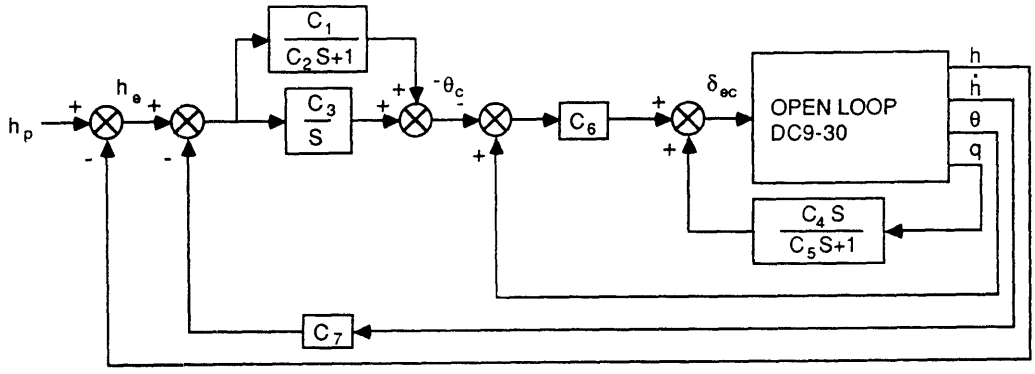

Figure 2-5 Block diagram of autopilot for McDonald Douglas DC9-30.

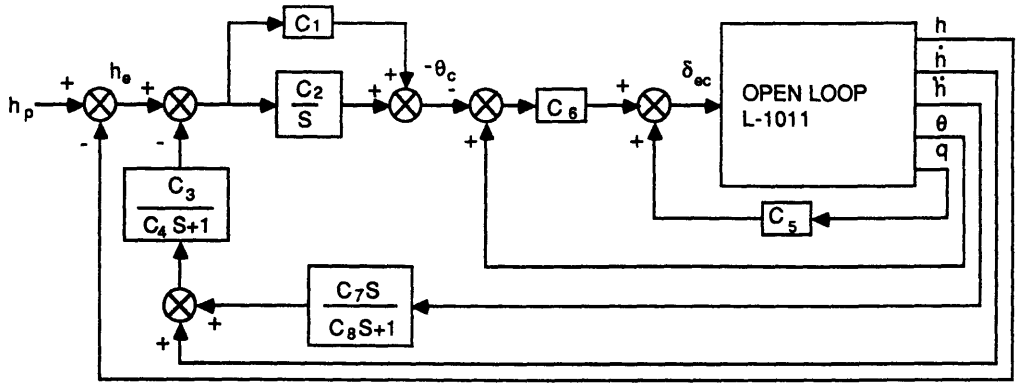

Figure 2-6 Block diagram of autopilot for Lockheed L-1011.

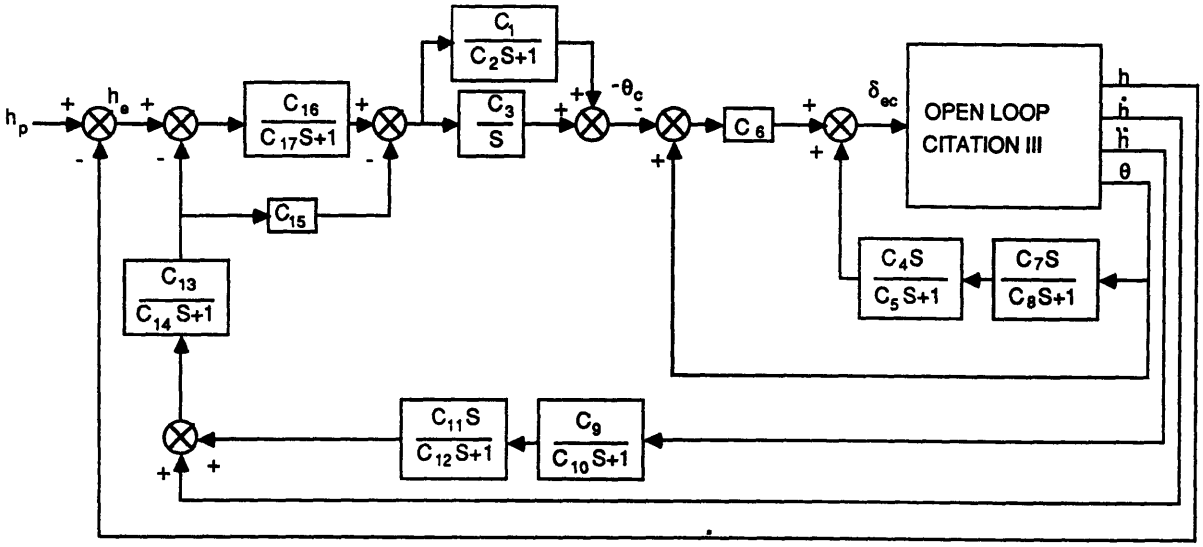

Figure 2-7 Block diagram of autopilot for Cessna Citation III.

2.2.4 Coupling of Disturbances into Aircraft-Autopilot Dynamics

The generation of the input coefficient matrix, $\underline{B}$, which models how fluctuations in the height of the assigned pressure surface, h_p, enter into the aircraft-autopilot dynamics is straightforward. As was indicated in Figures 2-4 - 2-7, pressure surface fluctuations enter the system through the autopilot at the summing node, where the height of the pressure surface is compared to the aircraft's height. The values of the coefficients which couple pressure surface fluctuations into the system dynamics are equivalent to the negative of the coefficients which couple changes in the aircraft's height into the system dynamics.

The vertical and horizontal gusts, g_z and g_x, which influence the aircraft's apparent wind, must be treated according to whether the aircraft model was derived in body axes or stability axes. For aircraft models in stability axes, g_x acts parallel to the aircraft's steady state velocity vector and, thus, has the effect of decreasing the perturbation velocity, v. Its influence on the system dynamics can be modeled using the negatives of the coefficients associated with v. The primary effect of g_z is to change the direction of the apparent wind. This results in a change in the aircraft's angle of attack due to the gust:

$$\alpha_g = -g_z/V \qquad (2\text{-}8)$$

where the minus sign reflects the fact that a downdraft

decreases the angle of attack. When this expression is linearized, the aircraft's velocity, V, is replaced by the steady state velocity, V_o. The effect of g_z on the system dynamics can be modeled using the coefficients associated with α divided by $-V_o$ and correcting for the fact that g_z does not influence $\dot{h}$ directly since it alters the aircraft's apparent wind but not the aircraft's inertial velocity.

For aircraft models derived in body axes, the gusts are incorporated by finding their components along the x_b and z_b axes and noting that the effect of the gusts is equivalent to the effect of perturbing u_b and w_b, except that the gusts have no direct effect on $\dot{h}$. The resulting equations for the change in the velocity components due to gusts are, after linearizing the projection equations:

$$u_g = \mathrm{Sin}(\Theta_o)g_z - \mathrm{Cos}(\Theta_o)g_x \qquad (2\text{-}9)$$

$$w_g = -\mathrm{Cos}(\Theta_o)g_z - \mathrm{Sin}(\Theta_o)g_x \qquad (2\text{-}10)$$

Using these relations, the coefficients from the state space aircraft models can then be used to investigate how each disturbance affects the rate of change of u_b, w_b, q, and θ.

2.3 Analysis Techniques

Two basic techniques were used to analyze the models of the aircraft-autopilot dynamics: time domain simulation and frequency response evaluation. Simulation was used primarily to investigate the response of the system to a step change in one of the atmospheric variables. Bode plots were used as the primary frequency domain technique to evaluate the aircraft-autopilot system's response to sinusoidal disturbances.

2.3.1 Step Responses

A system's step response is evaluated by using the system's model to perform a time-step simulation to investigate how the system responds when an input or a disturbance changes abruptly from one constant value (typically zero) to a new constant value (typically one for determining the 'unit step response' which effectively normalizes the output amplitude by the input amplitude). Two step response examples are shown in Figures 2-8 and 2-9. Figure 2-8 shows the response of an aircraft's height to a step change in the height of the pressure surface. Figure 2-9 shows the altitude error resulting from the same pressure surface step. The step response demonstrates two properties of the system. First, it shows how long the system takes to react to a change in an input or disturbance. Second, it indicates how well damped the system is. If the system is well damped, the step response will show it going to an equilibrium with little or no overshoot. If the system is

lightly damped, however, multiple oscillations about the equilibrium point will be observed in the step response.

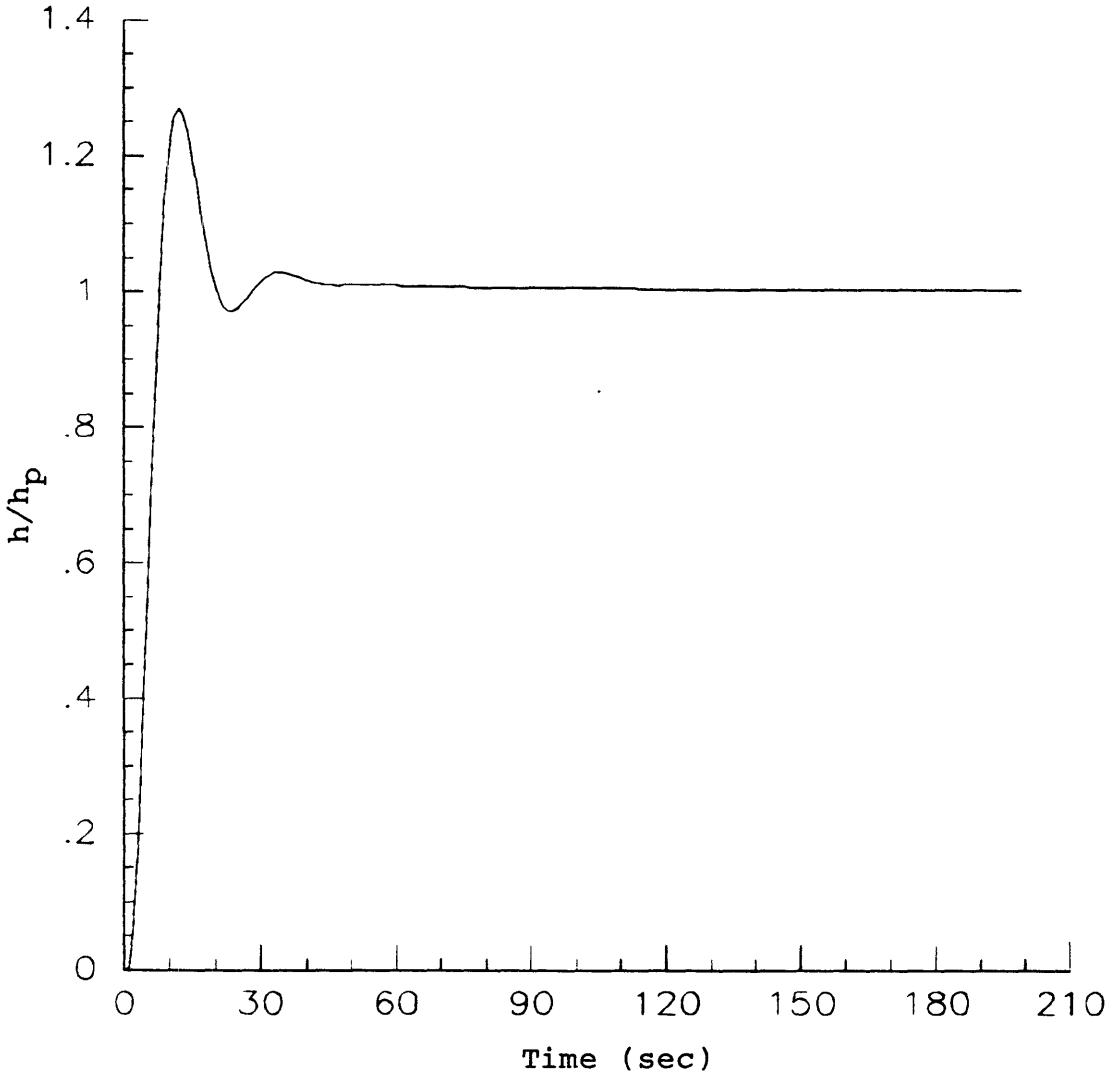

Figure 2-8 Typical response of aircraft height to step change in the height of the assigned pressure surface.

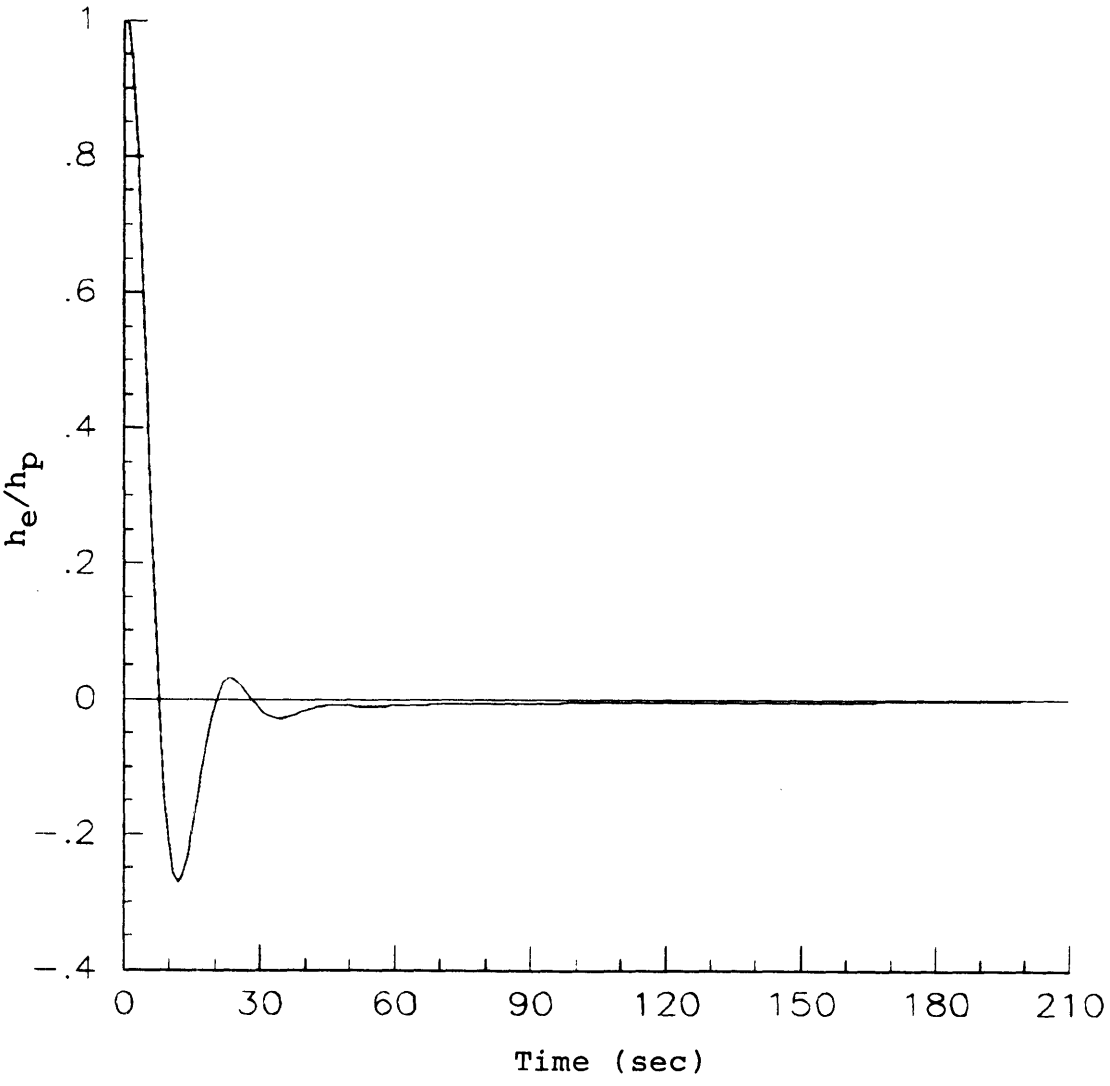

Figure 2-9 Typical response of aircraft altitude error to step change in the height of the assigned pressure surface.

Note that in the unit step response, the normalized altitude error resulting from changes in the height of the pressure surface is nondimensional since h_e and h_p are measured in the same units. The normalized altitude error resulting from gusts, however, will have units of seconds because h_e (which has units of distance) is normalized by g_z or g_x (which have units of distance per second)

2.3.2 Bode Plots

The effects of each atmospheric disturbance on the aircraft's altitude tracking accuracy were evaluated in the frequency domain by using the closed-loop models to generate Bode plots[7]. A property of linear systems (and linearized models) is that when they are excited by a sinusoidal input or disturbance of a given frequency, the output will be a sinusoid of the same frequency but usually of a different amplitude and phase. As an example, typical patterns of aircraft height and altitude error response to sinusoidal pressure surface fluctuations are shown in Figures 2-10, 2-11, and 2-12 for the model of a Boeing 737-100 at FL330. The three cases presented are examples of relatively low, moderate, and high frequency fluctuations. (Note that the frequency, f, of a disturbance can be converted to a wavelength measured along the flight path, λ, through the relation $\lambda = V/f$ where V is the aircraft's inertial velocity. V was typically between 780 and 800 ft/sec for the transport category aircraft and between 680 and 700 ft/sec for the Citation III). For each frequency, the first plot depicts

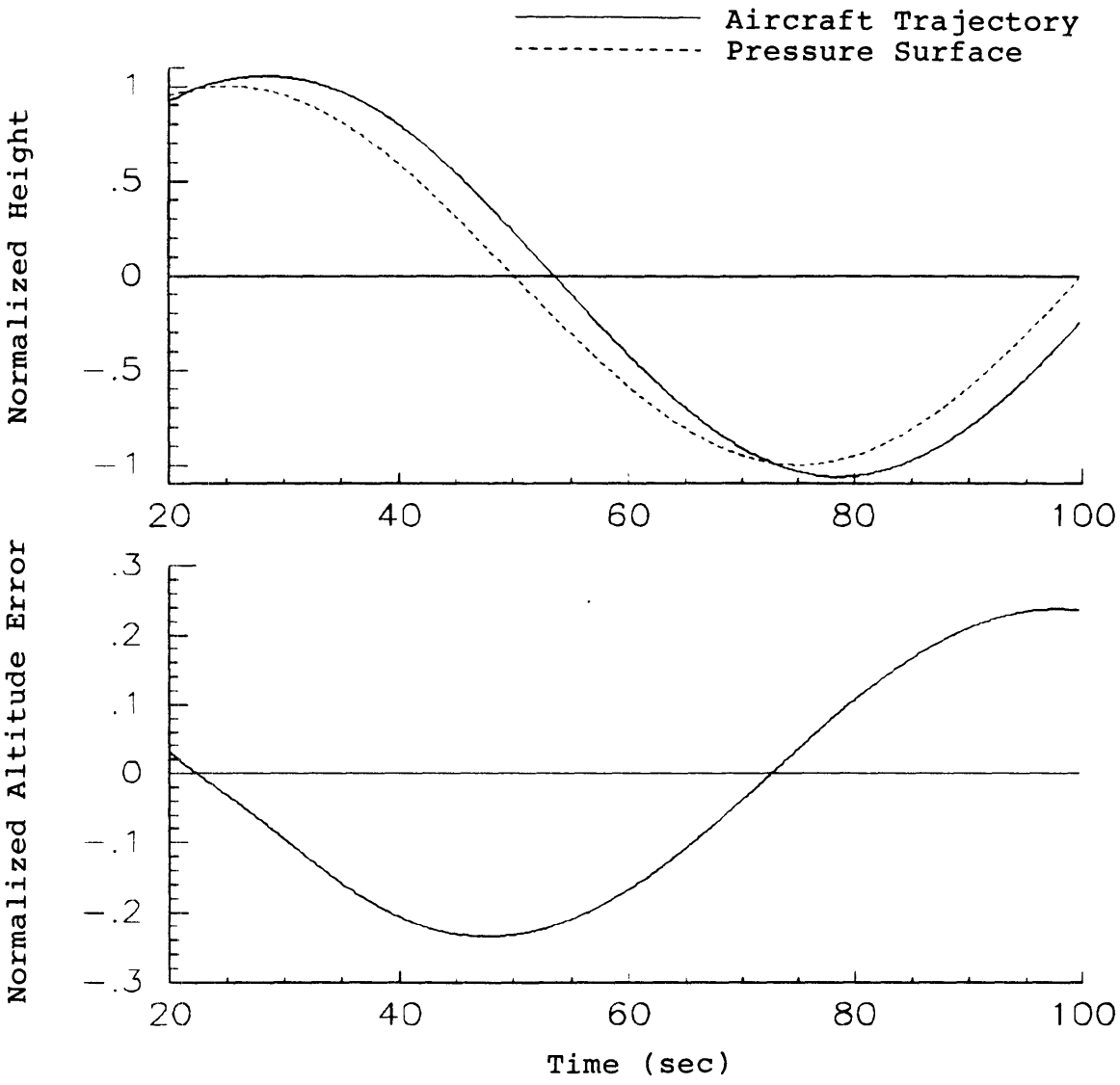

Figure 2-10 Typical aircraft-autopilot response to low-frequency pressure surface fluctuations.

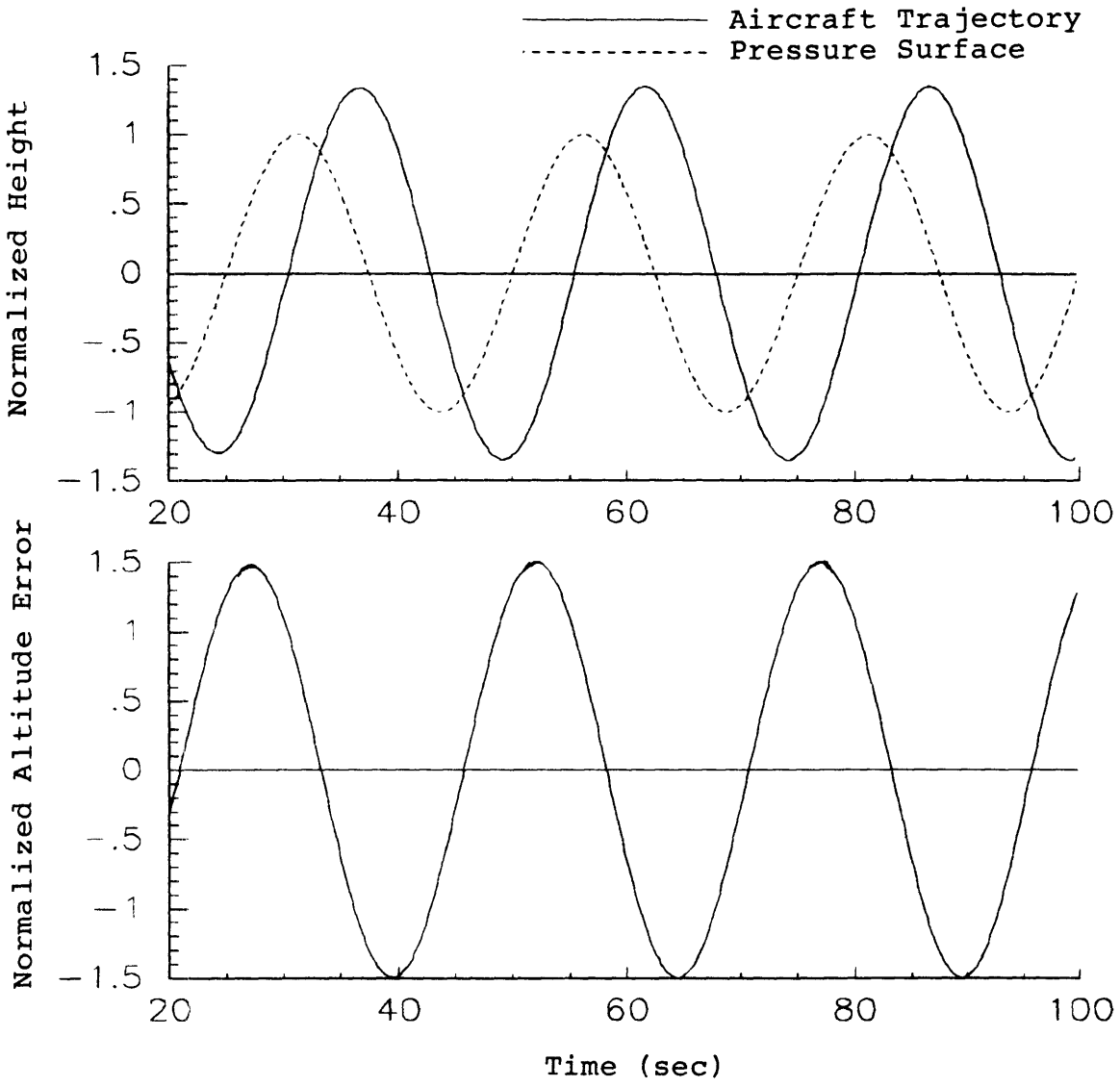

Figure 2-11 Typical aircraft-autopilot response to mid-frequency pressure surface fluctuations.

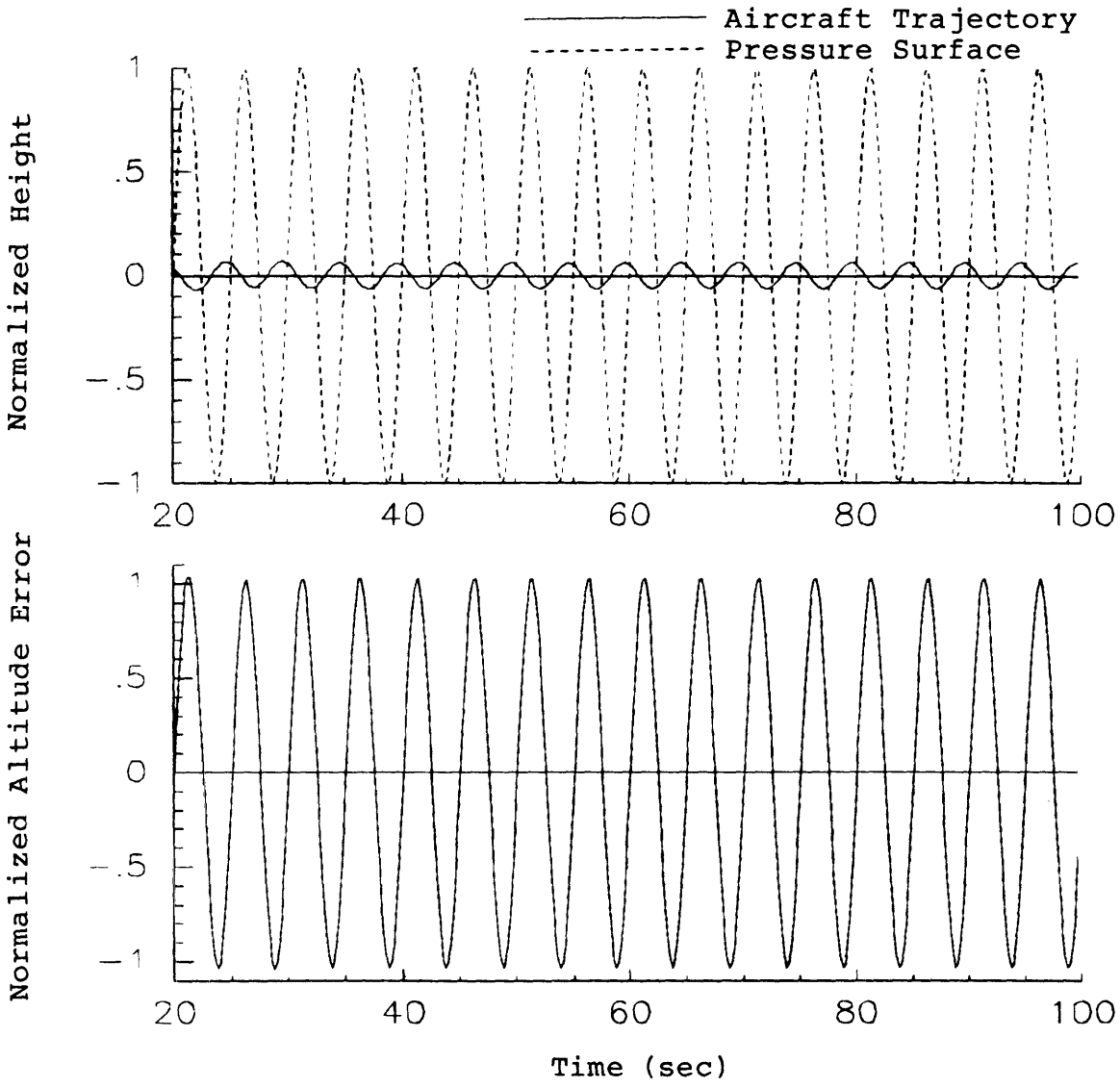

Figure 2-12 Typical aircraft-autopilot response to high-frequency pressure surface fluctuations.

the aircraft's trajectory and the desired pressure surface. The second plot indicates the time varying altitude tracking error. At low frequencies, the aircraft tracks the pressure surface fairly well, and the altitude error is relatively small. In the mid-frequency region, the aircraft tracks the pressure surface with a substantial phase lag and some overshoot, so the altitude error amplitude is larger than the pressure surface amplitude. At higher frequencies, the aircraft exhibits little vertical motion, so the altitude error is approximately equal to the pressure surface fluctuation. Note that both the amplitude of the altitude error and its phase shift relative to the pressure surface fluctuation vary with the frequency of the disturbance. The amplitude ratio and phase which relate a system's output to its input at a given frequency can be calculated directly using the state-space coefficient matrices.

The Bode plot, an example of which is given in Figure 2-13, presents the amplitude and phase information as a pair of graphs. The first graph, the Bode magnitude plot, charts the amplitude ratio, the ratio of the output amplitude to the input amplitude, as a function of frequency. The amplitude ratio is given in terms of decibels (1 dB = 20Log_{10}(amplitude ratio)), and the frequency is plotted on a logarithmic scale. The Bode magnitude plot can be thought of as indicating the output's sensitivity to sinusoidal inputs of various frequencies. Figure 2-13 shows the Bode plot relating altitude error to pressure surface fluctuations for the

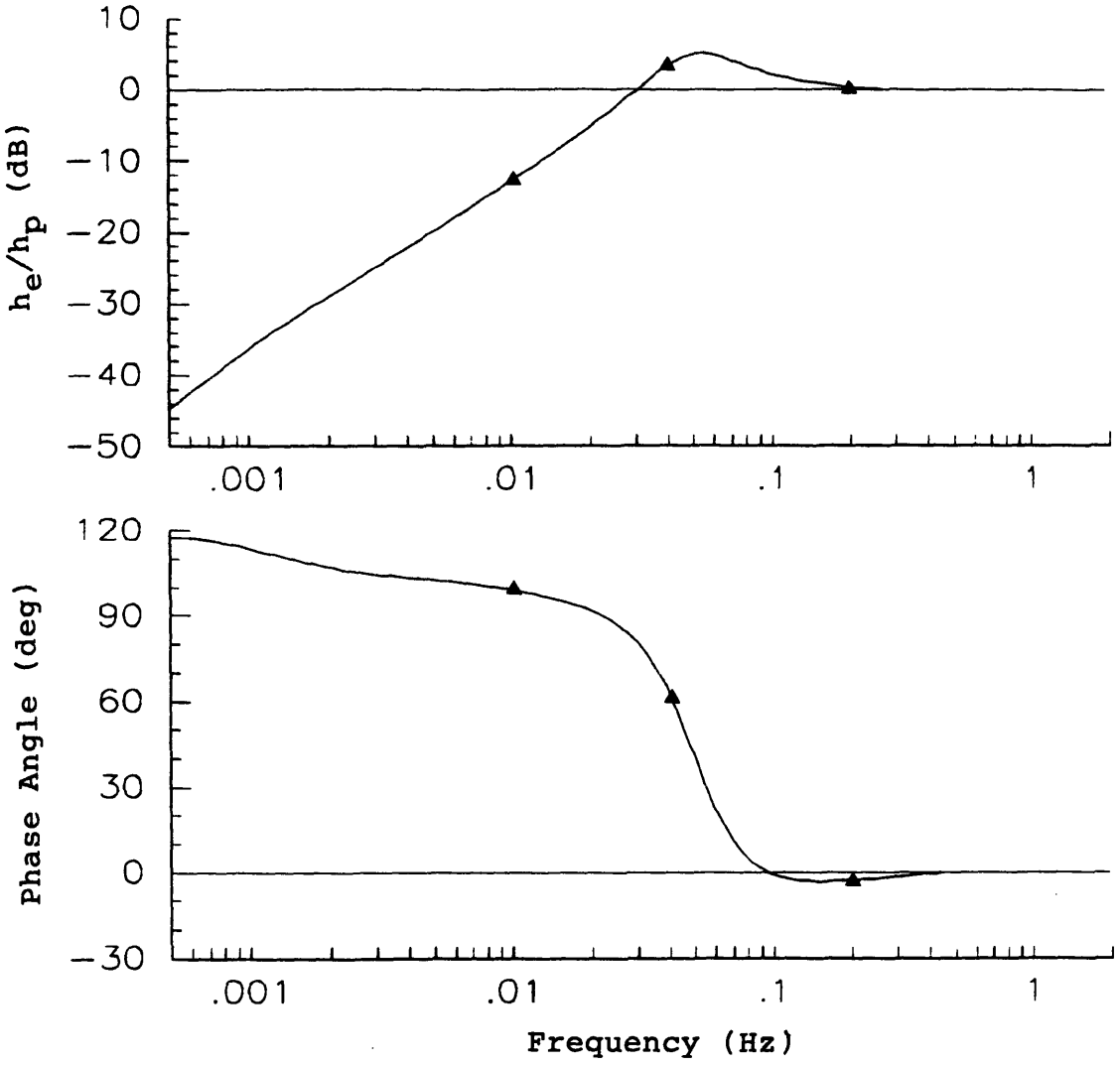

Figure 2-13 Typical altitude error sensitivity to pressure surface fluctuations.

aircraft-autopilot system used to generate the trajectories in Figures 2-10, 2-11, and 2-12. Note that the three points indicated on the two curves are at the frequencies used in the above trajectories. The low frequency example can be seen to have a negative magnitude in dB corresponding to an amplitude ratio of less than unity, which indicates that the altitude error amplitude is smaller than the pressure surface fluctuation amplitude and the system is relatively insensitive. The high frequency example has a magnitude of about zero dB corresponding to an amplitude ratio of unity, which indicates that the altitude error amplitude is equal to the pressure surface amplitude. The positive magnitude at mid-frequencies corresponds to an amplitude ratio greater than unity, which indicates that the altitude error amplitude exceeds the pressure surface amplitude.

Care must be used when looking at the Bode plots relating altitude errors to gust inputs. Since the amplitudes of the two quantities have intrinsically different units, the amplitude ratio is not nondimensional. In this analysis, consistent units were used to measure distance for altitude errors and gust velocities, and seconds were used as the time unit for the velocity. The amplitude ratio, therefore, is expressed in seconds, and the notation dB(sec) will be used to indicate when the amplitude ratio has units of seconds.

The second graph in a Bode plot charts the relative phase angle between the output sinusoid and the input

sinusoid as a function of frequency (again, on a logarithmic scale). When the phase angle is negative, the output is said to lag behind the input. When the phase angle is positive, the output is said to lead the input. The phase angle can be used to determine whether the altitude tracking errors of two aircraft will tend to decrease, increase, or have little effect on the aircraft's vertical separation as they pass one above the other. If two aircraft tend to be flying both above or both below their respective assigned altitudes at any given time, their tracking errors will have little effect on their vertical separation. If, on the other hand, one aircraft is above its assigned altitude while the other is below its assigned altitude or vice versa, their tracking errors will tend to either decrease or increase their vertical separation. The second situation, which is the more serious of the two, occurs for specific combinations of the two aircraft's altitude error phase angle. If the two aircraft are flying in the same direction, their vertical separation will be decreased or increased by as much as their combined altitude error if their phase angles differ by an odd multiple of 180^{o}. If the two are flying in opposite directions, the maximum potential reduction in vertical separation will occur if the sum of their phase angles is an odd multiple of 180^{o}.

Chapter 3

RESULTS

3.1 Overview

This chapter presents the results of the analysis which was performed using the methodology described in Chapter 2. Section 3.2 discusses the basic dynamics of the aircraft themselves so that differences in the behavior of each airframe can be noted. Sections 3.3, 3.4, and 3.5 present the effects of pressure surface fluctuations, vertical gusts and horizontal gusts on the ability of the aircraft-autopilot systems to track their assigned pressure altitudes. Within each section, the effect of step changes in the disturbance are evaluated first for each aircraft. Then, the frequency response is analyzed using Bode plots.

3.2 Open Loop Aircraft Behavior

The open-loop behavior (autopilot disengaged) of all four aircraft is similar in characteristic. Each exhibits a fairly well damped short period oscillatory mode in which the aircraft rotates but does not deviate significantly in altitude. Each also exhibits a lightly damped long period oscillatory mode, the phugoid mode, during which the aircraft slowly rises and sinks, exchanging kinetic and potential energy. The period and damping ratio of each aircraft's open loop phugoid mode at FL330 are given in Table 3-1. The

phugoid mode of the DC9 has the longest period and highest damping ratio. The L-1011 and Citation III have shorter periods and lower damping ratios. The 737 has the shortest phugoid period and lowest damping ratio.

Table 3-1 Open loop phugoid period and damping ratio at FL330.

Aircraft	Phugoid Period (sec)	Damping Ratio
737-100	63	0.034
DC9-30	105	0.21
L-1011	77	0.09
Citation III	75	0.12

3.3 Aircraft-Autopilot Response to Pressure Surface Fluctuations

The response of each aircraft-autopilot system's altitude error to a unit step in the height of the target pressure surface is shown at each altitude for each of the four aircraft in Figures 3-1 - 3-4. The response of each aircraft is quite similar. Each takes from eight to twelve seconds to reach the new height of the pressure surface, overshoots slightly, and then slowly settles. The response is reasonably fast, and the relatively small overshoots are indicative of fairly good damping. There is no significant variation in each aircraft's response from one altitude to another.

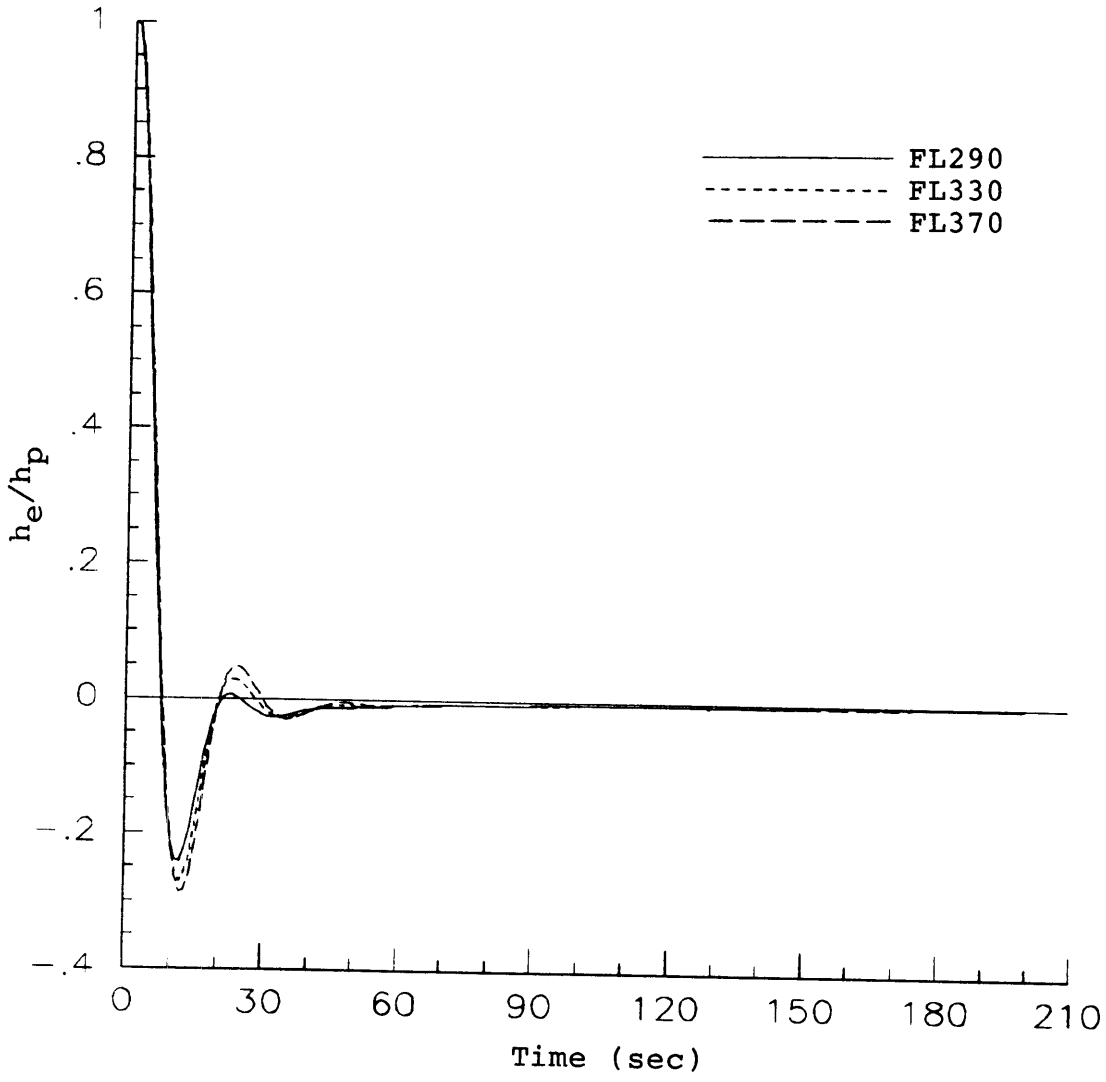

Figure 3-1 Altitude error resulting from step change in height of pressure surface for 737-100.

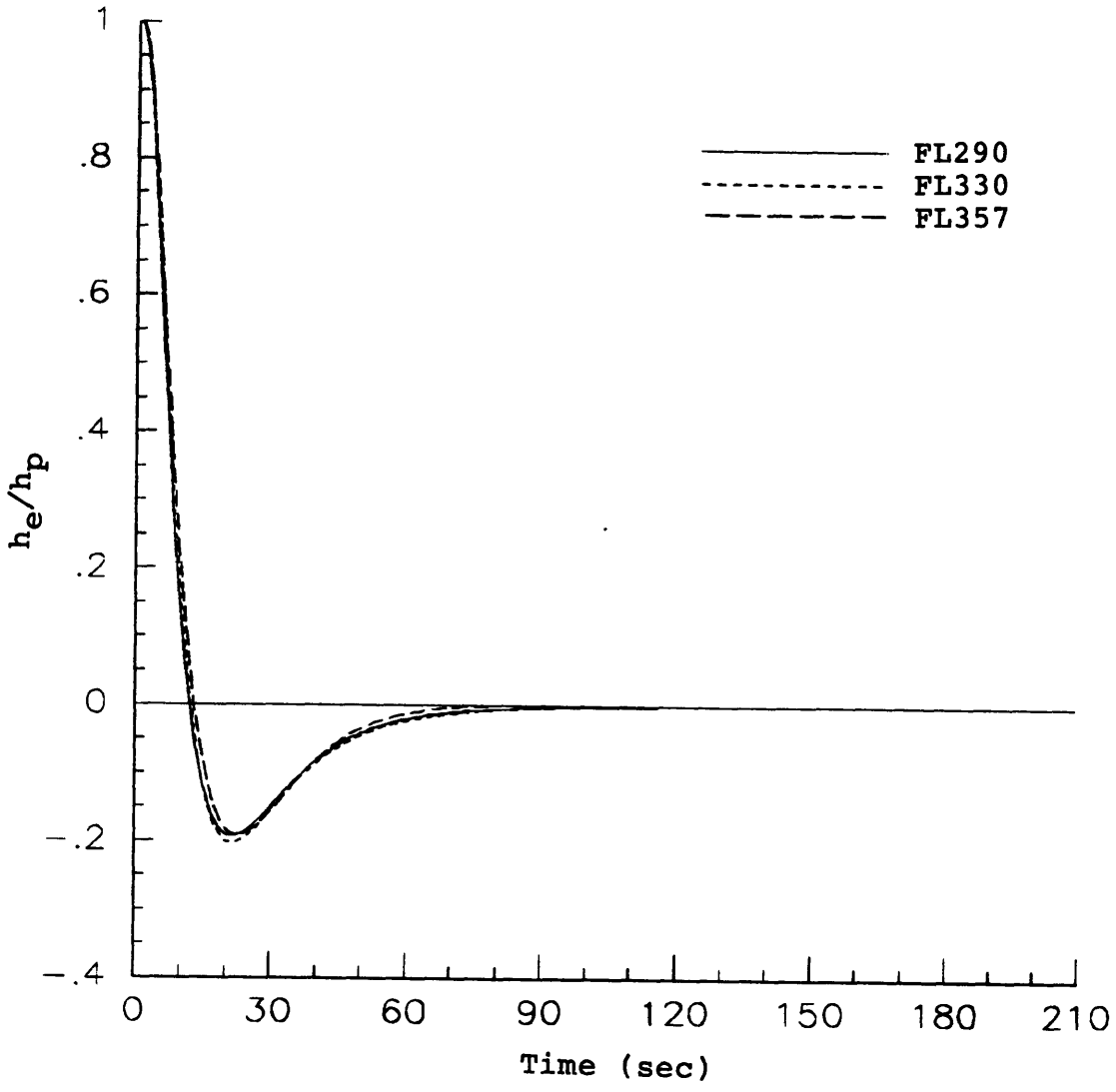

Figure 3-2 Altitude error resulting from step change in height of pressure surface for DC9-30.

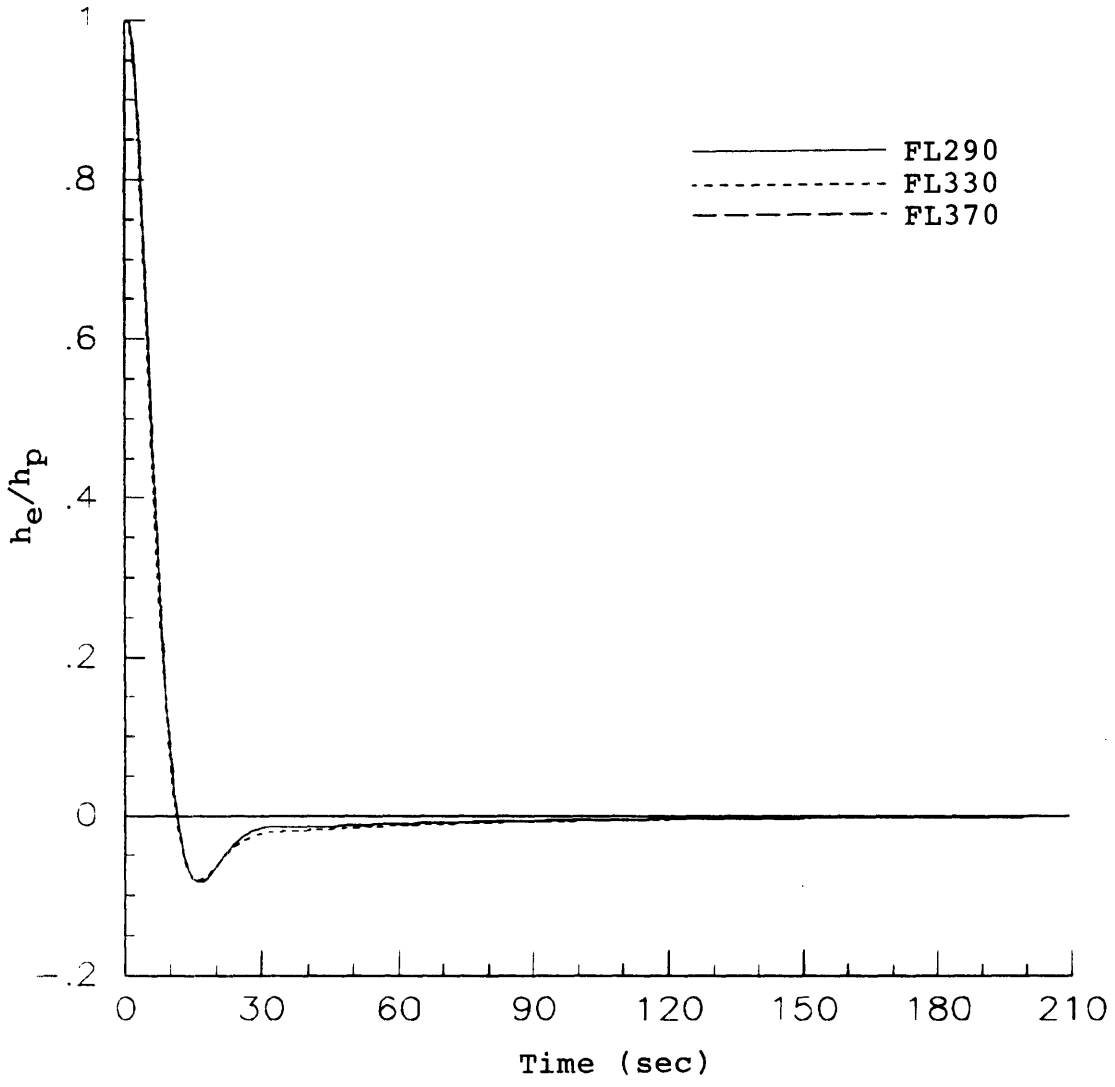

Figure 3-3 Altitude error resulting from step change in height of pressure surface for L-1011.

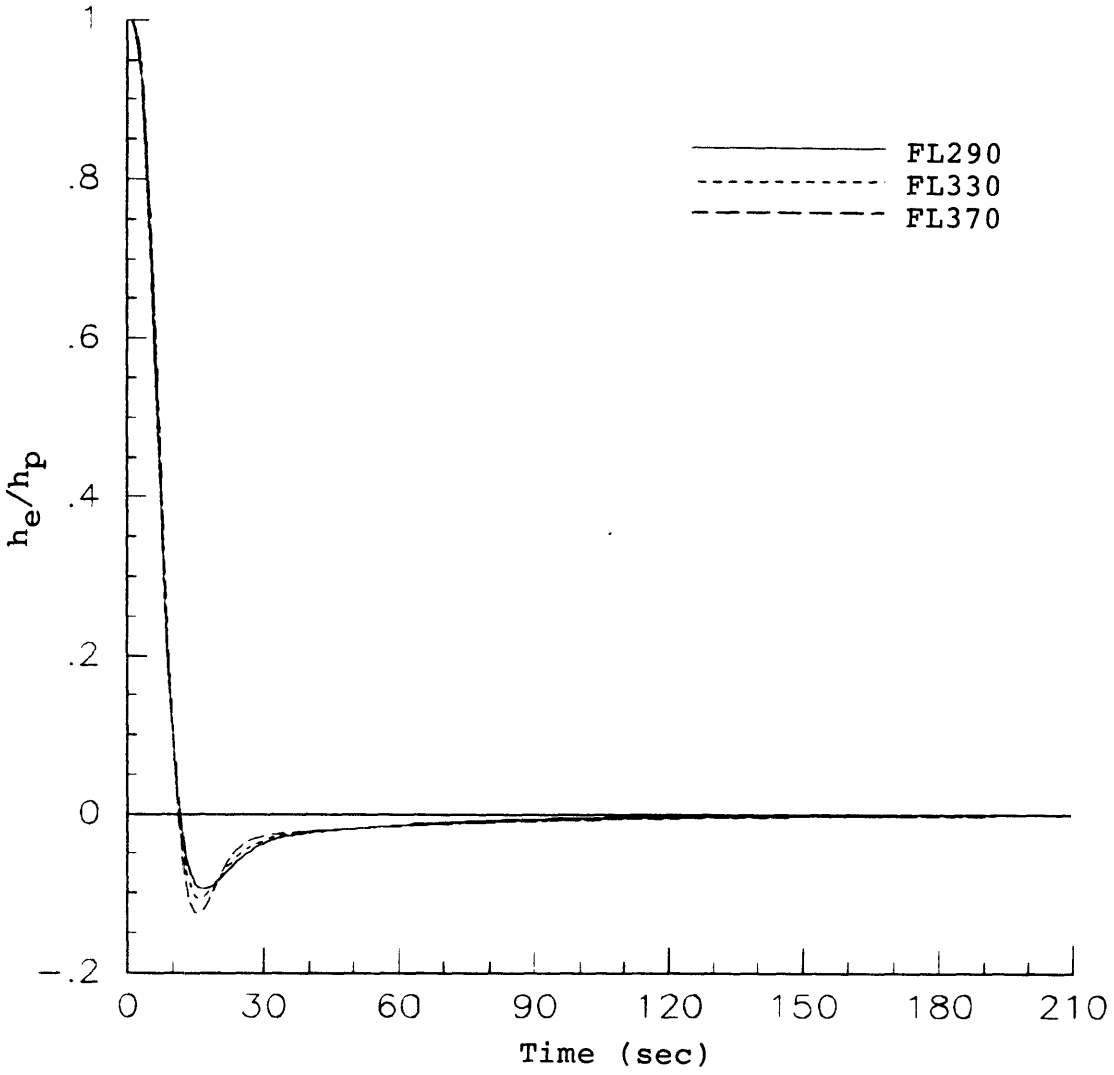

Figure 3-4 Altitude error resulting from step change in height of pressure surface for Citation III.

The response of each aircraft-autopilot system's altitude error to sinusoidal fluctuations in the height of the pressure surface at several altitudes is presented as Bode magnitude and phase plots in Figures 3-5 - 3-8. The closed-loop behavior of the four aircraft is quite similar despite the variations in their open loop phugoid periods and damping ratios mentioned in Section 3.2. This is most likely the result of similar design objectives for each autopilot. The results for each aircraft again show little variation with changes in altitude.

At low frequencies all of the autopilots are capable of keeping their aircraft at the proper altitude and the tracking error is much smaller than the pressure surface fluctuation as shown by the negative values in the Bode plot. This low frequency behavior is illustrated in Figure 3-9 for the 737-100 at FL330.

At high frequencies, the amplitude ratios approach unity (zero dB) because the aircraft-autopilot system cannot respond to these fast changes in the height of the pressure surface. As illustrated in Figure 3-10 for the 737 at FL330, the aircraft tends to ignore the high frequency disturbances and fly at a relatively constant level. The altitude error is, therefore, approximately equal in magnitude to the pressure surface fluctuation. The severity of the high frequency error is somewhat exaggerated because actual atmospheric pressure surface fluctuation amplitudes will tend to decrease considerably at these higher frequencies, since a

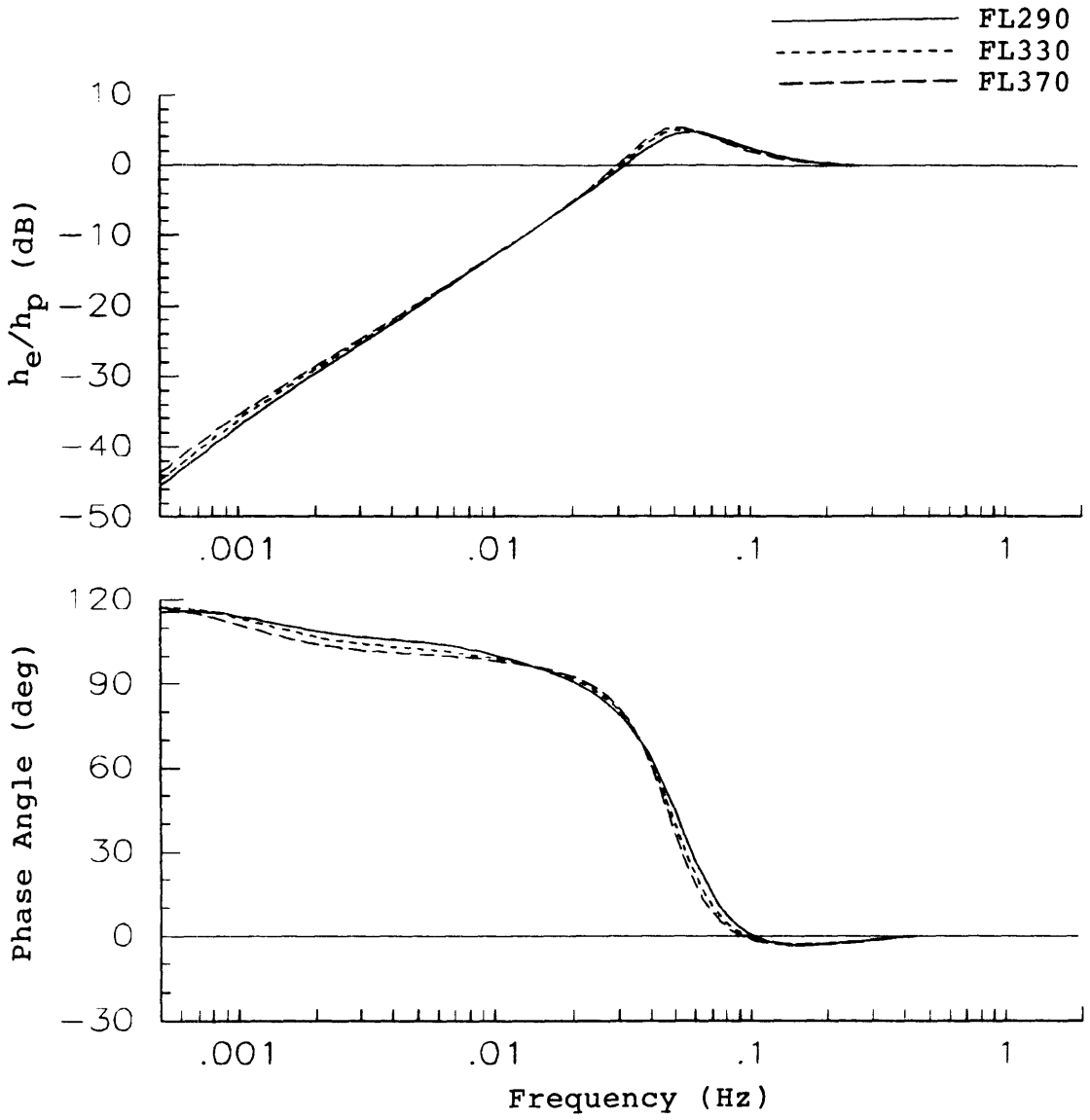

Figure 3-5 Altitude error sensitivity of 737-100 to pressure surface fluctuations.

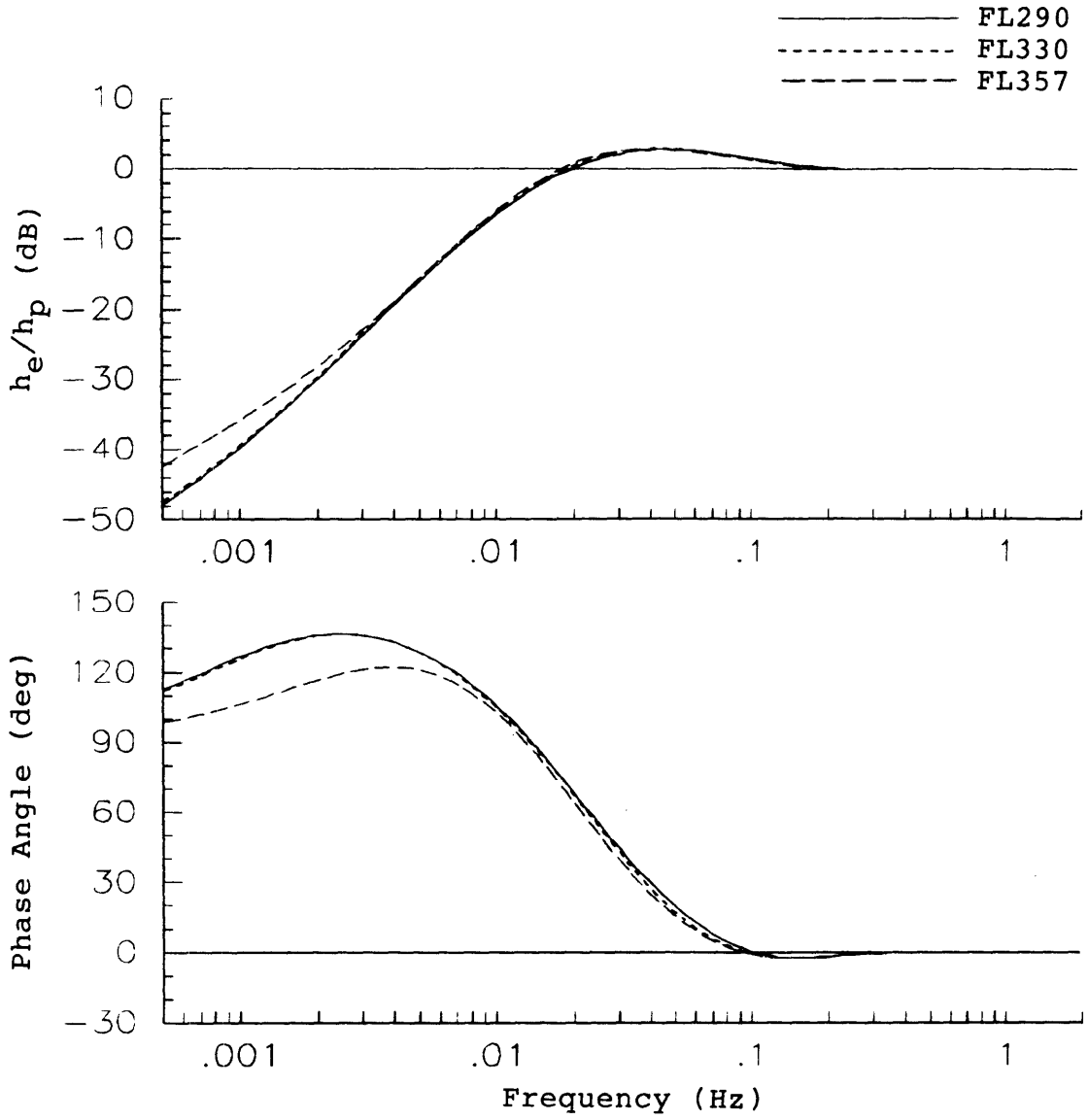

Figure 3-6 Altitude error sensitivity of DC9-30 to pressure surface fluctuations.

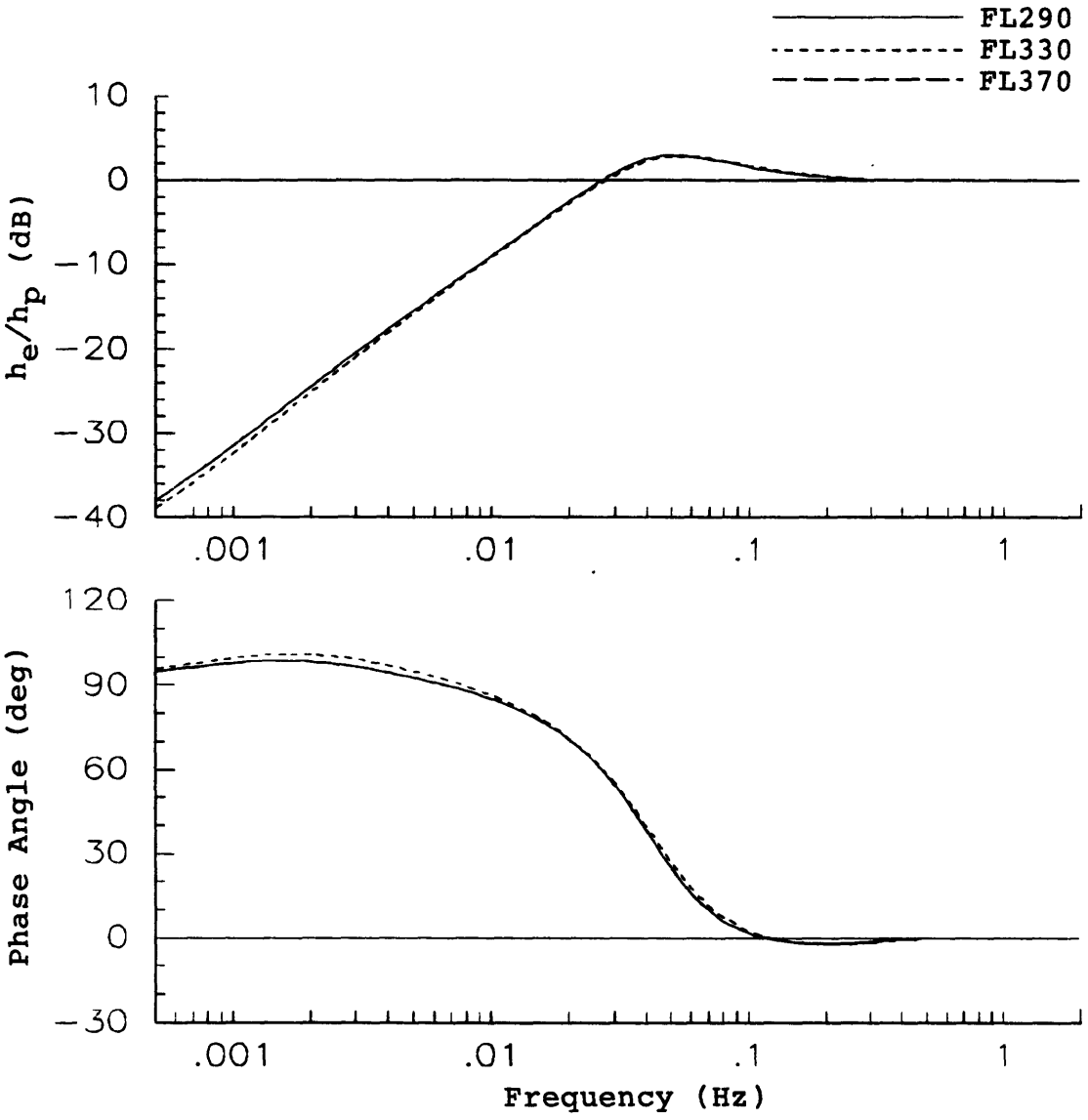

Figure 3-7 Altitude error sensitivity of L-1011 to pressure surface fluctuations.

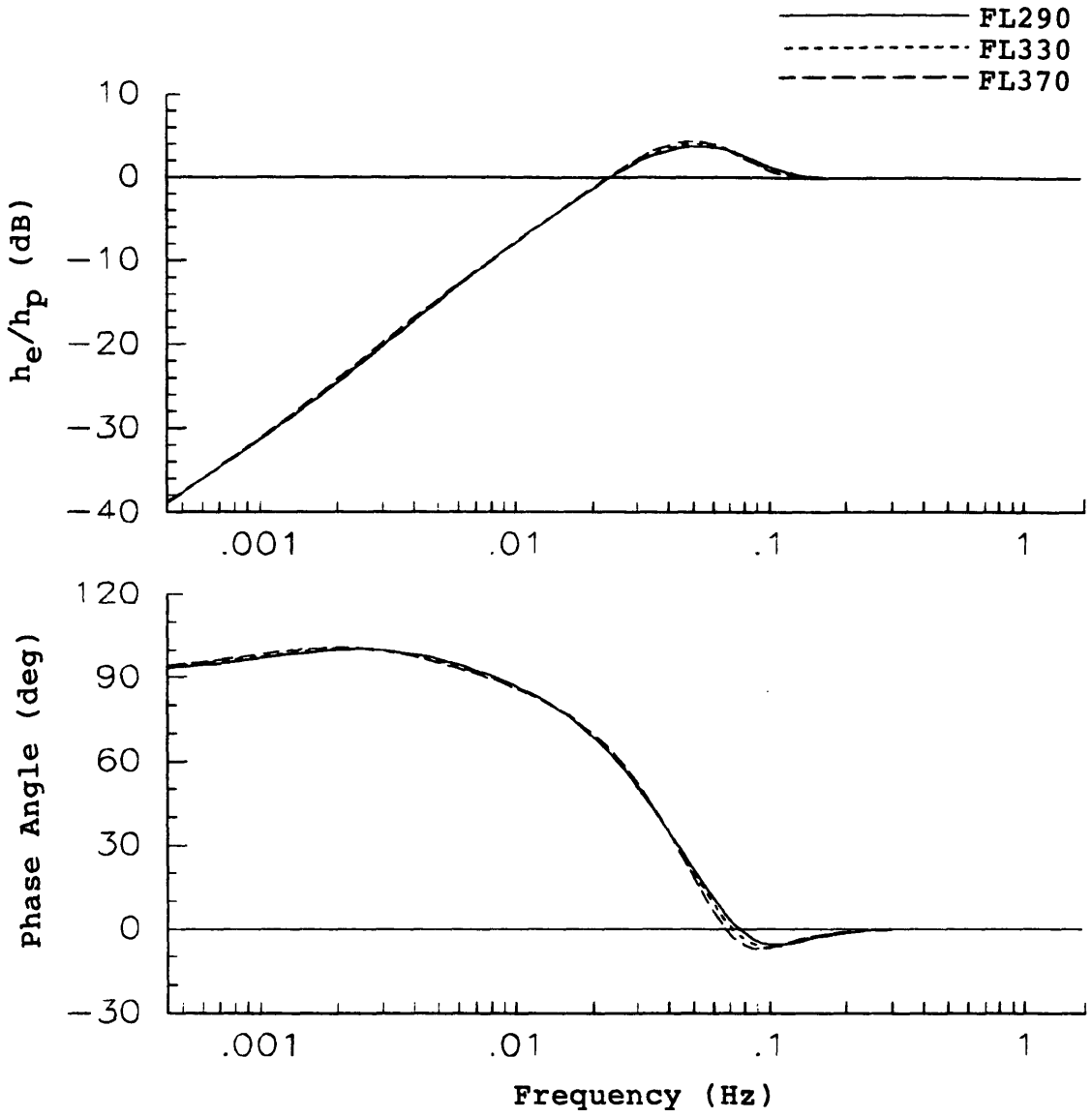

Figure 3-8 Altitude error sensitivity of Citation III to pressure surface fluctuations.

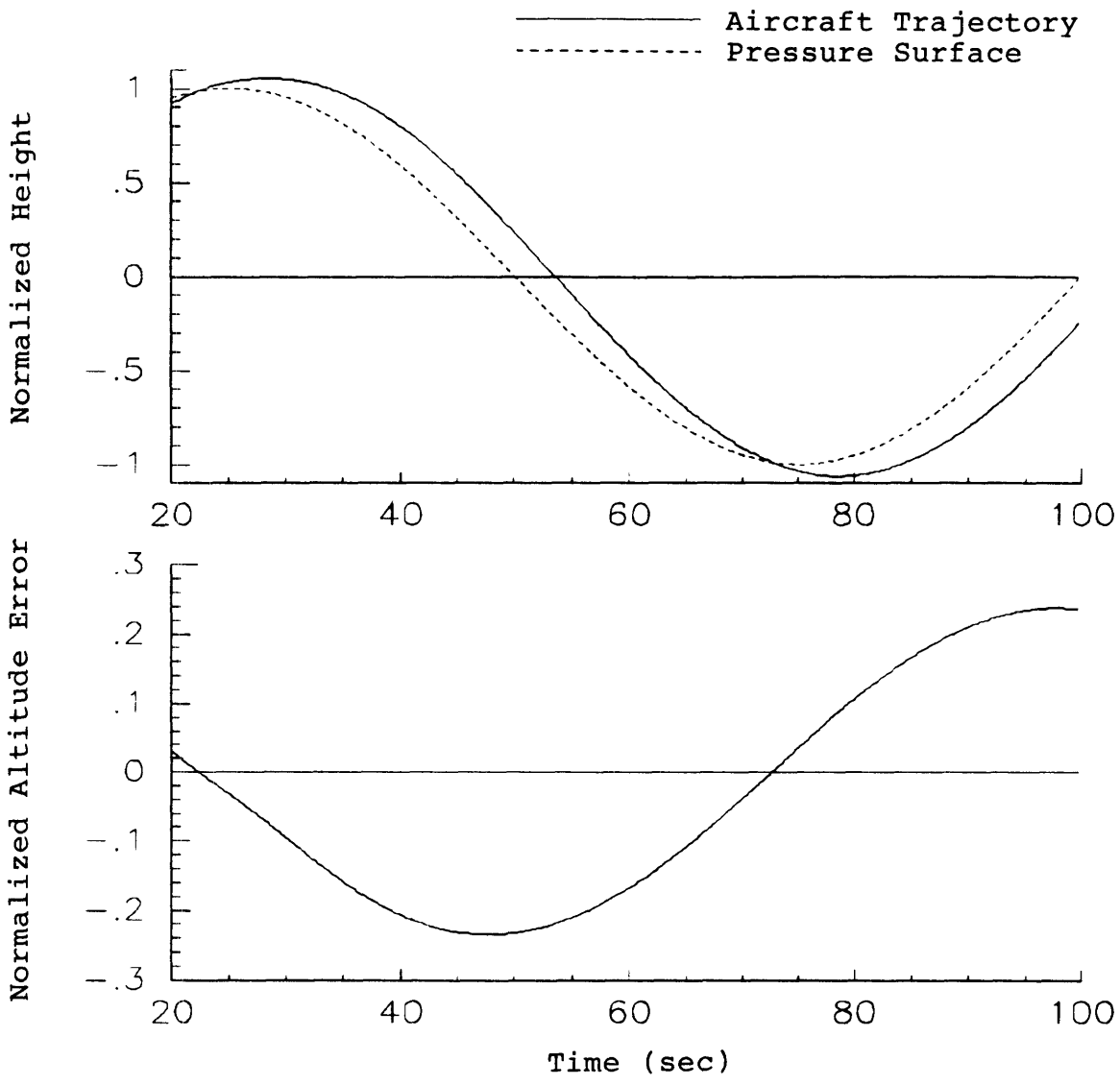

Figure 3-9 Response of 737 to low-frequency pressure surface fluctuations.

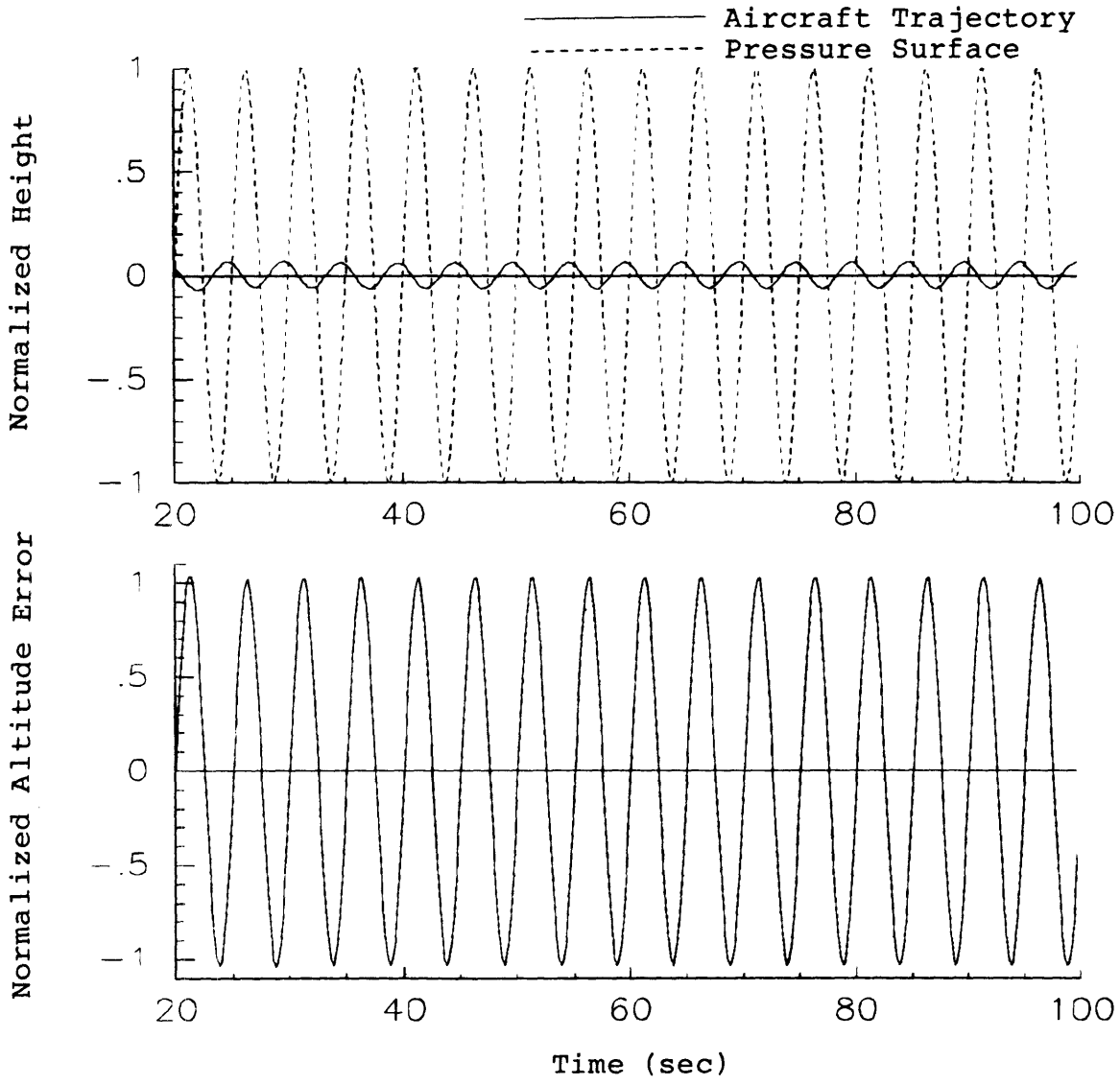

Figure 3-10 Response of 737 to high-frequency pressure surface fluctuations.

greater distortion of the pressure surface is required to produce large amplitudes at relatively short wavelengths.

In the mid-frequency region, each aircraft exhibits a peak in sensitivity to pressure surface fluctuations. This peak, which is most severe for the 737, is a result of the pressure surface fluctuation driving the closed-loop aircraft-autopilot system at resonance. As can be seen in Figure 3-11, which uses the 737 at FL330 as an example, the autopilot attempts to make the aircraft follow the pressure surface. The effective inertia of the aircraft and lags within the autopilot, however, cause the aircraft to lag behind the changing pressure surface so that, near the peak frequency, the aircraft is significantly out of phase with the pressure surface. The net result is that the amplitude of the altitude error actually exceeds the amplitude of the input disturbance in this region.

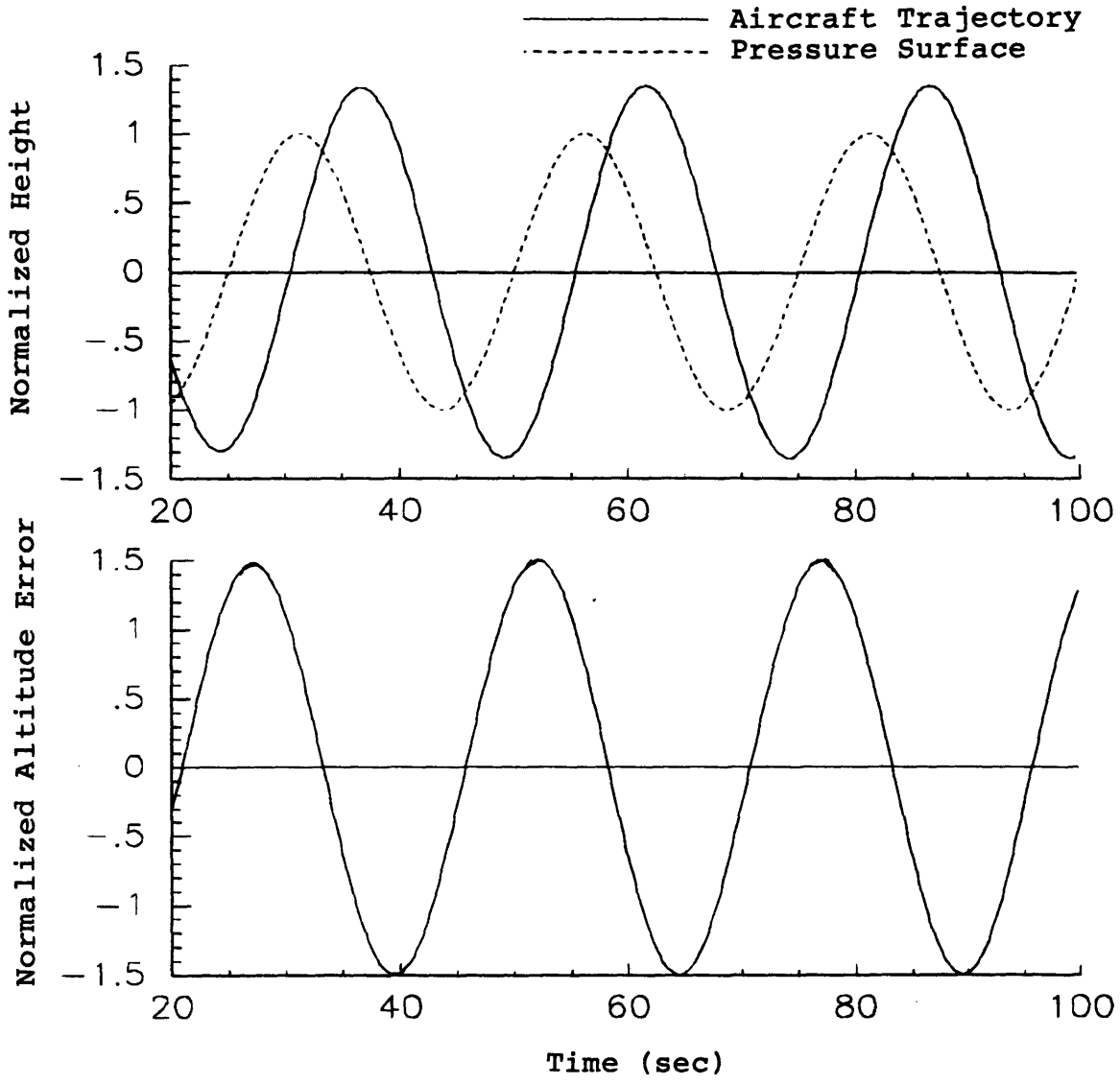

Figure 3-11 Response of 737 to mid-frequency pressure surface fluctuations.

3.4 Aircraft-Autopilot Response to Vertical Gusts

The normalized altitude error resulting from a step change in the vertical wind is shown at several altitudes for each aircraft in Figures 3-12 - 3-15. (Note units). All of the aircraft exhibit a fast partial recovery, but then take a much longer time to return to their assigned altitude completely. The Citation III exhibits a peak altitude error in response to vertical gust steps which is twice that of any of the transport aircraft. Each aircraft's response shows only a mild dependence on altitude.

The response of each aircraft-autopilot system's altitude error to sinusoidal vertical gusts at several altitudes is presented as Bode magnitude and phase plots in Figures 3-16 - 3-19. The shape of the curves on the Bode plots is similar for all four aircraft. The magnitude of the resonance peaks, however, differs greatly. While the results for each aircraft do vary some with changes in altitude, these changes are relatively small.

As was the case for pressure surface fluctuations, when the vertical gusts are oscillating at a low frequency, the aircraft are able to track the desired altitude fairly well. When the gusts occur at high frequencies, the inertia of the aircraft tends to limit the effect of the vertical gusts on the aircraft's altitude and the sensitivity is again small. In the mid-frequency range, however, there appears to be a fair amount of coupling between the vertical gusts and the dynamics of the closed-loop aircraft-autopilot system.

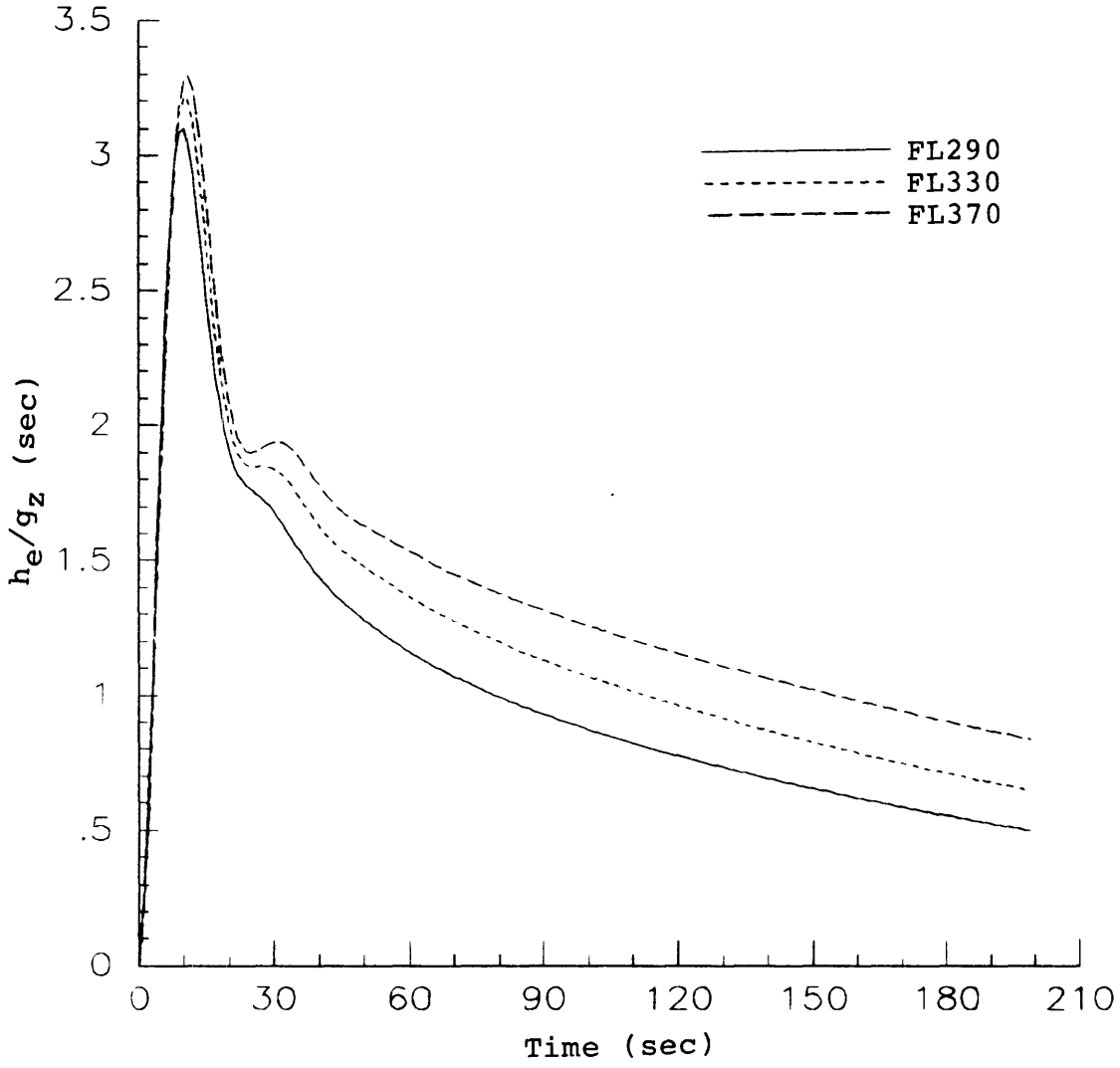

Figure 3-12 Altitude error resulting from step change in vertical gust velocity for 737-100.

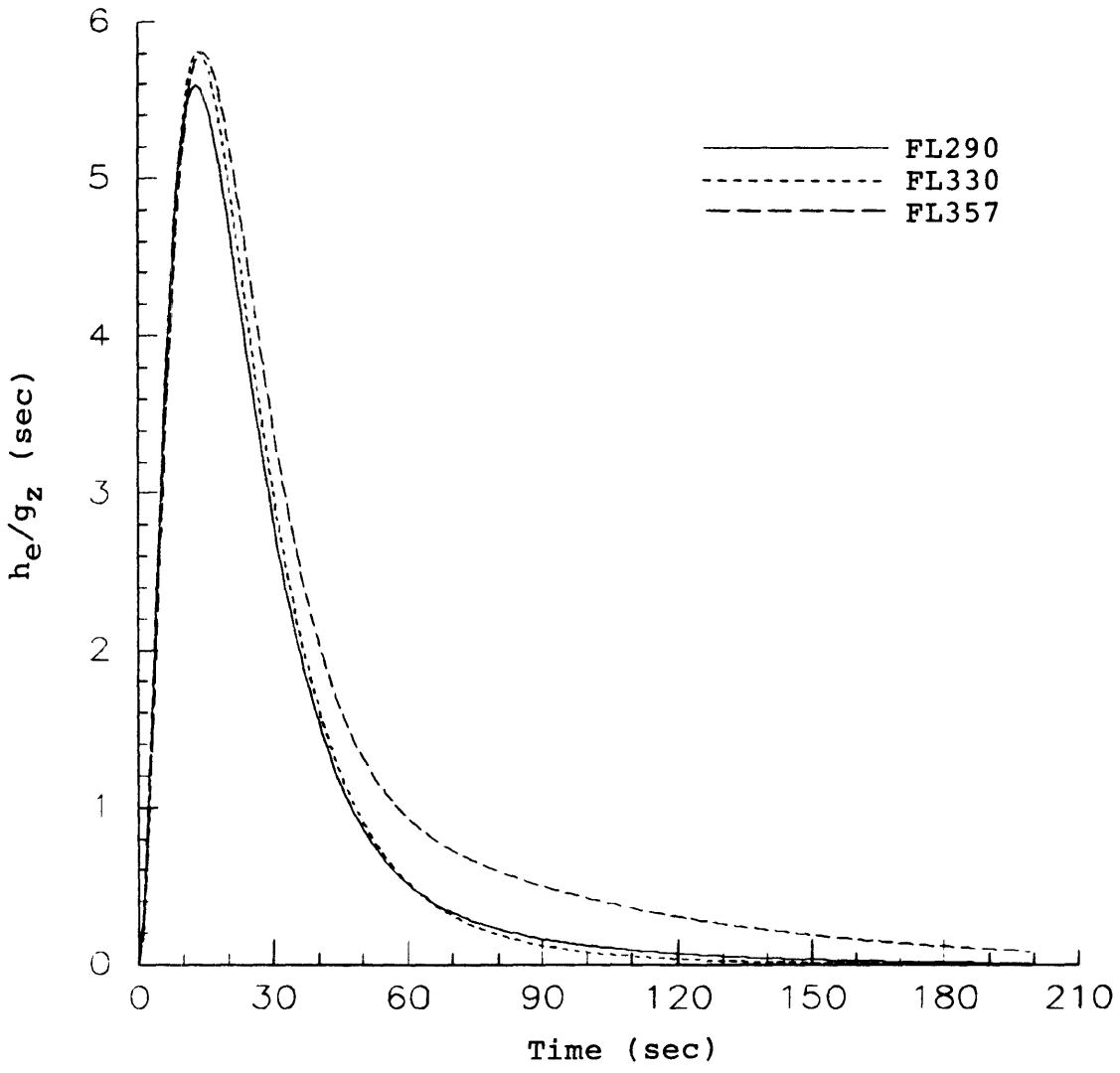

Figure 3-13 Altitude error resulting from step change in vertical gust velocity for DC9-30.

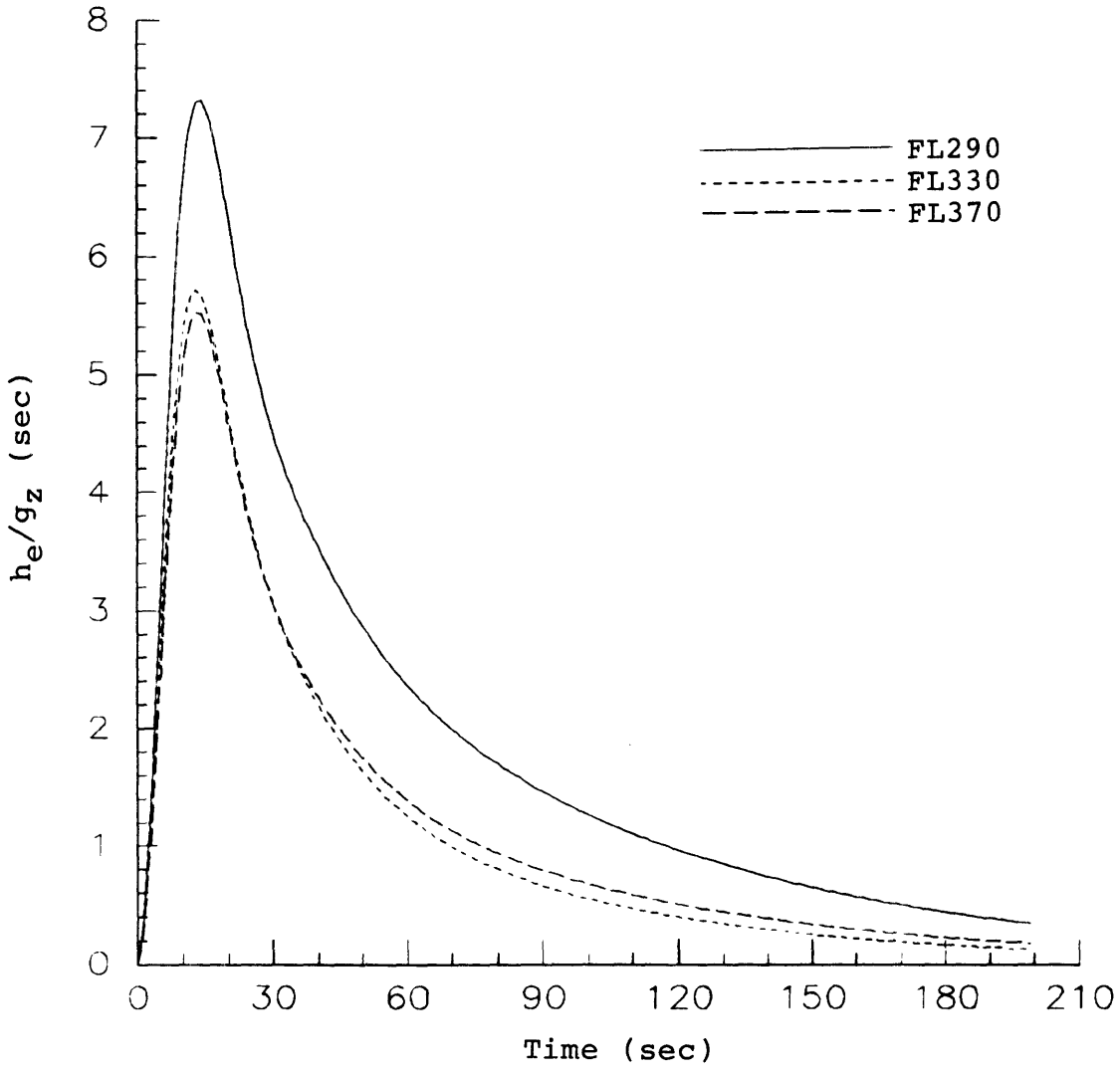

Figure 3-14 Altitude error resulting from step change in vertical gust velocity for L-1011.

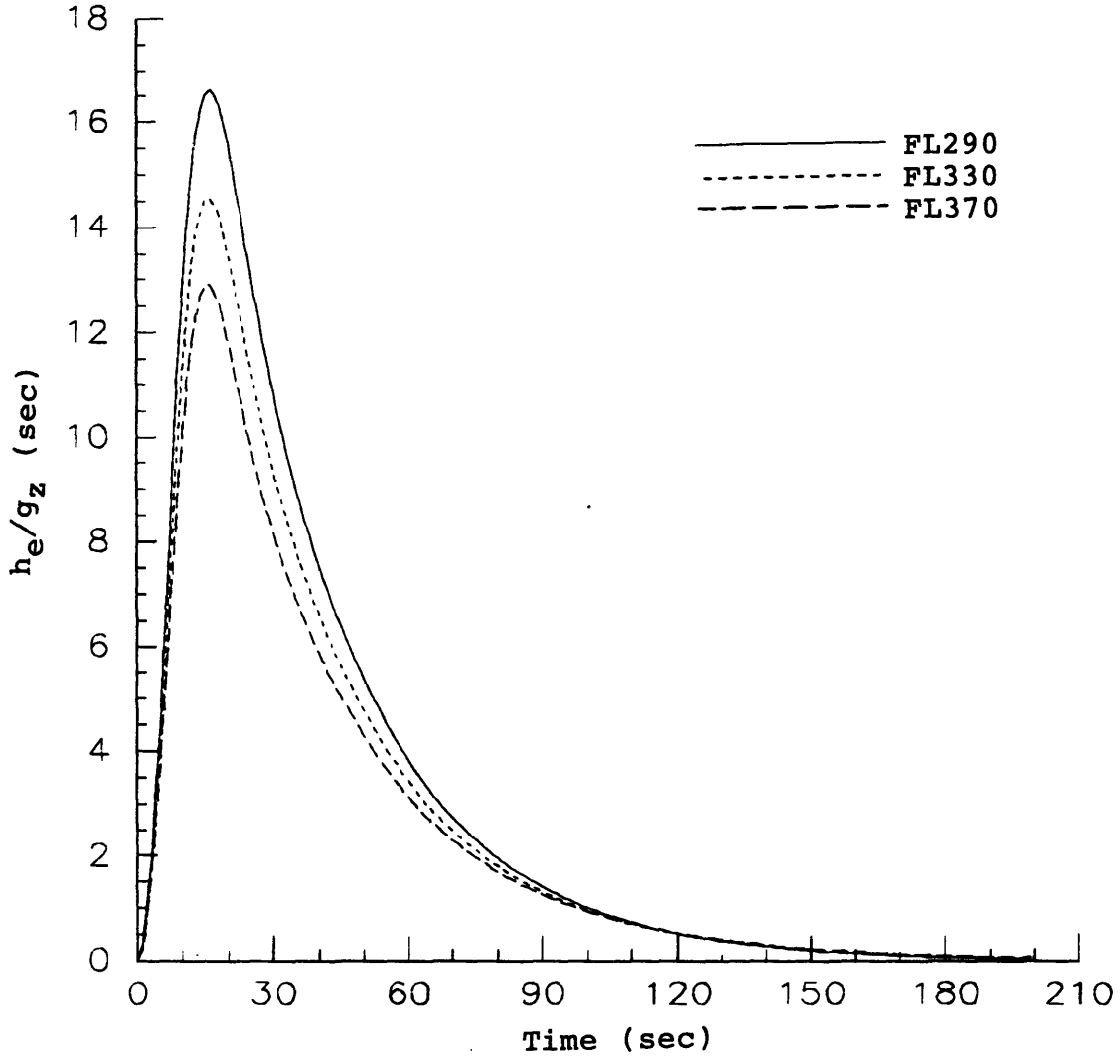

Figure 3-15 Altitude error resulting from step change in vertical gust velocity for Citation III.

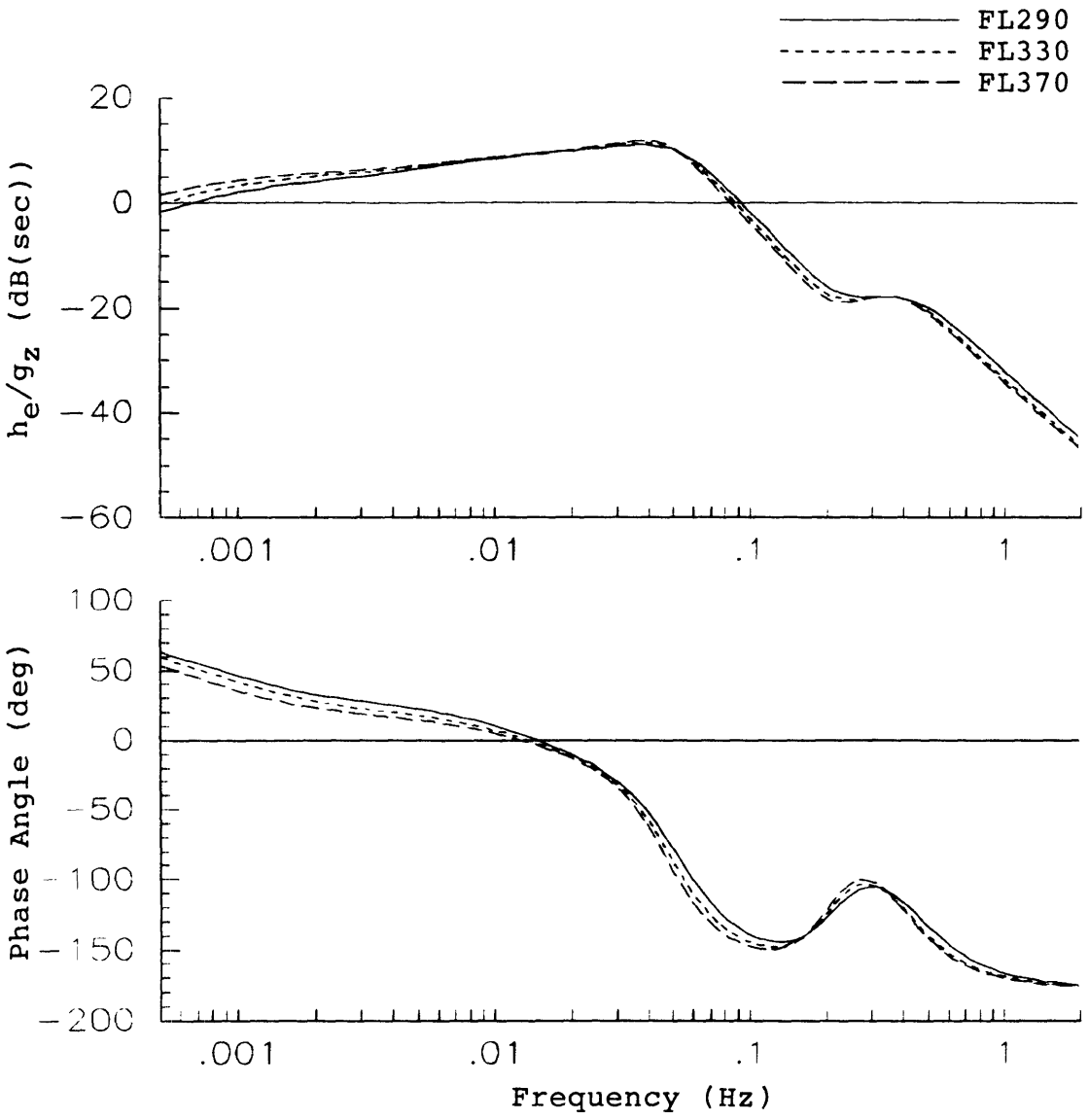

Figure 3-16 Altitude error sensitivity of 737-100 to vertical gusts.

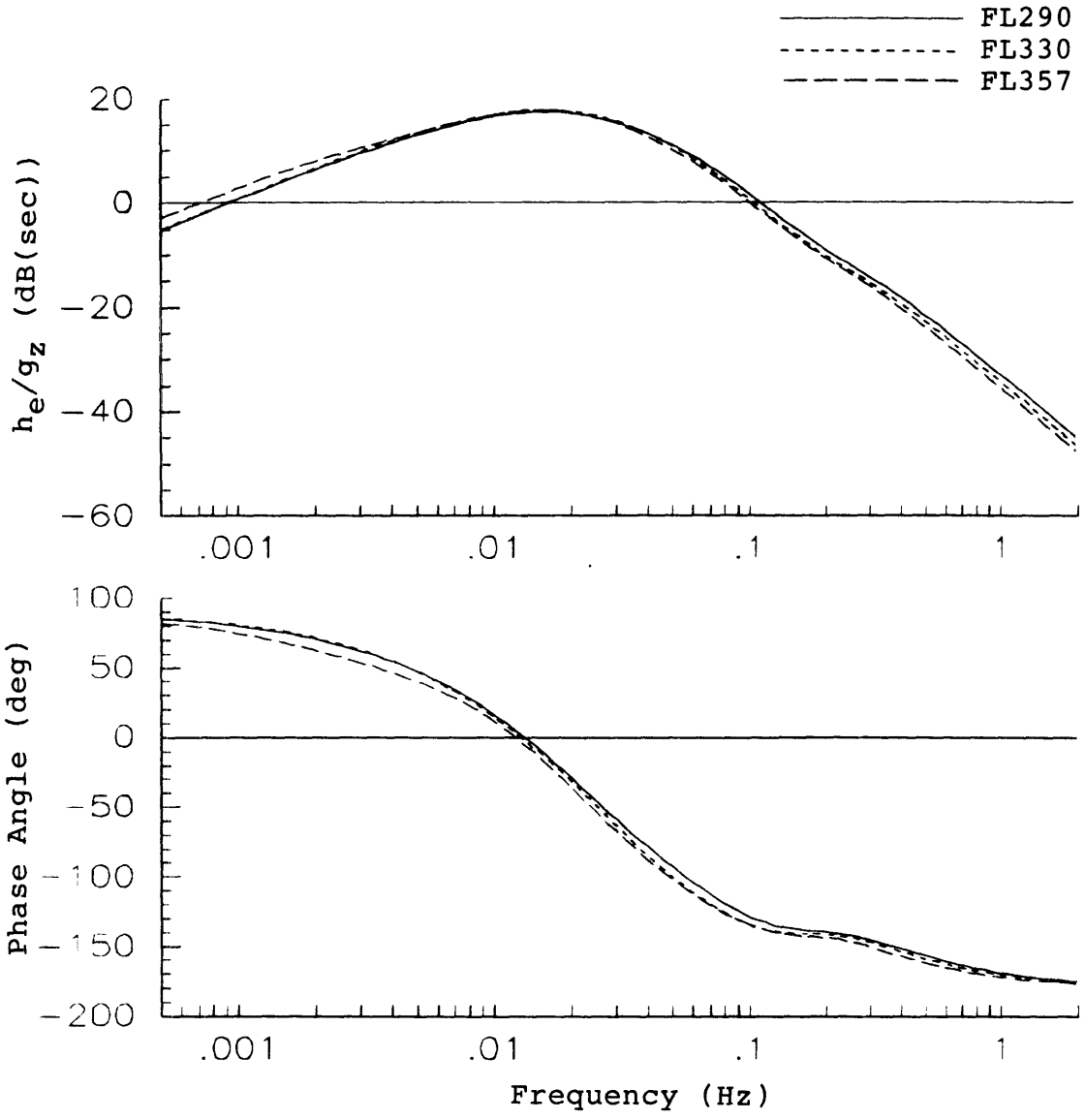

Figure 3-17 Altitude error sensitivity of DC9-30 to vertical gusts.

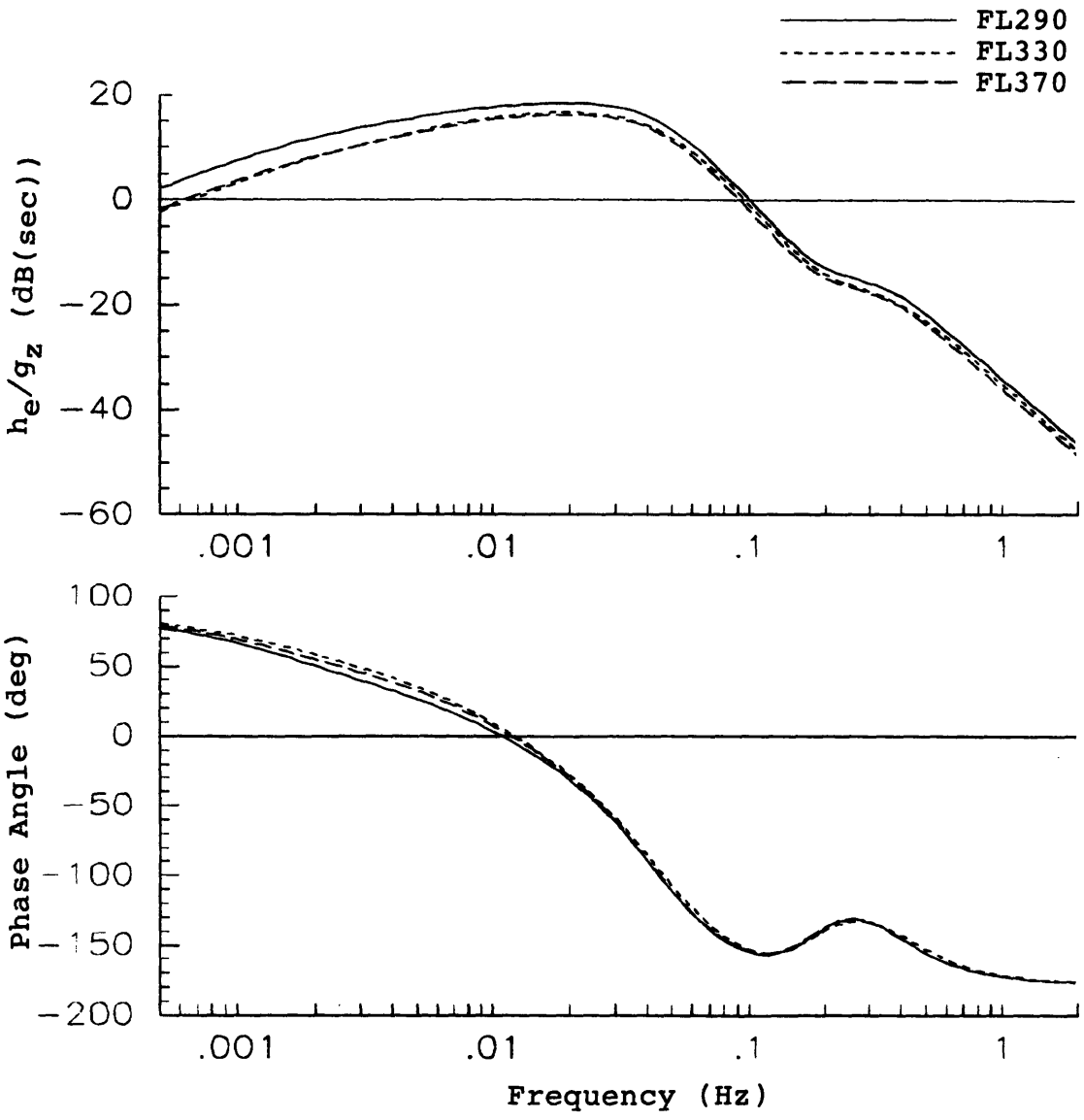

Figure 3-18 Altitude error sensitivity of L-1011 to vertical gusts.

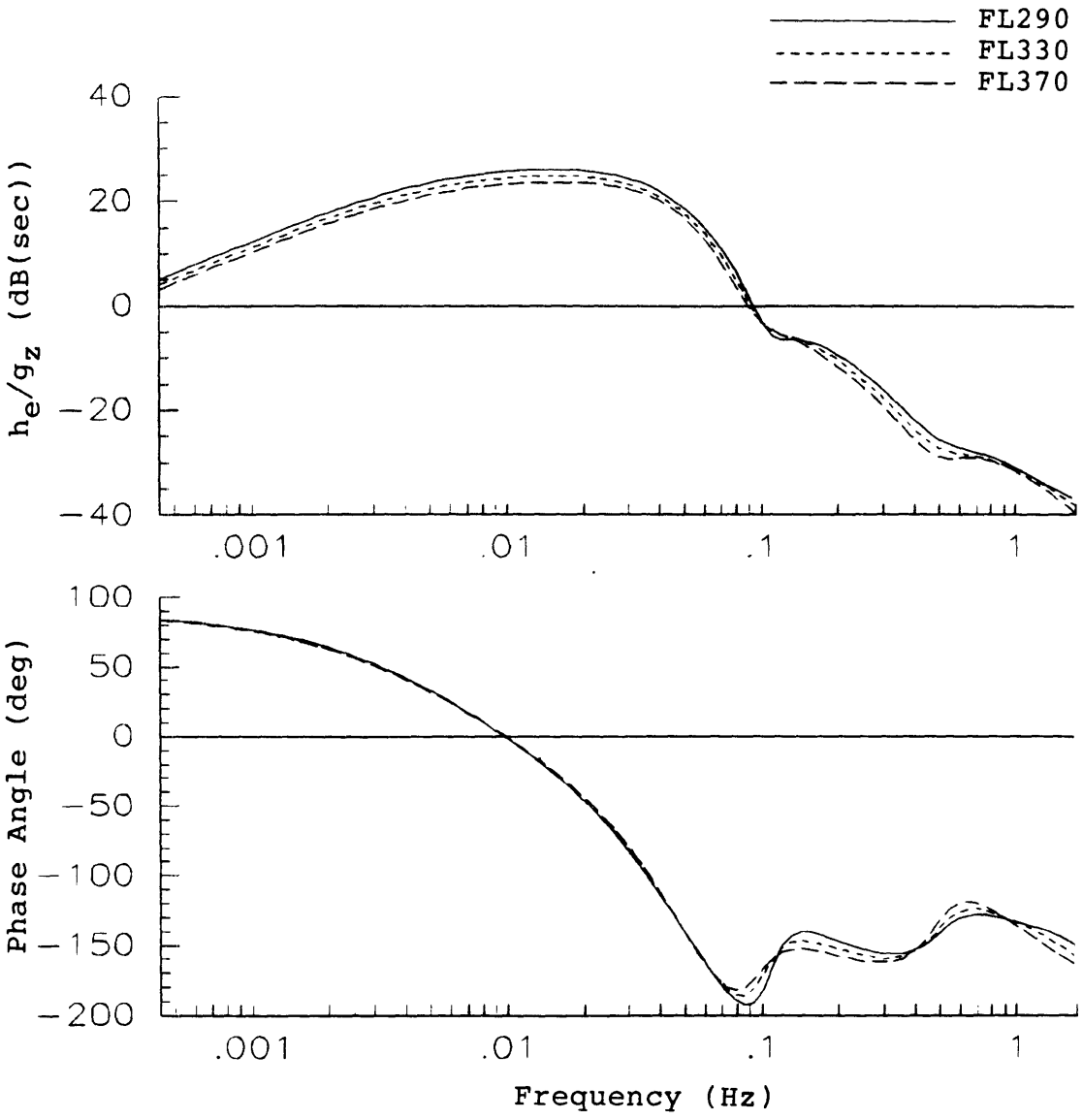

Figure 3-19 Altitude error sensitivity of Citation III to vertical gusts.

This coupling results in a resonance peak which is observed to be at a slightly lower frequency than the frequency of peak sensitivity to pressure surface fluctuations. This shift of peak sensitivity to lower frequencies could also have been surmised from the slower response to step vertical gusts than to steps in the pressure surface. Care should be exercised in comparing the responses to gusts with the responses to pressure surface fluctuations due to the dimensional dissimilarity.

3.5 Aircraft-Autopilot Response to Horizontal Gusts

Figures 3-20 - 3-23 indicate the responses of each aircraft to step changes in the longitudinal horizontal wind. The corresponding Bode magnitude and phase plots are included in Figures 3-24 - 3-27. The reaction of the aircraft to horizontal gusts is similar to their reaction to vertical gusts in both the shape of the curves and the frequency at which the peak sensitivity occurs. All four aircraft exhibit less sensitivity to horizontal gusts than to vertical gusts of equal amplitude. This is due to the vertical gusts directly affecting altitude by changing the angle of attack and thus changing the lift whereas the horizontal gusts indirectly affect altitude through airspeed-altitude coupling.

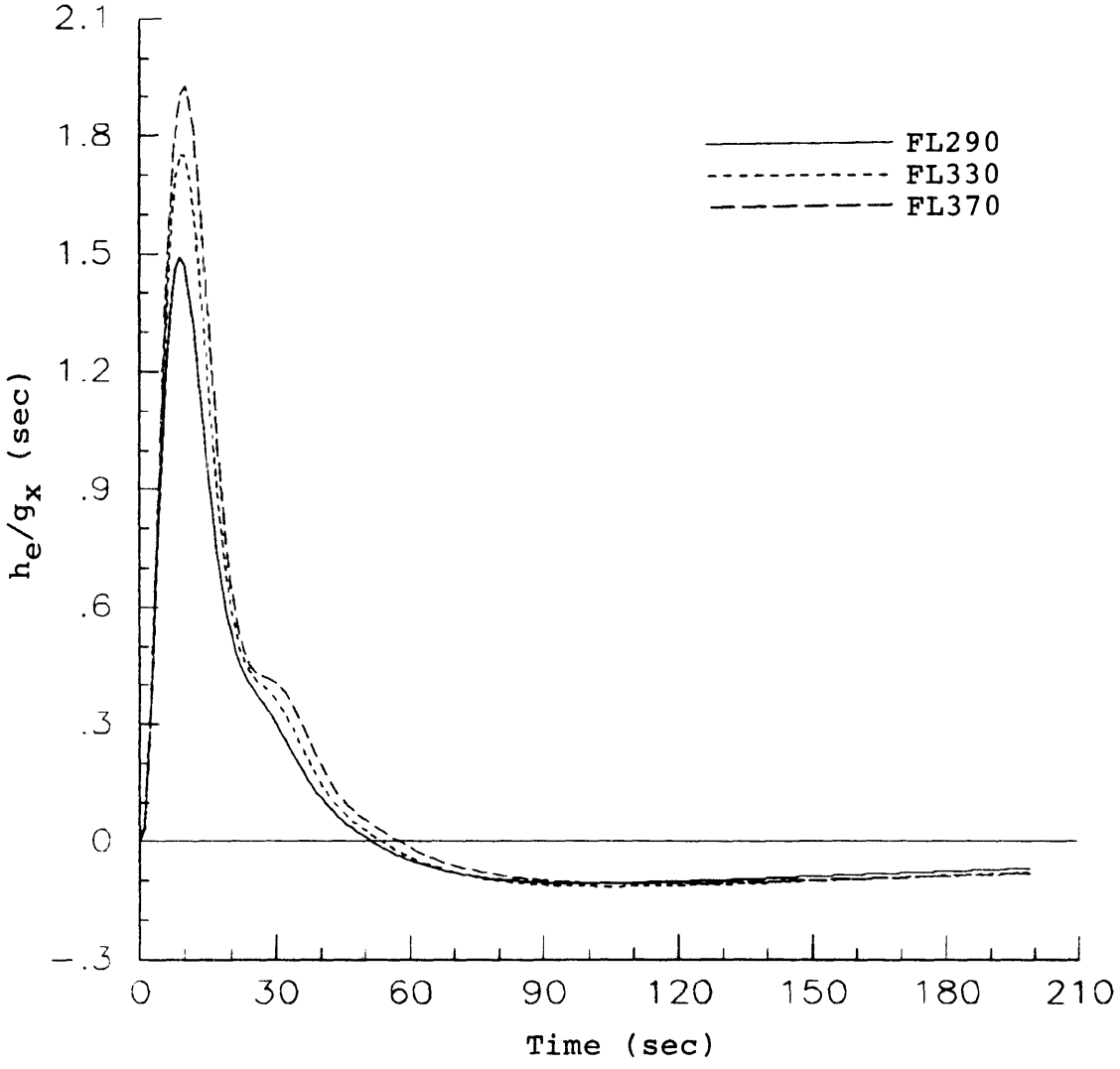

Figure 3-20 Altitude error resulting from step change in horizontal gust velocity for 737-100.

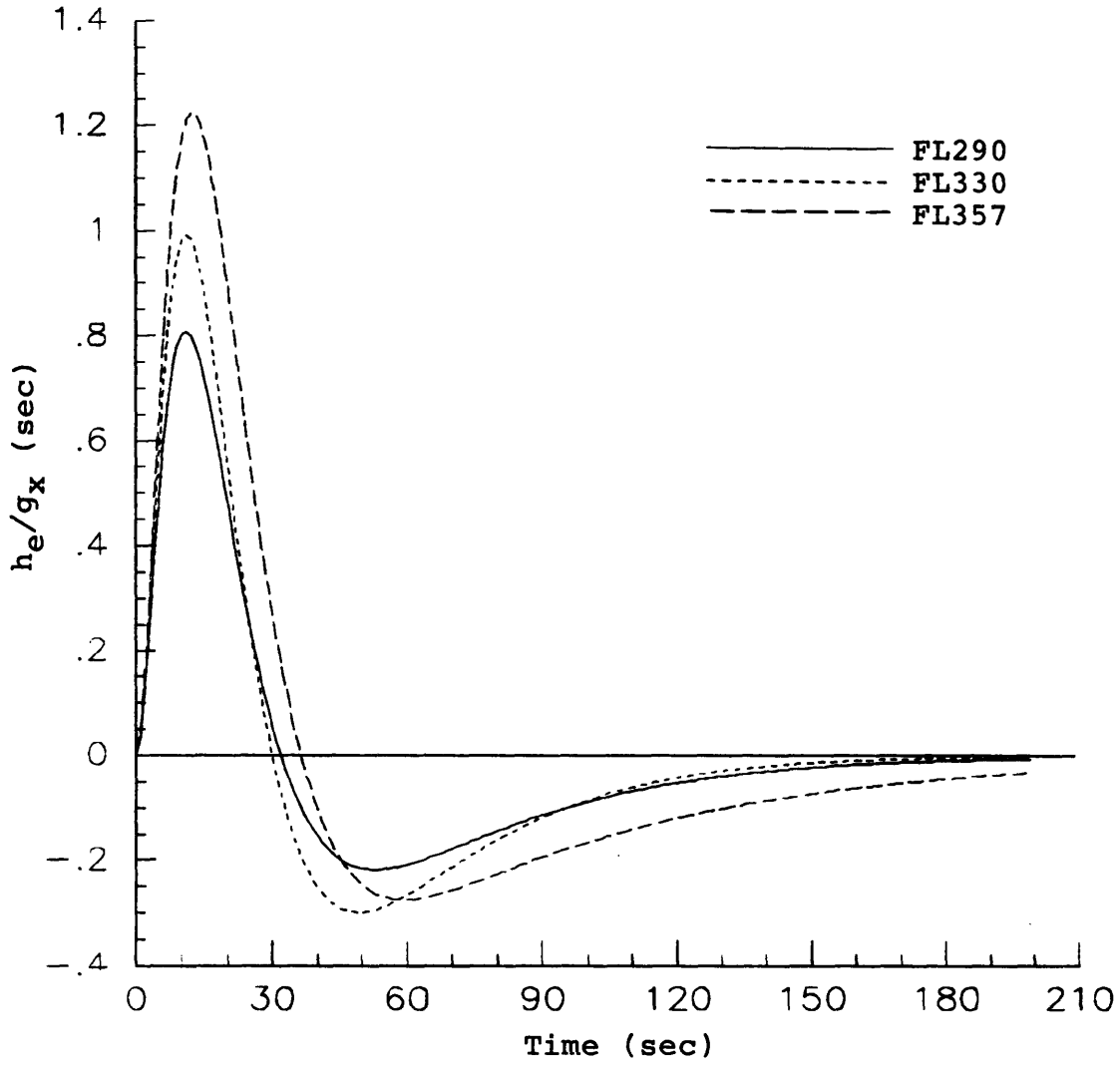

Figure 3-21 Altitude error resulting from step change in horizontal gust velocity for DC9-30.

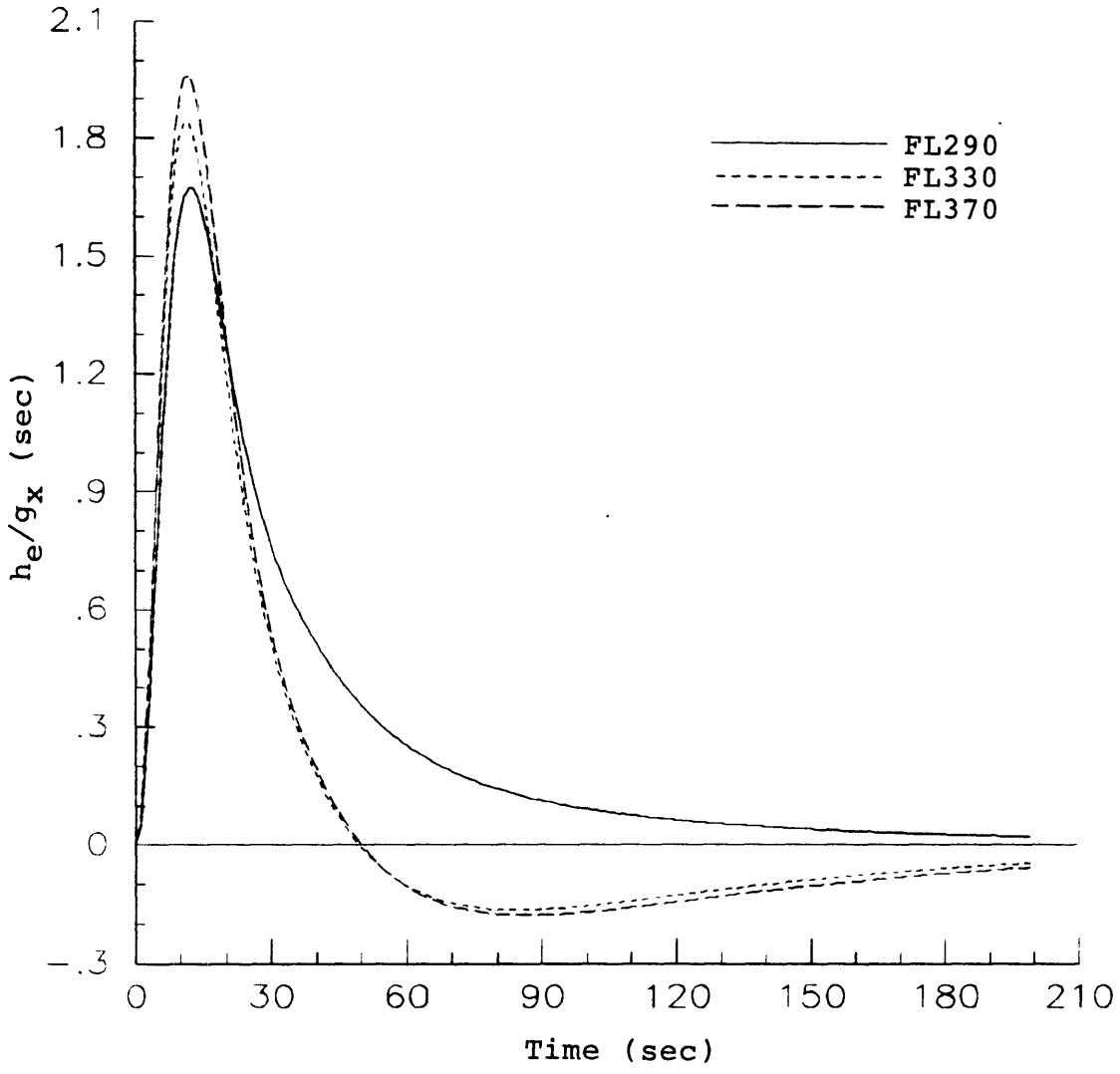

Figure 3-22 Altitude error resulting from step change in horizontal gust velocity for L-1011.

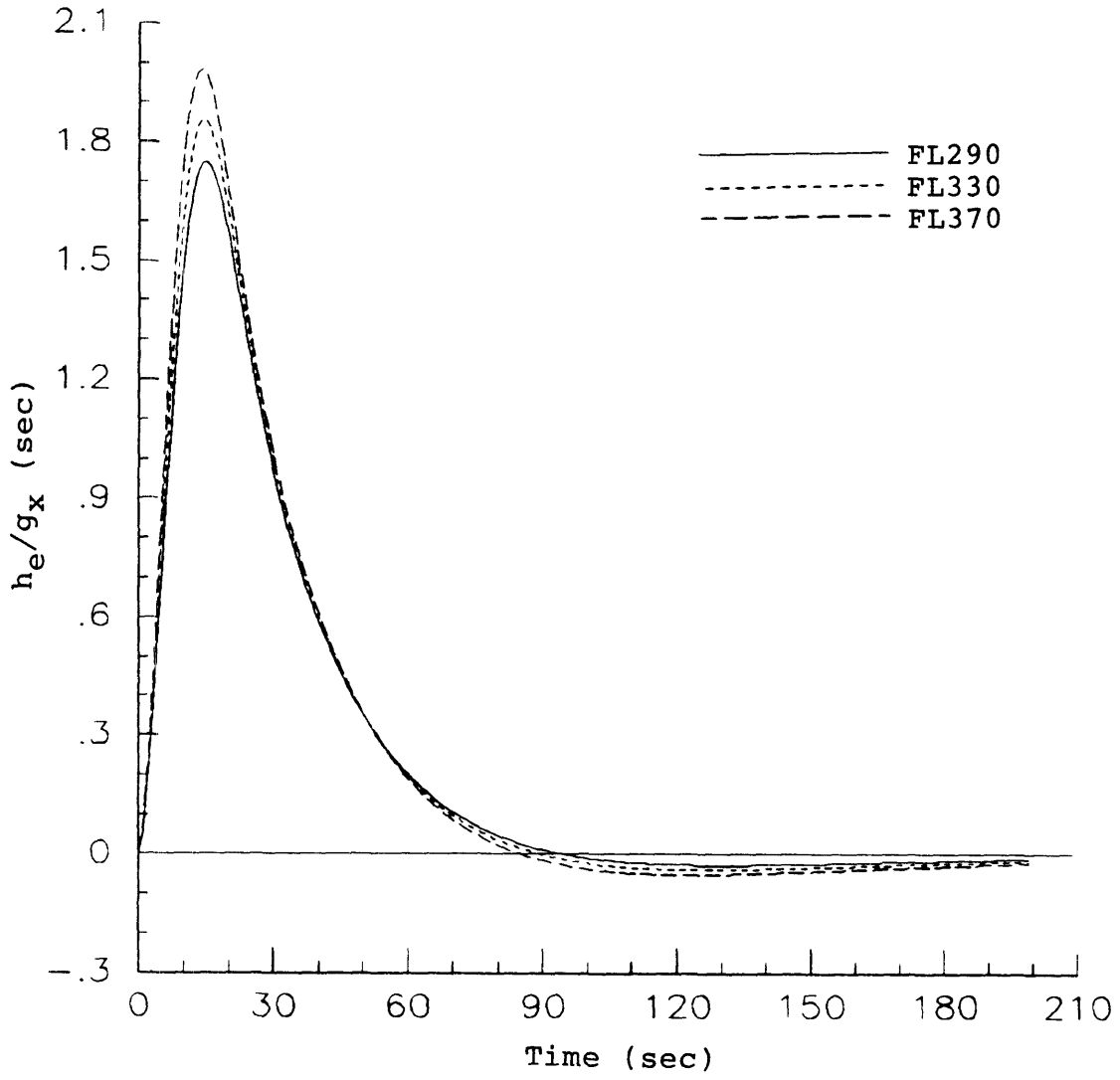

Figure 3-23 Altitude error resulting from step change in horizontal gust velocity for Citation III.

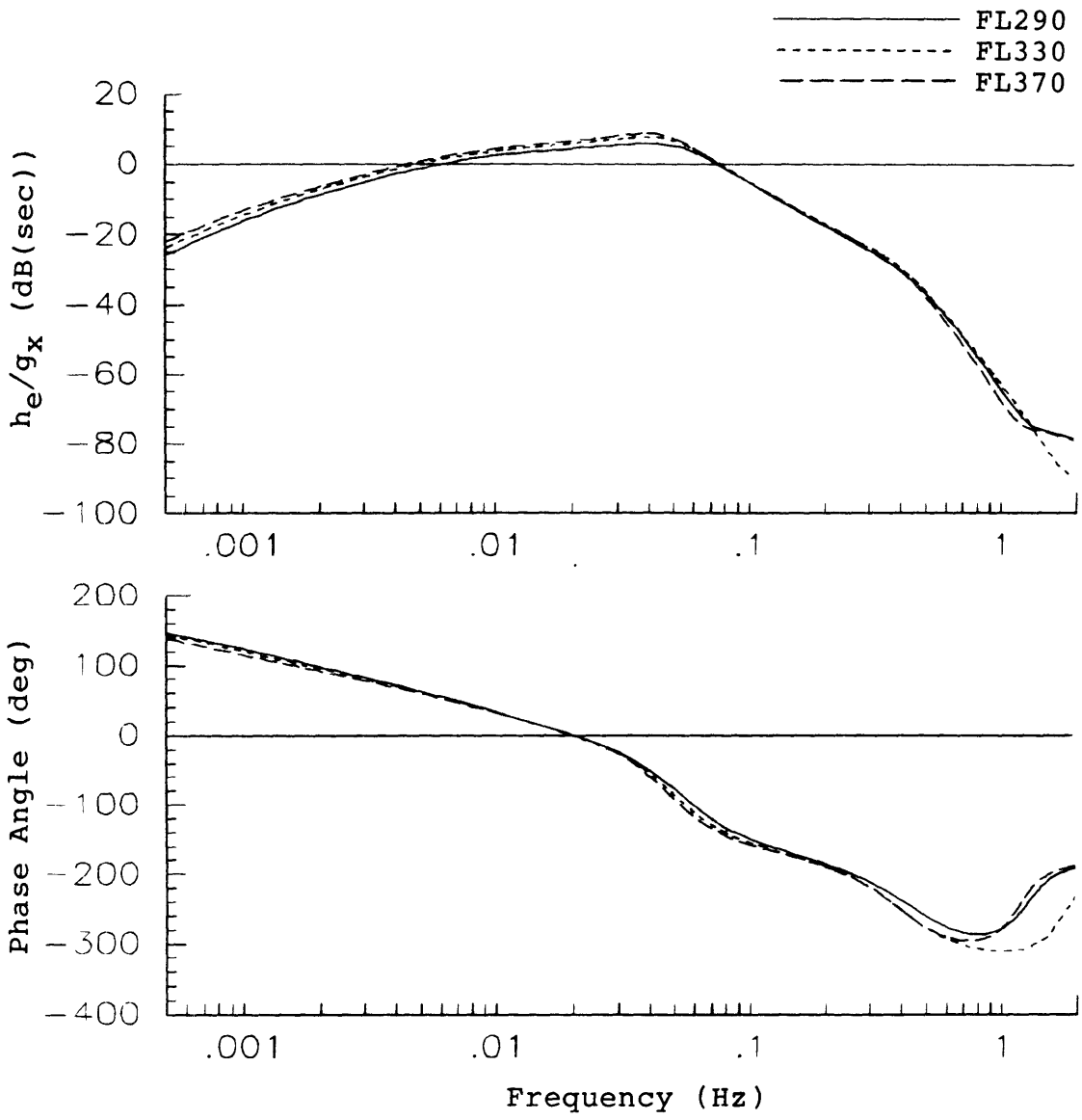

Figure 3-24 Altitude error sensitivity of 737-100 to horizontal gusts.

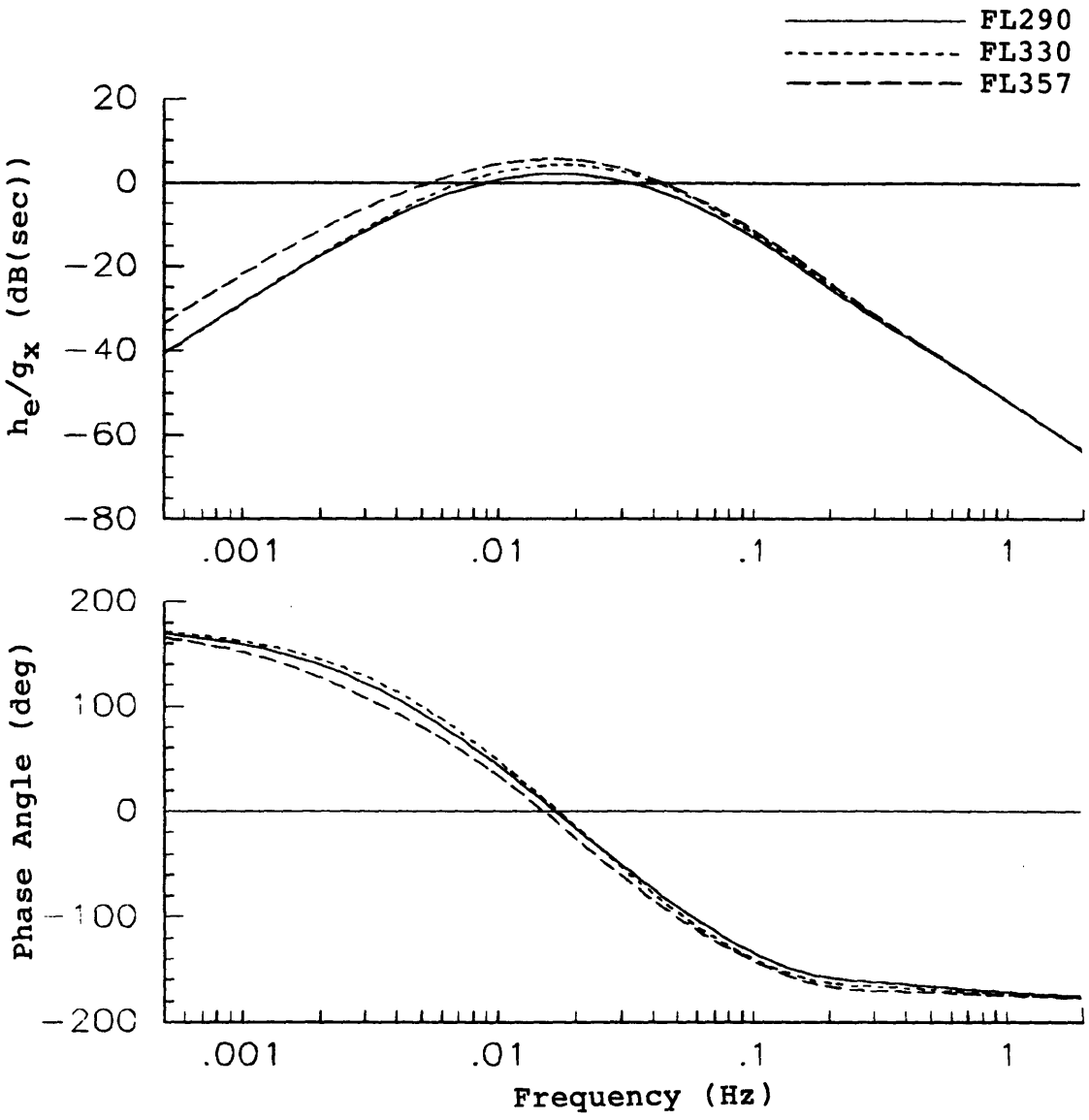

Figure 3-25 Altitude error sensitivity of DC9-30 to horizontal gusts.

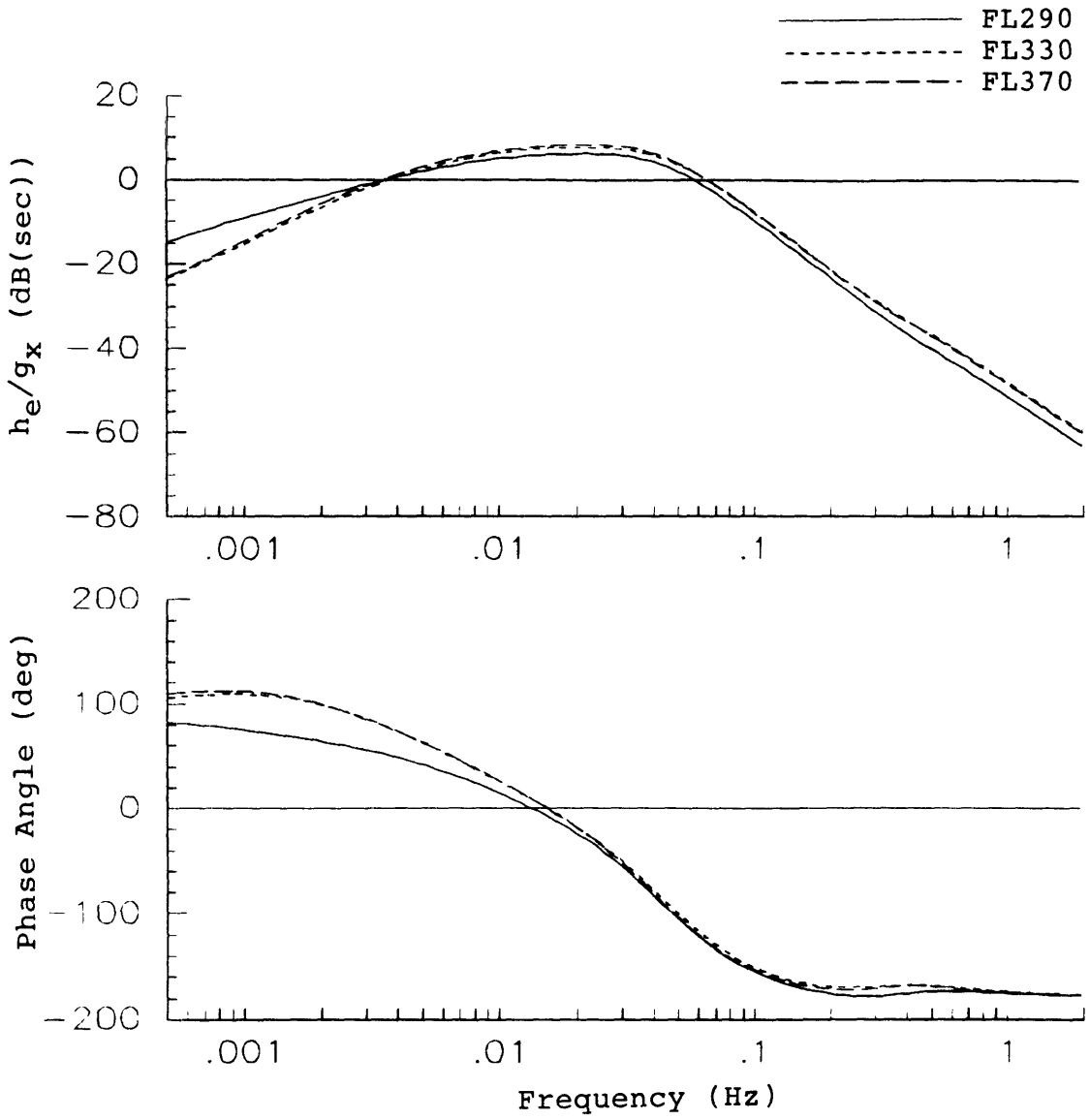

Figure 3-26 Altitude error sensitivity of L-1011 to horizontal gusts.

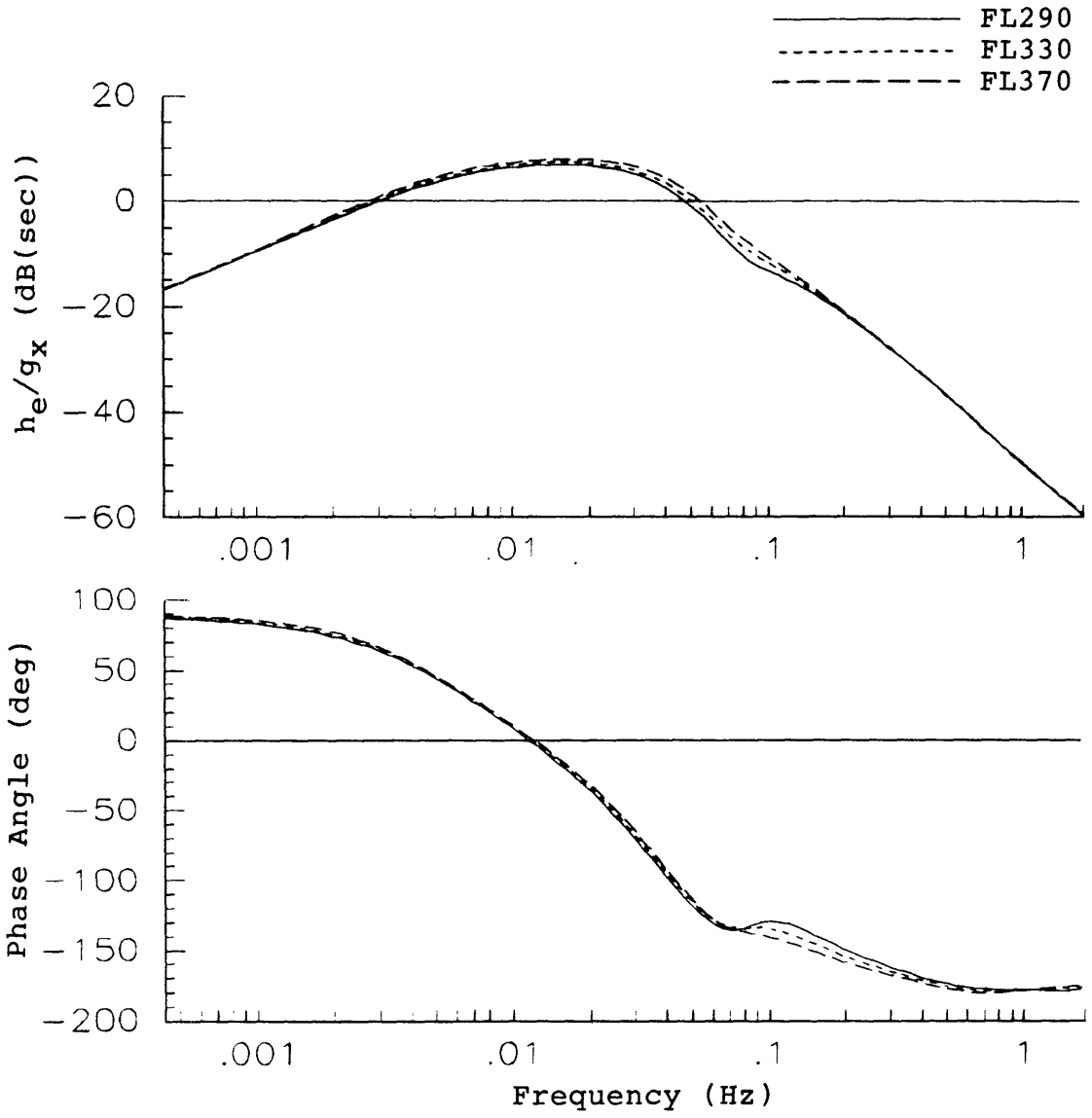

Figure 3-27 Altitude error sensitivity of Citation III to horizontal gusts.

Chapter 4

IMPLICATIONS FOR HIGH ALTITUDE WAVE ENCOUNTERS

4.1 Overview

The potential sources of large amplitude atmospheric disturbances with wavelengths observed to be important to the dynamics of altitude tracking are: 1) Orographic waves that form in the lee of mountains and 2) Gravity shear waves which are most often found at the edge of the jetstream. The physical processes that cause these waves to form are fairly well understood.[12] Due to the difficulty of collecting data, however, only a limited number of measurements of pressure surface fluctuation and gust amplitudes have been reported for mountain lee waves, and even fewer have been reported for gravity shear waves. Because of the lack of gravity wave data, no attempt was made to quantitatively investigate their effect on aircraft.

Section 4.2 presents a partial compilation of actual measurements of pressure surface fluctuations and vertical gusts in mountain waves that have been reported in the meteorological literature. The effect that each of these observed disturbances would have on the altitude tracking performance of one of the aircraft studied is presented in Section 4.3. In Section 4.4, a method is demonstrated for performing a useful manipulation of the altitude error sensitivity data presented in Chapter 3. This manipulation

converts the data into a form that is more convenient for evaluating which combinations of disturbance amplitude and wavelength are likely to cause a particular aircraft to deviate significantly from its assigned altitude.

4.2 Mountain Lee Waves

Mountain waves typically form in the lee of mountain ranges when the wind blowing across the mountain range triggers a natural vertical oscillation of the airmass. As the airmass oscillates, it drifts with the prevailing wind with the result that each constant pressure surface forms a series of waves (which look like ocean swells) whose crests are parallel to the mountain range. These waves in the pressure surfaces are illustrated in Figure 4-1 and discussed in Atkinson[12]. The horizontal distance between successive crests in the pressure surface, the pressure surface's wavelength λ_w, is directly influence by the speed of the prevailing wind. The faster the prevailing wind is blowing, the longer the wavelength will be. Since the strength of the prevailing wind typically varies with altitude, the wavelength of each pressure surface can be a function of the mean height of that pressure surface. Downwind of the mountain range, the variation in wavelength with altitude can result in the pressure surfaces getting slightly skewed relative to each other so that the peak of one surface does not necessarily occur directly above the peak of a lower surface.

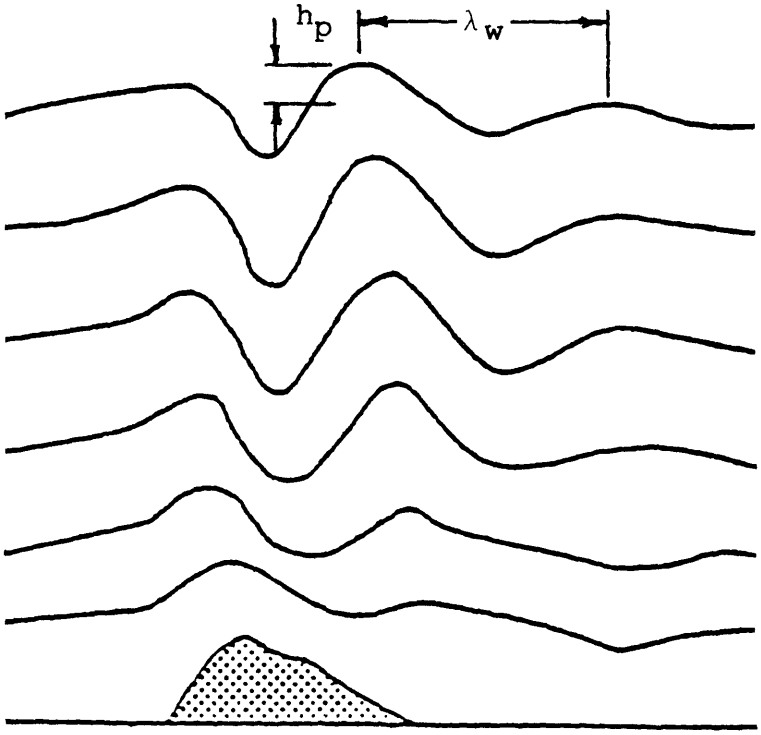

Figure 4-1 Mountain lee wave isobaric surfaces.

Figures 4-2 and 4-3 indicate observed pressure surface fluctuation and vertical gust amplitudes for mountain waves plotted against their observed wavelengths as compiled by Atkinson.[12] This data was obtained from a variety of meteorological studies including aircraft penetrations, surface pressure measurements, radar, and satellite observations. Due to the varied nature of the observations there is some uncertainty in this data. For this reason, several extremely large amplitude cases which were well outside the data cluster have been omitted in Figures 4-2 and 4-3. From these observations, it can be inferred that common disturbance wavelengths in mountain waves are between 5 and 15 nautical miles (nm). Pressure surface fluctuation amplitudes (half of the crest to trough distance) can be as high as several thousand feet, and vertical gust amplitudes can be as large as 20 ft/sec.

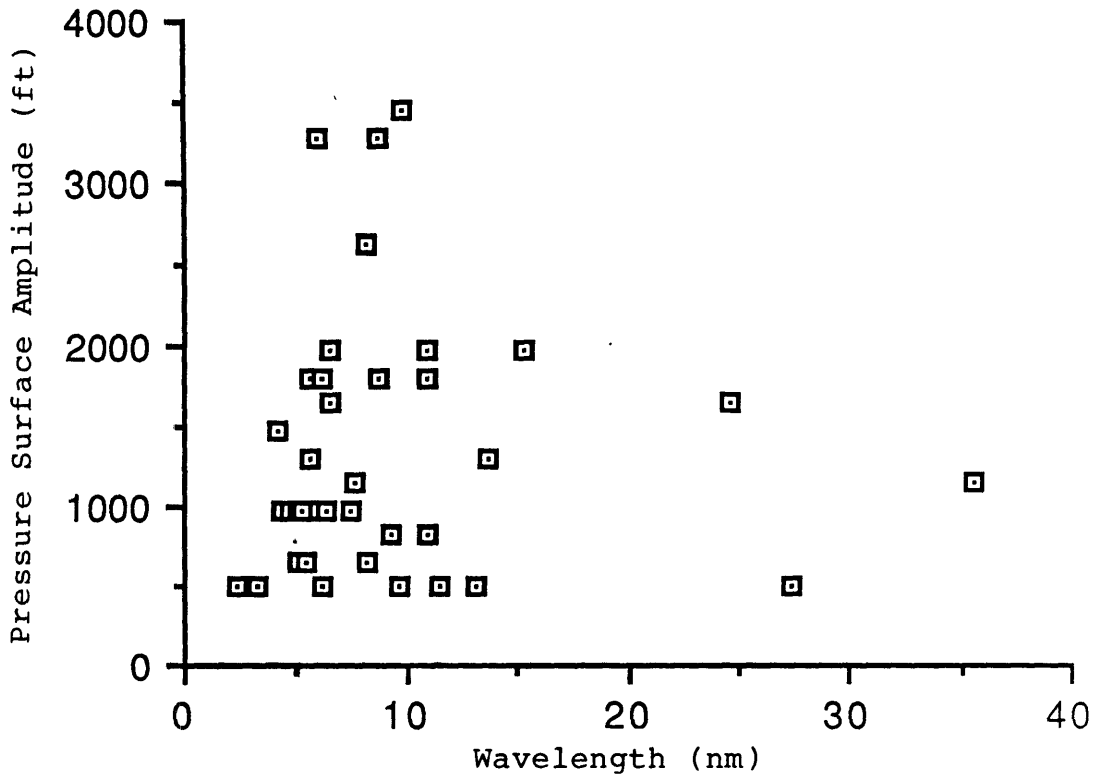

Figure 4-2 Pressure surface fluctuation amplitudes and wavelengths observed in mountain waves.

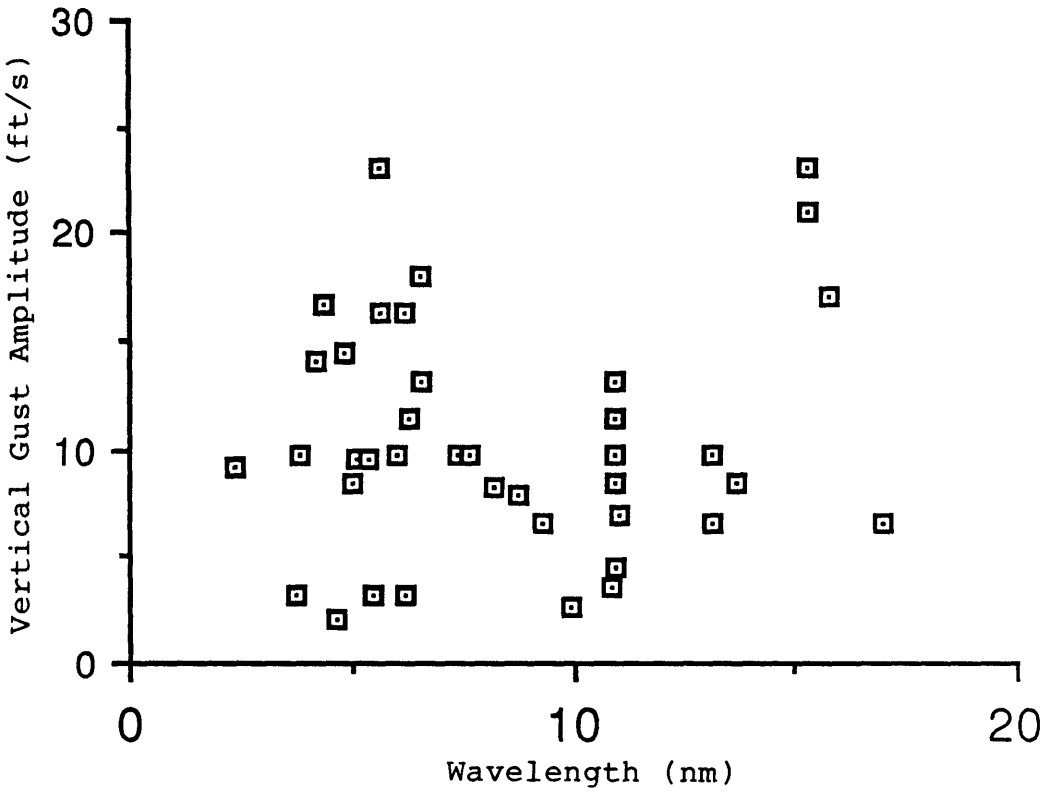

Figure 4-3 Vertical gust amplitudes and wavelengths observed in mountain waves.

4.3 Effect of Mountain Wave Disturbances on Altitude Tracking Performance

The mountain wave data presented in Section 4.2 can be examined in the context of the altitude tracking performance sensitivity data given in Chapter 3. An example is shown in Figure 4-4 which plots the expected error amplitude for the DC9-30 at FL330 subject to the mountain wave pressure fluctuations and vertical gusts shown in Figures 4-2 and 4-3. This data was generated by calculating the effective frequency of the disturbance using the disturbance's wavelength and the aircraft's equilibrium velocity and under the assumption that the aircraft is flying perpendicular to the wavefront. The frequency was then used to find the amplitude ratio from the appropriate Bode magnitude plot. The expected altitude error was then determined by multiplying the disturbance amplitude by the amplitude ratio.

The DC9-30 is presented because it has the greatest sensitivity to vertical gusts of the transport aircraft and only moderate sensitivity to pressure surface fluctuations. It is apparent that pressure surface fluctuations are reported which would result in altitude errors in excess of 1,000 feet if encountered by any of the four aircraft studied. (The actual values should be regarded with caution because of the potential inaccuracy of the disturbance data and because the assumption of small perturbations made in the linear models is not necessarily valid for the large errors). It is also clear that the altitude errors which could result

from the more severe pressure surface fluctuations are a factor of ten or more larger than the altitude errors which could result from the more severe vertical gusts. This implies that pressure surface fluctuations are the primary cause of altitude tracking error in severe mountain wave encounters.

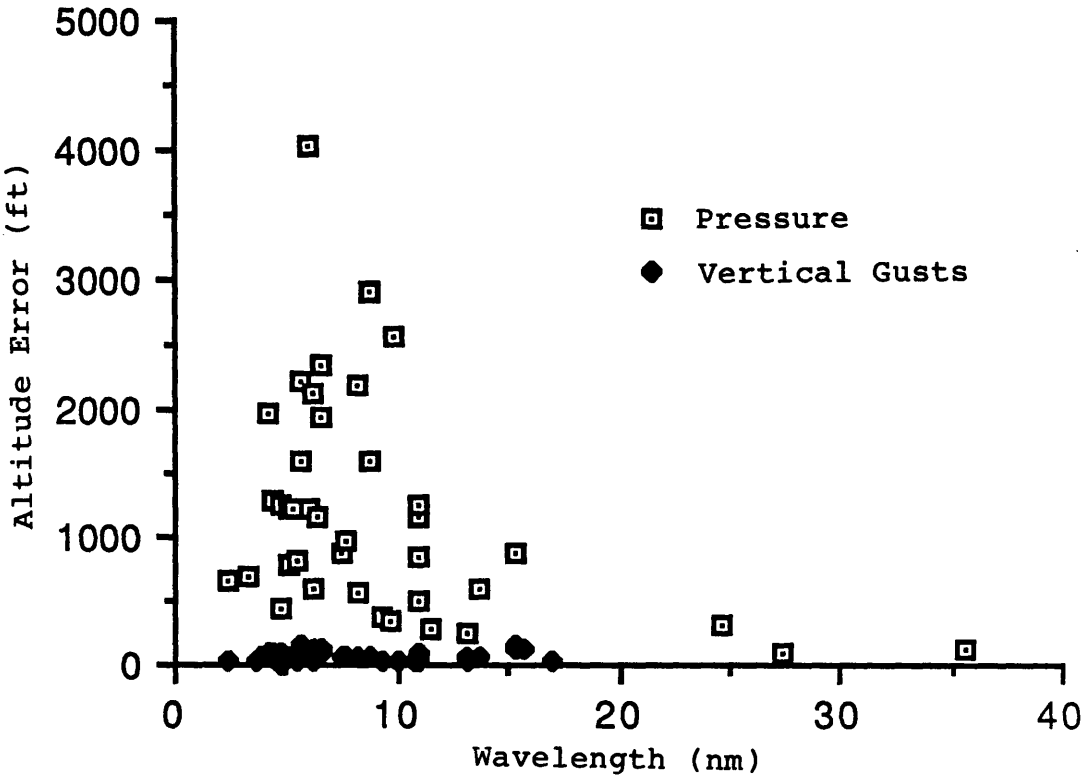

Figure 4-4 Predicted DC9 altitude errors resulting from observed pressure surface fluctuations and vertical gusts.

Figure 4-5 presents data obtained by the FAA from monitoring the Mode C altitude reporting transponder of a twin-engine Sabreliner jet aircraft. The Sabreliner was flying across the Continental Divide near Denver, Colorado during a period of reported mountain wave activity at an assigned altitude of 37,000 feet with its autopilot engaged. The Mode C data clearly shows that the aircraft experienced a 700 foot assigned altitude deviation during a period of apparently unsteady flight.

Figure 4-6 presents similar Mode C data from a Dassault Falcon 20 flying at 39,000 feet on autopilot in the Denver area during another period of mountain wave activity. This data also indicates that the aircraft exhibited a large assigned altitude deviation during a period of unsteady flight.

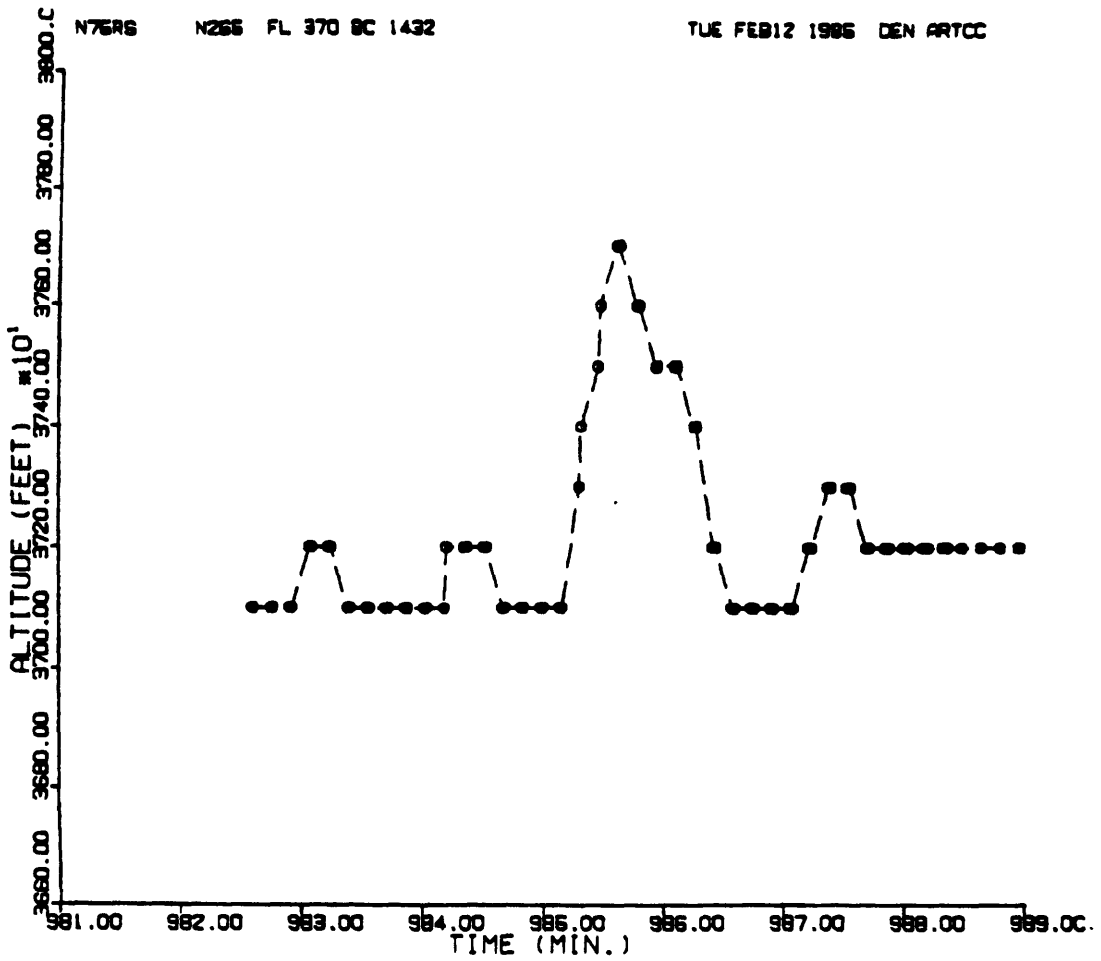

Figure 4-5 Mode C data from a Sabreliner flying in mountain waves.

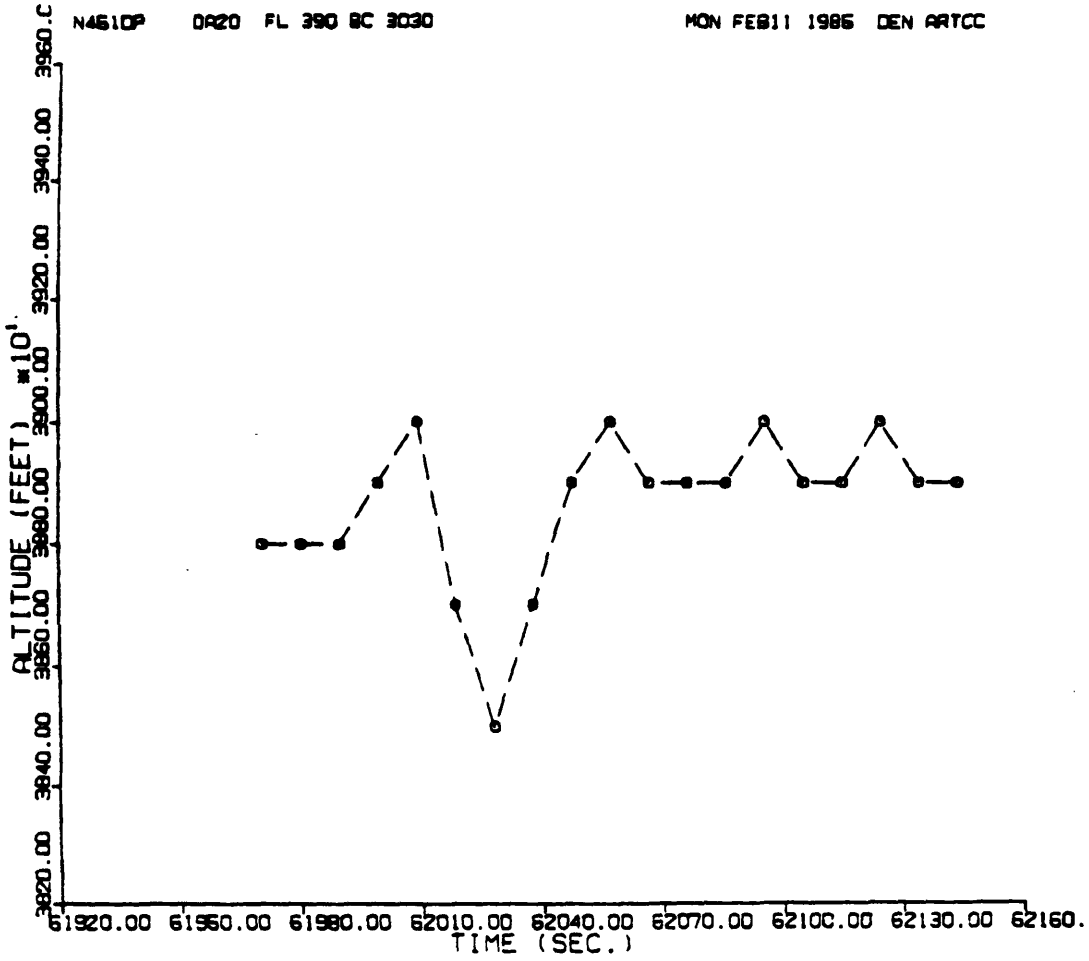

Figure 4-6 Mode C data from a Falcon 20 flying in mountain waves.

4.4 Determination of Critical Pressure Surface Fluctuation Amplitudes

Since pressure surface fluctuations seem to be the primary cause of altitude tracking errors in mountain wave encounters, it is desirable to be able to identify critical values of pressure surface fluctuation amplitude above which an aircraft's altitude tracking error will exceed a specified tolerance. This critical amplitude can be determined for any aircraft and wavelength (frequency). It is found by dividing the altitude error tolerance by the amplitude ratio from a Bode magnitude plot of the aircraft's altitude error sensitivity to pressure surface fluctuations. By repeating this calculation for a number of wavelengths, a chart of the critical pressure surface fluctuation amplitude as a function of wavelength can be derived. If the amplitude of the pressure surface fluctuation of a given wavelength exceeds the critical amplitude for that wavelength, the aircraft's altitude error will exceed the tolerance for at least a small portion of its oscillatory cycle.

Figure 4-7 shows the result of such an analysis for each of the four aircraft studied with a specified altitude error tolerance of 300 feet. A plot representing the optimum performance for any aircraft if its peak vertical acceleration is limited to plus or minus 1/4g is also included for reference. This 1/4g line is constructed by adding the maximum amplitude for a sinusoidal height variation that can be achieved within the acceleration limit,

which represents how much the aircraft can move up and down to track the pressure surface, to the altitude error tolerance. Superimposed on this Figure is the data on observed mountain wave pressure surface fluctuations. It is readily seen that many of the observed mountain waves would cause all of the aircraft studied to exhibit altitude deviations well in excess of 300 feet.

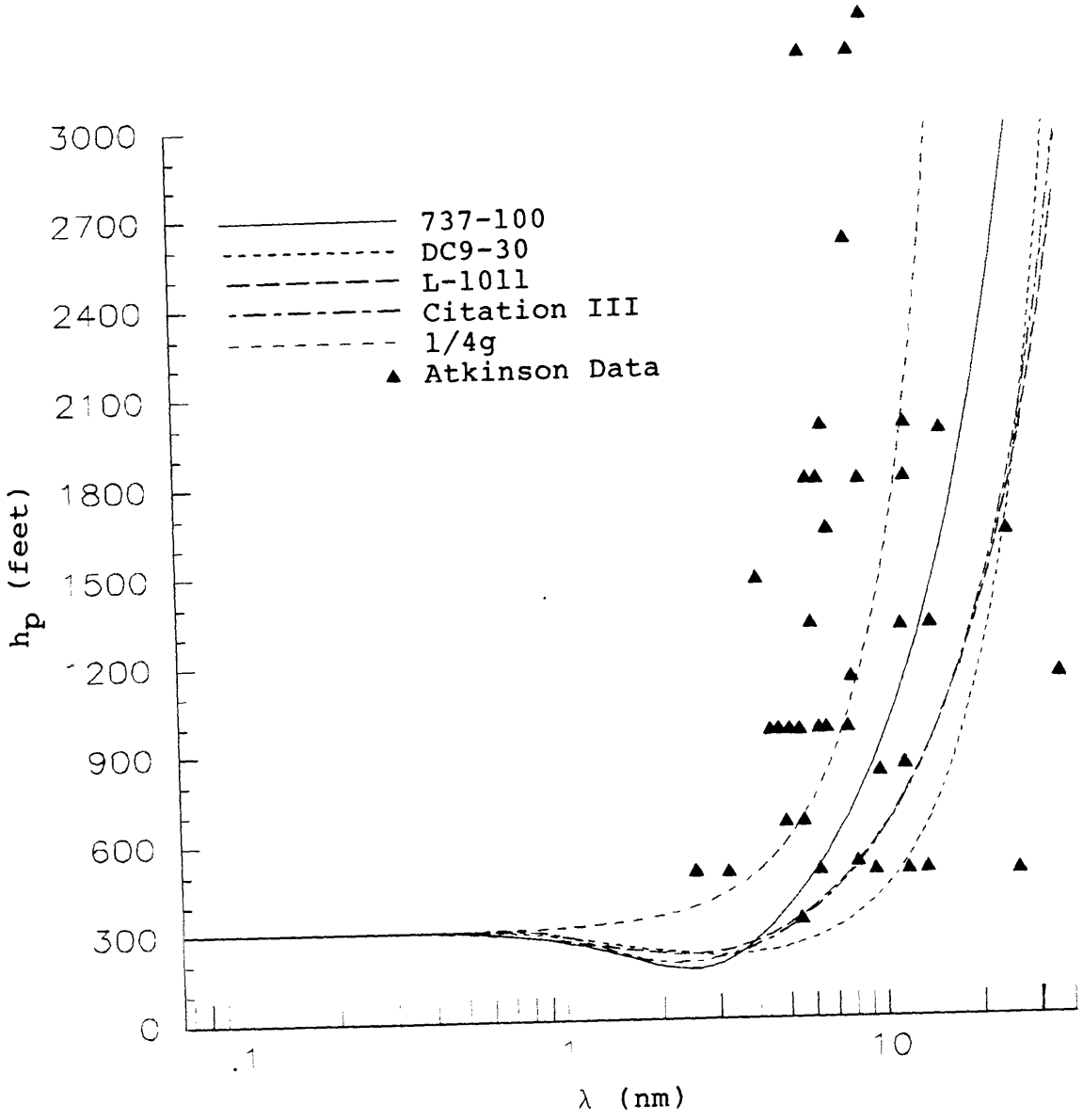

Figure 4-7 Tolerable pressure surface fluctuations for a specified altitude error limit of 300 feet.

Chapter 5

SUMMARY AND CONCLUSIONS

The recent interest in reducing the vertical separation standard at high altitude has motivated a series of investigations into how accurately aircraft track their assigned pressure altitude. Prior studies of altitude tracking performance have focussed on error sources in the aircraft's static pressure and altimetry systems. Evidence has been gathered by the FAA from monitoring the Mode C altitude reporting transponders of commercial, military, and general aviation aircraft, however, which suggests that large altitude tracking errors can be caused by factors other than incorrect measurement of altitude. This study sought to examine one source of these assigned altitude deviations, altitude tracking errors induced by the dynamic interaction of aircraft-autopilot systems with atmospheric disturbances.

Linearized models of aircraft and autopilot dynamics at several altitudes were developed for four common jet aircraft. These models were then used to investigate the dynamic interaction of aircraft-autopilot systems with three types of atmospheric disturbances: pressure surface fluctuations, vertical gusts, and horizontal gusts. Simulations were performed to determine the response of each aircraft-autopilot system to step changes in each disturbance. These step responses were used to develop a

sense of how quickly the aircraft responded and how well damped their response was. Bode plots were then used to asses the sensitivity of each system's altitude tracking performance to sinusoidal disturbances of various frequencies.

The step responses showed a fair degree of uniformity between the four aircraft in their respective responses to each of the disturbances. The aircraft returned to their assigned altitudes much faster after being upset by a step change in the height of the pressure surface than after being upset by a step change in either type of gust. The Bode plots showed that each aircraft is quite insensitive to fairly low frequency pressure surface fluctuations. At high frequencies, the aircraft tend to penetrate through the pressure surface fluctuations instead of trying to follow them. A mid-frequency region was identified in which each aircraft-autopilot system is especially sensitive to pressure surface fluctuations. All of the aircraft were fairly insensitive to high and low-frequency gusts. In the mid-frequency region, however, the altitude tracking performance of each aircraft showed some sensitivity to gusts.

Data collected on atmospheric disturbances resulting from mountain lee waves was used to evaluate the sensitivity data which has been generated for the four aircraft. This analysis demonstrated that in mountain wave activity atmospheric disturbances do exist which can cause aircraft to exhibit large assigned altitude deviations. It was also

noted that pressure surface fluctuations were the dominant cause of these altitude deviations. Further analysis demonstrated that the sensitivity data could be used to determine critical amplitudes for pressure surface fluctuations. The critical amplitudes set the boundaries for which an aircraft's altitude tracking error will be within a specified limit.

In summary, the following conclusions were drawn from this investigation:

1. Atmospheric conditions do occur which can cause aircraft to exhibit significant assigned altitude deviations due to their interaction with the dynamics of the aircraft-autopilot system.

2. The effect of atmospheric disturbances is strongest when they have a wavelength which couples strongly with the dynamics of the aircraft-autopilot system.

3. Analysis of available meteorological data suggests that fluctuations in the height of the pressure surface tend to be the largest source of altitude errors for flights through mountain waves.

4. If the aircraft and autopilot dynamics are known, a maximum amplitude of pressure surface fluctuation can be defined for any wavelength such that the aircraft will remain within a specified margin of its assigned altitude upon encountering such a disturbance.

5. Additional meteorological data is required to assess the probability of an aircraft exhibiting a significant assigned altitude deviation due to atmospheric disturbances.

The results of this work should help both in identifying which meteorological data must be examined in order to determine the viability of reducing vertical separation standards and in determining which meteorological conditions would cause aircraft to exhibit significant assigned altitude deviations.

REFERENCES

1 Anon., Third Meeting of the Vertical Separation Panel, ICAO Bulletin, Vol. XIV, No. 2, 1959.

2 Anon., ICAO Panel on Vertical Separation Reports to the Air Navigation Commission, ICAO Bulletin, Vol. XI, No. 4, 1956.

3 Gracey, William, The Measurement of Pressure Altitude on Aircraft, NACA TN 4127, 1957.

4 Gracey, William, The Measurement of Aircraft Speed and Altitude, NASA Reference Publication 1046, Langley Research Center, Hampton, Virginia, 1980.

5 Harlan, Raymond, Final Report - Survey and Preliminary Evaluation of Barometric Altimetry Techniques, RE-61, M.I.T. Measurement Systems Laboratory, Cat. 10, Special Printing 291, October 10, 1969.

6 Sizoo, David G., The Effects of Dynamic Error Sources on the Altitude Hold Performance of Aircraft Tracking a Pressure Altitude, S.M. Thesis, Massachusetts Institute of Technology, September 1986.

7 Reid, J. Gary, Linear System Fundamentals, McGraw-Hill, Inc., New York, 1983.

8 Personal communications with Richard M. Hueschen, Aero-Space Technologist, NASA Langley Research Center/Guidance and Control Division.

9 Personal communications with Randy Nelson, Section Supervisor, Cessna Aircraft Company.

10 Blakelock, John, Automatic Control of Aircraft and Missiles, John Wiley and Sons, Inc., New York, 1965.

11 Personal Communications with Bill Carter, Engineering Section Head, Honeywell, Sperry Commercial Flight Systems Division.

12 Atkinson, B. W., Meso Scale Atmospheric Circulations, Academic Press, New York, 1981.

Appendix A

AIRCRAFT STATE SPACE MODELS

A.1 Boeing 737-100 State Space Models

This section presents the state vector, equilibrium condition and coefficient matrices for the three state space models of the 737-100's longitudinal dynamics.

Five variables are included in the state vector, $\underline{x}$, of the 737. They are:

$$\underline{x} = \begin{bmatrix} u_b \text{ (ft/sec)} \\ w_b \text{ (ft/sec)} \\ q \text{ (rad/sec)} \\ \theta \text{ (rad)} \\ h \text{ (ft)} \end{bmatrix}$$

The control vector, $\underline{u}$, is the elevator defection, δ_e, which is in degrees. These variables were defined in Section 2.2.1.

The three trim conditions and their corresponding coefficient matrices are as follows:

737 Trim Condition I

Altitude:	29,000 ft
Speed:	799.4 ft/sec (Mach 0.8)
Pitch angle:	0.0229 rad
Weight:	85,000 lbs
$X_{c.g.}$:	0.20

$$\underline{A} = \begin{bmatrix} -.666e\text{-}2 & .464e\text{-}1 & -.183e+2 & -.322e+2 & .0 \\ -.593e\text{-}2 & -.873 & .797e+3 & -.738 & .0 \\ .218e\text{-}2 & -.744e\text{-}2 & -.984 & .0 & .0 \\ .0 & .0 & .100e+1 & .0 & .0 \\ .229e\text{-}1 & -.100e+1 & .0 & .799e+3 & .0 \end{bmatrix}$$

$$\underline{B} = \begin{bmatrix} .160e\text{-}1 \\ -.697 \\ -.925e\text{-}1 \\ .0 \\ .0 \end{bmatrix}$$

737 Trim Condition II

Altitude: 33,000 ft

Speed: 790.3 ft/sec (Mach 0.8)

Pitch angle: 0.0317 rad

Weight: 85,000 lbs

$X_{c.g.}$: 0.20

$$\underline{A} = \begin{bmatrix} -.674e\text{-}2 & .498e\text{-}1 & -.250e+2 & -.322e+2 & .0 \\ .122e\text{-}1 & -.738 & .788e+3 & -.102e+1 & .0 \\ .245e\text{-}2 & -.625e\text{-}2 & -.846 & .104e\text{-}13 & .0 \\ .0 & .0 & .100e+1 & .0 & .0 \\ .317e\text{-}1 & -.100e+1 & .0 & .790e+3 & .0 \end{bmatrix}$$

$$\underline{B} = \begin{bmatrix} .191e\text{-}1 \\ -.601 \\ -.802e\text{-}1 \\ .0 \\ .0 \end{bmatrix}$$

737 Trim Condition III

Altitude:	37,000 ft
Speed:	778.4 ft/sec (Mach 0.8)
Pitch angle:	0.0373 rad
Weight:	85,000 lbs
$X_{c.g.}$:	0.20

$$\underline{A} = \begin{bmatrix} -.595e\text{-}2 & .525e\text{-}1 & -.290e+2 & -.321e+2 & .0 \\ .156e\text{-}2 & -.688 & .776e+3 & -.120e+1 & .0 \\ .231e\text{-}2 & -.602e\text{-}2 & -.771 & .0 & .0 \\ .0 & .0 & .100e+1 & .0 & .0 \\ .373e\text{-}1 & -.999 & .0 & .799e+3 & .0 \end{bmatrix}$$

$$\underline{B} = \begin{bmatrix} .206e\text{-}1 \\ -.553 \\ -.736e\text{-}1 \\ .0 \\ .0 \end{bmatrix}$$

A.2 McDonald Douglas DC9-30 State Space Models

The variables in the state vector for the DC9-30 model are similar to those in the 737-100's state vector except that there is an additional state for the elevator deflection.

The six variables included in the state vector, $\underline{x}$, of the DC9 are:

$$\underline{x} = \begin{bmatrix} u_b \text{ (ft/sec)} \\ w_b \text{ (ft/sec)} \\ q \text{ (rad/sec)} \\ \theta \text{ (rad)} \\ h \text{ (ft)} \\ \delta_e \text{ (deg)} \end{bmatrix}$$

The control vector, $\underline{u}$, is the commanded elevator defection, δ_{e_c}, which is in degrees. These variables were defined in Section 2.2.1.

The three trim conditions and their corresponding coefficient matrices are as follows:

DC9 Trim Condition I

Altitude:	29,000 ft
Speed:	799.4 ft/sec (Mach 0.8)
Pitch angle:	0.0218 rad
Weight:	95,000 lbs
$X_{c.g.}$:	0.25

$$\underline{A} = \begin{bmatrix} -.285e\text{-}1 & .183e\text{-}1 & -.174e+2 & -.322e+2 & -.118e\text{-}3 & .0 \\ -.845e\text{-}1 & -.863 & .799e+3 & -.701 & .118e\text{-}2 & .0 \\ .169e\text{-}3 & -.382e\text{-}2 & -.344e+1 & -.140e\text{-}14 & -.670e\text{-}6 & -.435e\text{-}1 \\ .0 & .0 & .100e+1 & .0 & .0 & .0 \\ .218e\text{-}1 & -.100e+1 & .0 & .799e+3 & .0 & .0 \\ .0 & .0 & .0 & .0 & .0 & -.200e+2 \end{bmatrix}$$

$$\underline{B} = \begin{bmatrix} .0 \\ .0 \\ .0 \\ .0 \\ .0 \\ .200e+2 \end{bmatrix}$$

DC9 Trim Condition II

Altitude: 33,000 ft

Speed: 785.5 ft/sec (Mach 0.8)

Pitch angle: 0.0315 rad

Weight: 95,000 lbs

$X_{c.g.}$: 0.25

$$\underline{A} = \begin{bmatrix} -.362e\text{-}1 & .221e\text{-}1 & -.247e+2 & -.322e+2 & -.126e\text{-}3 & .0 \\ -.821e\text{-}1 & -.732 & .785e+3 & -.101e+1 & .120e\text{-}2 & .0 \\ .259e\text{-}3 & -.333e\text{-}2 & -.290e+1 & .396e\text{-}14 & -.906e\text{-}6 & -.358e\text{-}1 \\ .0 & .0 & .100e+1 & .0 & .0 & .0 \\ .315e\text{-}1 & -.100e+1 & .0 & .786e+3 & .0 & .0 \\ .0 & .0 & .0 & .0 & .0 & -.200e+2 \end{bmatrix}$$

$$\underline{B} = \begin{bmatrix} .0 \\ .0 \\ .0 \\ .0 \\ .0 \\ .200e+2 \end{bmatrix}$$

DC9 Trim Condition III

Altitude: 35,700 ft

Speed: 776.0 ft/sec (Mach 0.8)

Pitch angle: 0.0396 rad

Weight: 95,000 lbs

$X_{c.g.}$: 0.25

$$\underline{A} = \begin{bmatrix} -.411e-1 & -.149 & -.308e+2 & -.322e+2 & -.200e-3 & .0 \\ -.805e-1 & -.651 & .775e+3 & -.128e+1 & .127e-2 & .0 \\ .349e-3 & -.231e-2 & -.256e+1 & -.255e-14 & -.231e-7 & -.313e-1 \\ .0 & .0 & .100e+1 & .0 & .0 & .0 \\ .396e-1 & -.999 & .0 & .776e+3 & .0 & .0 \\ .0 & .0 & .0 & .0 & .0 & -.200e+2 \end{bmatrix}$$

$$\underline{B} = \begin{bmatrix} .0 \\ .0 \\ .0 \\ .0 \\ .0 \\ .200e+2 \end{bmatrix}$$

A.3 Lockheed L-1011 State Space Models

The variables in the state vector for the L-1011 model are different than those in the state vectors for the 737-100 and the DC9-30. The six variables included in the state vector, $\underline{x}$, of the L-1011 are:

$$\underline{x} = \begin{bmatrix} v \text{ (ft/sec)} \\ \alpha \text{ (deg)} \\ q \text{ (deg/sec)} \\ \theta \text{ (deg)} \\ h \text{ (ft)} \\ \delta_e \text{ (deg)} \end{bmatrix}$$

The control vector, $\underline{u}$, is the commanded elevator defection, δ_{e_c}, which is in degrees. These variables were defined in Section 2.2.1.

The three trim conditions and their corresponding coefficient matrices are as follows:

L-1011 Trim Condition I

Altitude:	29,000 ft
Speed:	799.1 ft/sec (Mach 0.8)
Weight:	360,000 lbs
$X_{c.g.}$:	0.25

$$\underline{A} = \begin{bmatrix} -.539e-2 & .112 & .533e-10 & -.562 & .362e-5 & -.945e-1 \\ -.794e-2 & -.760 & .977 & .398e-12 & .721e-4 & -.160 \\ .684e-2 & -.222e+1 & -.763 & .0 & -.141e-3 & -.587e+1 \\ .0 & .0 & .100e+1 & .0 & .0 & .0 \\ .0 & -.139e+2 & .0 & .139e+2 & .0 & .0 \\ .0 & .0 & .0 & .0 & .0 & -.588e+1 \end{bmatrix}$$

$$\underline{B} = \begin{bmatrix} .0 \\ .0 \\ .0 \\ .0 \\ .0 \\ .588e+1 \end{bmatrix}$$

L-1011 Trim Condition II

Altitude: 33,000 ft

Speed: 787.7 ft/sec (Mach 0.8)

Weight: 360,000 lbs

$X_{c.g.}$: 0.25

$$\underline{A} = \begin{bmatrix} -.212e-1 & .909e-1 & -.858e-10 & -.562 & -.512e-4 & -.100 \\ -.113e-1 & -.650 & .980 & -.231e-10 & .658e-4 & -.139 \\ .944e-3 & -.189e+1 & -.651 & .0 & -.122e-3 & -.501e+1 \\ .0 & .0 & .100e+1 & .0 & .0 & .0 \\ .0 & -.137e+2 & .0 & .137e+2 & .0 & .0 \\ .0 & .0 & .0 & .0 & .0 & -.588e+1 \end{bmatrix}$$

$$\underline{B} = \begin{bmatrix} .0 \\ .0 \\ .0 \\ .0 \\ .0 \\ .588e+1 \end{bmatrix}$$

L-1011 Trim Condition III

Altitude: 37,000 ft

Speed: 774.8 ft/sec (Mach 0.8)

Weight: 360,000 lbs

$X_{c.g.}$: 0.25

$$\underline{A} = \begin{bmatrix} -.270e-1 & -.206 & -.965e-10 & -.562 & -.123e-5 & -.166 \\ -.111e-1 & -.585 & .983 & .380e-12 & .112e-3 & -.127 \\ .166e-2 & -.172e+1 & -.545 & .0 & -.890e-4 & -.450e+1 \\ .0 & .0 & .100e+1 & .0 & .0 & .0 \\ .0 & -.135e+2 & .0 & .135e+2 & .0 & .0 \\ .0 & .0 & .0 & .0 & .0 & -.588e+1 \end{bmatrix}$$

$$\underline{B} = \begin{bmatrix} .0 \\ .0 \\ .0 \\ .0 \\ .0 \\ .588e+1 \end{bmatrix}$$

Appendix B

CESSNA CITATION III TRIM CONDITIONS

This Appendix presents the equilibrium conditions for the three state space models of the Cessna Citation III's longitudinal dynamics.

Citation III Trim Condition I

Altitude:	29,000 ft
Speed:	699.7 ft/sec (Mach 0.7)
Weight:	15,700 lbs
$X_{c.g.}$:	0.30

Citation III Trim Condition II

Altitude:	33,000 ft
Speed:	685.8 ft/sec (Mach 0.7)
Weight:	15,700 lbs
$X_{c.g.}$:	0.30

Citation III Trim Condition III

Altitude:	37,000 ft
Speed:	677.5 ft/sec (Mach 0.7)
Weight:	15,700 lbs
$X_{c.g.}$:	0.30

Appendix C

AUTOPILOT GAINS

The values for the constants used in the transport aircraft block diagrams that were shown in Figure 2-4 - 2-6 are as follows:

	Autopilot		
Constant	737-100	DC9-30	L-1011
C_1	$19/V_o$(ft/sec)	0.998E-2	0.218E-1
C_2	0.65	0.65	0.109E-2
C_3	$0.95/V_o$(ft/sec)	0.529E-3	3.00
C_4	0.213	1.24	2.00
C_5	0.66	0.8	0.40
C_6	0.735	2.9	0.40
C_7	1.14	0.73	40
C_8	-	-	20

Each autopilot uses units of feet for lengths, seconds for time, and degrees for angles.